Silesian University of Technology
Faculty of Civil Engineering
Department of Structural Engineering

PhD thesis

MSc Eng Marcin Kozłowski

Experimental and numerical analysis of hybrid timber-glass beams

Supervisor: DSc Eng Jacek Hulimka, SUT professor

Gliwice, 2014

The figures on the front page are: Upper left: An architectural visualisation of the pilot project, within this thesis, made by A. Kozłowska, A. Klich | AK^2. Upper right: A photograph from one of the experiments on adhesives, within this thesis, taken by Marcin Kozłowski. Middle left: A photograph from one of the experiments on life-size beam specimens, within this thesis, taken by Marcin Kozłowski. Middle right: A strain map obtained from Aramis system, within the thesis. Lower center: A figure from one of the FE analyses, within this thesis.

Front page design: A. Kozłowska | AK^2

The modern men need space, light, clearness, peace, nothing should limit the space.
We open our rooms to the sun and sky to big window surfaces,
and this way we intake the surroundings into our rooms.
They seem to be spacious without being big.

Heinrich Lauterbach (1893-1973)

Preface

The thesis was prepared in the Structural Engineering Department in the Faculty of Civil Engineering at the Silesian University of Technology in Gliwice (Poland). It was started in October 2010 and lasted four years.

Part of the research on materials (glass, timber) and experimental investigation on small-size beam specimens were carried out at the laboratory of the Faculty of Civil Engineering at the Silesian University of Technology (Gliwice, Poland). Part of the research on materials (glass, timber and adhesives) and experimental investigation on life-size beam specimens were performed in collaboration with the research group in the Department of Building and Energy Technology at the Linnaeus University (Växjö, Sweden) within the European research project "The WoodWisdom-programme: Load Bearing Timber Glass Composites (LBTGC)".

Abstract

Current trends in modern architecture are focused on minimising the boundaries between the external environment and interior of the building. This requires a continuous increase of the amount of translucent surfaces allowing natural sunlight to enter the building, not only in facades but also as interior elements. The research project on hybrid timber-glass beams is based on an assumption that timber and glass work together to carry external loads. Glass no longer acts as a filling, as in traditional solutions, but actively participates in load transfer. The research project involves the most important mechanical properties of very different materials: the stiffness and strength of glass and ductile nature of timber to build a modern, safe and durable building components.

The research project involves a single pane web made of annealed float glass and timber block flanges bonded together with an adhesive. Even if the glass web fails, due to overloading or an act of vandalism, the glass shards are held in place by the timber flanges and the beam can still withstand loading. The bottom flange with the bond line adhesive connection acts as a bridge: the tensile forces that before failure were carried by the tensile zone of the web are now transferred by the timber flange. Therefore, the concept prevents brittle failure of the beam, provides ductility and offers a high post-breakage strength after possible glass failure. The post-breakage strength relates to an increased value of the load at final collapse of a beam in relation to the load at which an initial crack in the web occurs.

Experimental investigation on materials used in the research (glass, timber and adhesives) was conducted in order to better understand the behaviour of the materials and determine the basic material properties used in the numerical and analytical models.

Tests on small- and life-size specimens were conducted in order to estimate the load-bearing capacity, bending stiffness and post-breakage strength. Also the influence of different adhesives covering the full range of stiffness from low (1-3 MPa) to high stiffness (1500 MPa) and types of glass (annealed float and heat-strengthened glass) on global glass beam behaviour was analysed.

Advanced 3D numerical models of beam specimens were implemented using Finite

Element Code ABAQUS. Explicit solver and *Brittle cracking* material model for glass were used to simulate cracking of glass. The Influence of element geometry, element size and value of fracture energy on results were analysed. From these studies the most suitable model parameters were chosen for final models of small- and life- size hybrid timber-glass beams. The models were validated by comparing their results with experimental studies.

A simple analytical method for preliminary design of hybrid glass beams (determination of the load at first cracking of glass and the initial bending stiffness) was proposed by modification of the gamma-method included in PN-EN-1995-1-1. The method was validated by comparing its results with experimental studies.

Acknowledgements

Over the past four years, I have received support and encouragement from many different people, organizations and companies but herein I would like to acknowledge those who have made a particularly important contribution.

First, I would like to express my special appreciation and thanks to my supervisor professor Jacek Hulimka. I would like to thank you for your support, guidance, listening my ideas and fruitful discussions. Thank you for encouraging my research and allowing me to grow as a research scientist.

I would also like to thank my colleagues from the Department of Structural Engineering at the Faculty of Civil Engineering at Silesian University of Technology (Gliwice, Poland) for valuable comments and suggestions from different perspectives. Special thanks to my colleagues Agnieszka Knoppik-Wróbel and Marta Kadela for careful reading, remarks and interesting suggestions.

During several research stays in Sweden I had a pleasure to meet many great people, but I would like to thank three of them in particular: professor Erik Serrano, Michael Dorn and Bertil Enquist. Thanks to them each stay in Växjö was pleasant and productive. Thank you Erik for the opportunity to join the timber-glass research group at the Department of Building and Energy Technology at the Linnaeus University, your help, being always positive to my ideas, guidance and time we spent discussing scientific issues. Michael, thank you for your cooperation, friendship and help. Bertil, it was great time working with you in the laboratory preparing test specimens and performing experiments.

A large part of the time devoted to preparation of the thesis was spent in the laboratory. I would like to thank Władysław Marchacz for his brilliant skills and commitment. I would also like to thank Michał Pieron and Rafał Siwek from Sika Poland for support during preparation of small-size specimens.

The thesis and several stays at the Linnaeus University was founded by the statutory activities for young scientists - research task "Analysis of breakage strength of hybrid timber-glass beams" (project number BK345/RB6/2012 and BK547/RB6/2013), Supporting Innovative Grants Forum Technology "SWIFT" (Center for Innovation and

Acknowledgements

Technology Transfer of the Silesian University of Technology), LLP/ERASMUS, the Programme "Research grants as an opportunity to develop the province of Silesia" (Poznań Academic Business Incubator) and the Visby Programme (the Swedish Institute). The contribution is gratefully acknowledged.

To my dear sister Agnieszka Kozłowska and Adam Klich, thank you for help with graphic design of the front page and architectural visualization of the pilot project.

Finally, a special thanks to my family and friends, especially for constantly asking me "are you done yet?". Thank you all for your encouragement, support in moments of doubt and understanding that sometimes the time I should devote to you I decided to spent working on the thesis. I appreciate your warm words and keeping your fingers crossed until the happy ending.

Thank you all!

Marcin Kozłowski
Chorzów, June 2014

Contents

Nomenclature

Greek letters

ΔT	temperature change
$\Delta \sigma$	increment of stress
$\Delta \sigma_{axial}$	increment of axial stress
$\Delta \varepsilon_{axial}$	increment of axial strain
ΔF	increment of load
Δl	axial elongation
Δu	increment of displacement
Δ_{exp}	variation of results of analytical solution and experimental testing
Δ_{local}	difference between EI_{global} and EI_{local}
Δ_{num}	variation of results of numerical analysis and experimental testing
Δ_t	time increment
δ_u	crack normal displacement
γ	connection efficiency factor
λ	Lame constant
μ	Lame constant
ν	Poisson's ratio
ρ	material density
$\rho(\varepsilon_{crack})$	material density

Nomenclature

σ	stress
σ_{axial}	axial stress
$\sigma_{f,c}$	stress in flange (centroid)
σ_f	stress in flange (outer edge)
$\sigma_{t,t}$	true stress
$\sigma_{t,u}$	maximal tensile stress
σ_t	nominal stress
σ_w	stress in web (edge)
ε	strain
ε_{axial}	axial strain
$\varepsilon_{crack,max}$	material parameter
ε_{crack}	crack opening strain
$\varepsilon_{lateral}$	lateral strain
$\varepsilon_{t,u}$	maximal tensile strain
ε_t	nominal strain

Latin letters

a	distance between loading position and the nearest support
A_0	nominal area of cross-section
A_i	cross-section area of i-component
a_i	distance from center of gravity of i-component and entire cross-section
b	width of cross-section
b_1	width of specimen
b_2	width of specimen (narrowing)
b_f	width (thickness) of web
b_f	width of flange
c^d	dilatational wave speed

E	modulus of elasticity
E_i	modulus of elasticity of i-component
E_v	comparative modulus of elasticity of i-component
E_{dyn}	dynamic modulus of elasticity
E_{global}	modulus of elasticity based on global deflection
E_{local}	modulus of elasticity based on local deflection
$E_{t,e}$	elastic tensile modulus
$E_{t,p}$	plastic tensile modulus
EI	bending stiffness
EI_{global}	bending stiffness calculated from global deflection
EI_{local}	bending stiffness calculated from local deflection
F	load
f	fundamental frequency
f_t	maximal tensile stress
F_{crack}	load at initial cracking in glass
$F_{t,u}$	ultimate load
f_{te}	ultimate tensile stress in elastic domain
G	shear modulus (uncracked)
G_{crack}	post-cracking shear modulus
G_f^I	fracture energy of glass
h	height of specimen
h_f	height of flange
h_w	height of web
h_{fg}	height of groove
I	moment of inertia
$I_{e,eff}$	effective moment of composite cross-section with i-components
$I_{e,ef}$	effective moment of composite cross-section

$I_{y,i}$	moment of inertia of i-component
K_k	stiffness of bond connection
L	length of specimen
l	length of specimen
L^e	characteristic element length
l_0	extensometer base length
l_1	distance between load introduction points
l_2	distance between supports
l_3	length of specimen
M	bending moment
MOE	modulus of elasticity
n_i	ratio of E_i to E_v
P	load
p	material parameter
r	radius
u	deflection
v_{global}	global deflection
v_{local}	local deflection
w_{fg}	width of groove
y_{fs}	distance from bottom side to center of gravity of flange

1 Introduction to the research

This chapter provides an introduction to the research. Background, motivation and problem definition are described. The chapter presents also main objectives, hypotheses, main research aspects and methodology.

1.1 Background and motivation

"The modern men need space, light, clearness, peace, nothing should limit the space. We open our rooms to the sun and sky to big window surfaces, and this way we intake the surroundings into our rooms. They seem to be spacious without being big" - the quote by Heinrich Lauterbach (1893-1973), one of the most renowned architects of Wrocław city during II World War period, despite many years after his death is still valid. Current trends in modern architecture are focused on minimising the boundaries between the external environment and interior of the building. This requires a continuous increase of the amount of translucent surfaces allowing natural sunlight to enter the building, not only in facades but also as interior elements, see Figure 1.1.

Figure 1.1: Pilot project. Hybrid timber-glass beams as load-bearing components of roof structure and conservatory (Authors: A. Kozłowska, A. Klich | AK^2)

.

Contact with the outside living environment is one of the most important psychological aspect [1]. It is indisputable that natural sunlight has positive impact on health and quality of life of people living or working in buildings [2]. For this reason, the possibility of increasing the translucent surfaces by the use of glass structural components is desirable. Besides, modern trends in architecture are oriented towards the high quality of life and low energy consumption, into which modern glass and wood products fit perfectly [3].

Nowadays, timber and glass are widely used in many architectural applications. Solutions such as glass panes bonded to timber frames were known for a long time. However, traditional solutions assume that glass only fills the frame - it does not contribute in the total load-bearing behaviour, only transfers wind load to the structural frame. Thus the glass pane requires a substructure to bear external loading.

The research project on hybrid timber-glass beams is based on a different assumption - namely, that timber and glass work together to carry external loads. Glass no longer acts as a filling but actively participates in load transfer. It becomes equivalent to timber, a structural element.

Timber is a natural material, environmentally friendly and perfectly in line with principles of sustainable development. Its high strength-to-weight ratio in combination with its low thermal conductivity makes timber a strong alternative to other constructional materials. In addition, an increased use of timber as a material for structural purposes will allow the European countries to reduce CO_2 emissions, mitigating climate change in accordance with international agreements such as The Kyoto Protocol [4].

The research project focuses on the combination of glass and timber materials in a way to work in synergistic cooperation. It involves the most important mechanical properties of very different materials: the stiffness and strength of glass and ductile nature of timber to build modern, safe and durable building components.

1.2 Problem definition

Although glass is known for thousands of years, only in the last few decades has been used as a load-bearing material for various structural elements, such as beams, walls and columns [5, 6]. The glass components were applied in a number of realizations, e.g. roof structures, facade structures, conservatories, footbridges and canopies [7–14].

Despite the undeniably desirable properties of glass, such as translucency, strength and durability the material glass itself poses many difficulties in structural considerations. Firstly, it is an extremely brittle material - thus unsafe, when overloaded breaks immediately into shards within a second. In contrast to for example steel, in case of which failure is preceded by large plastic deformation, glass fails with no warning. Secondly, glass is extremely susceptible to stress concentrations due to inability to redistribute stresses by local yielding of the material. Therefore, it is a big challenge to design proper structural connections between glass elements avoiding solutions that do not cause stress

peaks. Finally, glass is much weaker in tension than in compression, therefore it limits its scope of application especially in bending and tension components.

A traditional approach to design glass elements takes into account presented before aspects and involves the use of tempered glass. Tempered glass has a considerably higher strength than annealed float glass, but breaks into small shards and thus presents no post-breakage strength. Besides that, the commonly used approach is to laminate a few panes together to minimise the probability of total glass failure. In case of breakage of one pane the remaining are designed to carry the load. Finally, current design approaches are based on the use of very high safety factors and application of sacrificial sheets to the laminate to protect the load-bearing core. The conservative approaches are uneconomical and do not fully take advantage of the material glass.

The research project is based on another concept, different from traditional approaches. The hybrid timber-glass concept is presented in Figure 1.2. The concept involves a single pane web made of annealed float glass and timber block flanges bonded together with an adhesive [15]. Even if the glass web fails, the glass shards are held in place by the timber flanges and the beam can still withstand loading. The bottom flange with the bond line adhesive connection acts as a bridge: the tensile forces that before failure were carried by the tensile zone of the web are now transferred by the timber flange. Therefore, the concept prevents brittle failure of the beam, provides ductility and offers a high post-breakage strength after possible glass failure (caused by overloading or vandalism). The post-breakage (residual) strength relates to an increased value of the load at final collapse of a beam in relation to the load at which an initial crack in the web occurs, see Figure 1.2.

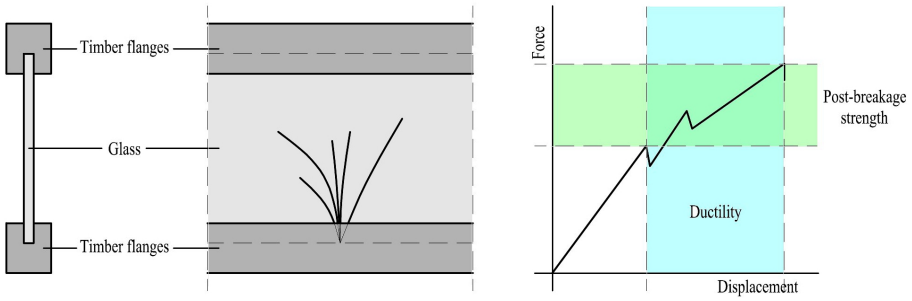

Figure 1.2: Schematic representation of hybrid timber-glass beam concept: cross-section of hybrid beam (left), side-view of hybrid beam with cracked glass web (middle), force-displacement diagram showing ductility and post-breakage strength.

In the last few decades several projects of combining glass with other materials were started [16, 17]. The projects can be divided into two categories: research on reinforced and hybrid glass beams. The first presents an analogy to reinforced concrete - a reinforcing material is not inside the main material but bonded to the tensile side of a glass web. The idea is to strengthen a glass beam with a strip made of steel [18–21],

carbon fibre [22] or glass fibre [23] bonded to the tensile side of the element. The other category presents analogy to composite structures. The hybrid glass beam concept is to combine a glass web and flanges made of different materials [16, 17]. It involves flanges made of steel [24–26], concrete [27] or timber [28–34]. In general, all research projects show tendency to seek ductility and post-breakage safety.

However, not all aspects of hybrid timber-glass beams are yet fully investigated. There is a need to continue experimental investigation on beam specimens of life-size dimensions. Moreover, numerical models of hybrid beams which include, in most cases, only the elastic phase, but also cracking in glass would contribute to current state of knowledge. Finally, a simple analytical tool for initial dimensioning would be of interests.

The current research project therefore focuses on broadening the knowledge and understanding the structural response of hybrid timber-glass beams. It includes experimental investigations on material of components, small-size (1800 mm long) and life-size (4800 mm long) specimens. Furthermore, numerical models are performed to simulate the behaviour of hybrid timber-glass beam elements under loading. They include not only the elastic phase but also post-cracking behaviour. Finally, a simple design method for dimensioning of hybrid timber-glass beam elements is provided.

1.3 Hypotheses and limitations

The previous section outlines the research area and defines the idea of the research project. However, when formulating the research problem, its boundaries and limitations should be carefully defined.

In the thesis the following hypotheses and limitations can be distinguished:

- **Hypothesis 1**
  Combination of a glass web and timber flanges bonded with adhesives provides a practical, durable and environmentally-friendly basis for a building system.
  Limitation: The thesis is limited to beam components as selected parts of a building system.

- **Hypothesis 2**
  Hybrid timber-glass beam components make possible predictable and safe structures by providing ductility and high post-breakage (residual) strength.
  Limitation: The thesis is limited to determination of a load-bearing strength of hybrid timber-glass beam components based on four-point bending test.

- **Hypothesis 3**
  The stiffness of a bond line adhesive connection influences the bending stiffness and load-bearing capacity of hybrid timber-glass beams.
  Limitation: The thesis is limited to three types of adhesives of different stiffness.

1.4 Objectives of the thesis

The main purpose of the thesis is to extend the knowledge about structural response of hybrid timber-glass beams. Moreover, it is focused on the try to simulate numerically the behaviour under loading and failure mechanism including formation and propagation of cracks in the glass web. In addition, it aims at a simple method to estimate the stiffness and load-bearing capacity of hybrid timber-glass beam components.

The following sub-goals can be distinguished:

- Prepare a literature review. Its main goals are to analyse and present the current state of knowledge including substantive findings as well as methodological contributions to the topic of hybrid timber-glass structural beams. The aim is to situate the current research within the work done by others;
- Investigate experimentally materials (glass, timber and adhesives) used for preparation of hybrid timber-glass specimens. Its main goal is to determine mechanical characteristics to use the values in numerical simulations and analytical considerations;
- Build and test nine 300 mm high and 1800 mm long hybrid timber-glass beams bonded with three different types of adhesives. The main goal is to test the concept and draw conclusions before manufacturing life-size specimens;
- Build and test twelve 240 mm high and 4800 mm long hybrid timber-glass beams bonded with three different types of adhesives;
- Model numerically the behaviour of hybrid timber-glass beams under loading and failure of a glass web including formation and propagation of cracks using Finite Element Methods (FEM);
- Investigate analytically the hybrid timber-glass beams regarding bending stiffness and load level at which initial cracking in glass occurs. Provide a simple analytical tool for initial dimensioning of hybrid timber-glass beams;
- Draw general conclusions based on findings from experimental investigations, numerical simulations and analytical considerations;
- Formulate directions for future research.

1.5 Research aspects and methodology

The experimental investigations are focused on understanding the behaviour under loading and mechanism of failure of hybrid timber-glass beams. The part consists of three main phases: testing of materials, small- and life-size specimens. The first phase deals with extending the knowledge about basic physical properties of materials used to build the hybrid beam specimens. Firstly, it includes determination of failure stress

of glass tested in standing position, modulus of elasticity and level of residual stress in heat-strengthened glass. Secondly, the timber is planned to be investigated in few configurations using different methods to determine its stiffness properties. Finally, three adhesives are tested in tension to specify the stiffness and Poisson's ratio. The experimental research on materials is focused on qualitatively rather than quantitatively. The parameters obtained in this phase are planned to be used in numerical models and analytical methods. The second phase includes experimental research on small-scale specimens (1800 mm long) by means of four-point bending tests. The aim is to investigate the differences in structural response of hybrid beam specimens built using three adhesives of different stiffness. The final phase is focused on experimental research on life-size specimens (4800 mm long). The main goal of this phase is to investigate the structural response of hybrid timber-glass beam specimens of life-size dimensions. Moreover, it allows to check the size-effect and answer the question if the results of small-size beams can be translated into the life-size specimens.

Numerical investigations are focused on the simulation of structural response of hybrid timber-glass beams. The numerical investigations make use of a 3D models and *brittle cracking model* available in ABAQUS/Explicit software [35]. The *brittle cracking model* is suited especially for modelling the response of brittle materials, in which the behaviour is dominated by tensile cracking. The crack initiation is governed by a simple criterion - a crack starts forming when the maximum principal stress exceeds the tensile strength of glass. Post-cracking behaviour of an element is based on fracture mechanics and loss of shear modulus associated with the magnitude of crack opening (shear retention model). Load-displacement curves and cracking patterns are derived from numerical models and compared with the experimental results. Moreover, the effects of various model parameters (e.g. element type, element size, fracture energy of glass) on the results are investigated.

A complex analytical model is not an aim of the thesis. The analytical investigation is focused rather on a simple design tool to be used by engineers who are not always familiar with complex FEM software or used to perform complex calculations. It provides an analytical method to estimate the stiffness and load-bearing capacity of hybrid timber-glass beams. The analytical tool can be also used for initial dimensioning of hybrid timber-glass beams.

1.6 Organization of the thesis

The thesis consists of 8 chapters, each dealing with separate subject.

Chapter 1 provides introduction to the research, background, motivation and problem definition. It presents objectives, hypotheses, main research aspects and methodology.

Chapter 2 presents a literature review, it provides the results of research projects on hybrid glass beam specimens made by others and an example of application of the hybrid timber-glass beam concept. It presents findings and methodological contributions to the subject. The motivation of the thesis is presented.

Chapter 3 focuses on experimental investigations on materials being the components of the specimens tested in following chapters. It characterizes mechanically glass, wood and adhesives.

Chapter 4 deals with with experimental testing of small-size beam specimens (l=1800 mm). It provides details of test specimens, test set-up and test procedures. It presents results, discussions and conclusions.

Chapter 5 deals with with experimental testing of life-size beam specimens (l=4800 mm). It provides details of test specimens, test set-up and test procedures. It presents results, discussions and conclusions.

Chapter 6 focuses on numerical modelling of structural response of hybrid timber-glass beams. It presents brief review of numerical methods used in the research. The experimental results, reported in Chapters 4 and 5, are used as a reference to validate the models. The findings from the numerical investigations are presented.

Chapter 7 presents a simple analytical tool to investigate the structural response of hybrid timber-glass beams regarding initial bending stiffness and the load at first cracking in glass. The test results presented in Chapters 4 and 5 are used as a reference to validate the models. The findings from the analytical investigations are presented.

Chapter 8 provides the conclusions from the research presented in the preceding chapters. It also presents the recommendations for future research.

2 Literature review

The chapter presents the current state of knowledge regarding hybrid glass beams within last twenty years. The chapter focuses mainly on hybrid timber-glass beams but provides also examples of combinations of glass and other materials. It gives the results of research projects on beam specimens. The chapter presents also an application of hybrid timber-glass concept in the roof structure of The Palafitte Hotel in Switzerland.

2.1 Hybrid timber-glass beams

The current knowledge about synergistic features of timber-glass composites relates to a few previously conducted research projects in European research centres within last twenty years.

Early examples of timber-glass composites were presented in the mid and late 1990s and early 2000s [36–39]. These research projects related to the basic studies on hybrid structural panels consisted of glass panes and frames made of timber, aluminium and glass fibre reinforced plastic, bonded with elastic connections. The projects showed a big potential and a need to develop the knowledge and continue the research on timber-glass composite elements.

More detailed technical research on timber-glass composites was made by Hamm in 2000 [28, 29]. Hamm investigated the influence of combining timber and glass based on I-shaped beam and plate elements using polyurethane adhesive, see Fig. 2.1. Eight 4000 mm long and 250 mm high beams were tested. The flanges consisted of two solid timber blocks bonded on both sides of the glass web. The dimensions of flanges varied from 30×50 mm to 50×60 mm. For all beams a 10 mm thick glass pane was used. Hamm observed an average increase of 200% of a load after first crack has appeared and average distance between cracks for all tested beams, which was 250 mm (Fig. 2.1). Despite high post-breakage strength of tested specimens, the idea of bonding two timber blocks on both sides of the glass web is questionable regarding proper load transfer from flanges to the web. Even minor imperfection of geometry may introduce unintended

eccentricities. Moreover, moisture exchange in wood can lead to its defects, such as warping, which in case of flange consisting of two elements may cause unpredictable effects.

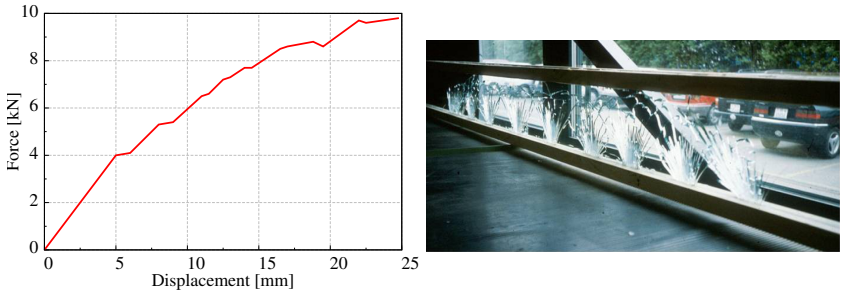

Figure 2.1: Force-displacement curve for 4000 mm long timber-glass composite beam (left) and the specimen after failure (right) [28].

Extensive research on I-shaped timber-glass composite beams including float, heat-strengthened and fully tempered glass was performed by Kreher in 2004 [30, 31]. Design of the beams was similar to Hamm's specimens but he used thinner pane thicknesses: 4 and 6 mm, also the length was reduced to 2000 mm likewise the height of beam to 150 mm. The dimensions of flanges varied from 30 $\times$ 30 mm to 50 $\times$ 50 mm. Kreher reported an average increase of 70% of a load after first crack has appeared before the total collapse of the beams with web made of annealed float glass (Fig. 2.2).

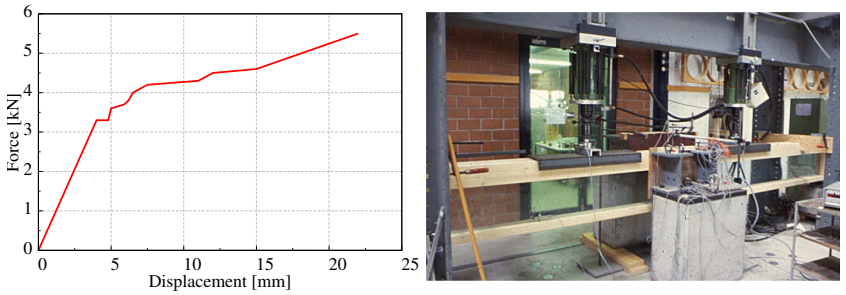

Figure 2.2: Force-displacement curve for a selected 2000 mm long timber-glass composite beam (left) and test set-up (right) [30].

The beams with web made of heat-strengthened glass and tempered glass showed no post-breakage strength. Kreher in his research used very thin glass panes (4 and 6 mm), probably due to small dimensions of specimens. This is understandable in terms of experimental investigations but it seems inadequate for practical applications due to its fragility.

Timber-glass composite beams were also researched by Cruz and Pequeno in 2008 [32]. Twenty beams were tested – 15 composite beams, including I-shaped and rectangular section, four timber beams and one glass beam. All composite beams were 550 mm high and consisted of a glass web and timber flanges 70 × 100 mm. The span of the beams varied from 650 to 3200 mm. The web was a laminate glass which consisted of two 6 mm thick annealed float glass panes with PVB interlayer. For the composite beams three adhesives were used: polymer, silicone and polyurethane. Cruz and Pequeno observed post initial crack strength of almost 185%, which corresponds to an average increase of a load of 85%.

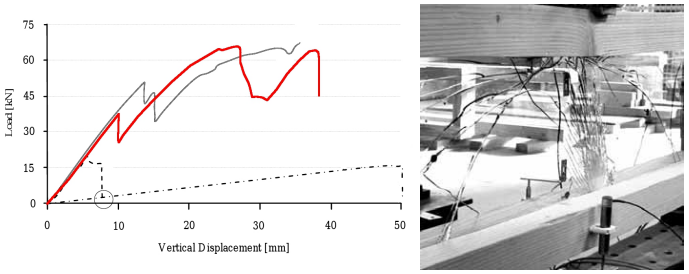

Figure 2.3: Force-displacement curve for a selected 3200 mm long timber-glass composite beam (left) the specimen after failure (right) [32].

The increase of load was observed for the 3200 mm long composite beam with polymer adhesive. However, Cruz and Pequeno state that silicone adhesive due to its great flexibility seems to be the most advisable for this application. Great flexibility and the associated smaller stiffness of hybrid beams are not desired in structural applications. When comparing force-displacement curves for tested specimens reported by Hamm, and Kreher (Fig. 2.1 and 2.2) and Cruz (Fig. 2.3) significant differences can be noticed. Cruz observed smaller number of cracks in glass web and the drops of forces were more pronounced. This leads to a conclusion that beams bonded with stiffer adhesives fail in more ductile manner and present more stable mechanism of failure in terms of structural behaviour.

Research on I-shaped timber-glass composite beams was also performed by Blyberg and Serrano in 2011 [33, 34]. All beams were 240 mm high and 3850 mm long. The section consisted of 10 mm thick glass pane 200 × 3850 mm made of annealed float glass and solid timber flanges 45 × 60 mm. Two types of glass edges were tested: roughly polished and non-treated after the traditional cutting. For the flanges laminated veneer lumber (LVL) was used. The glass web was bonded with adhesive in a groove milled in timber flanges. In the set, fourteen beams were tested: seven with non-treated edges, five with polished edges – both bonded with acrylic adhesive, and one bonded with silicone sealant with polished edges. Blyberg and Serrano observed an increase of load of 140% after formation of the first crack in the glass web before the maximum load was reached.

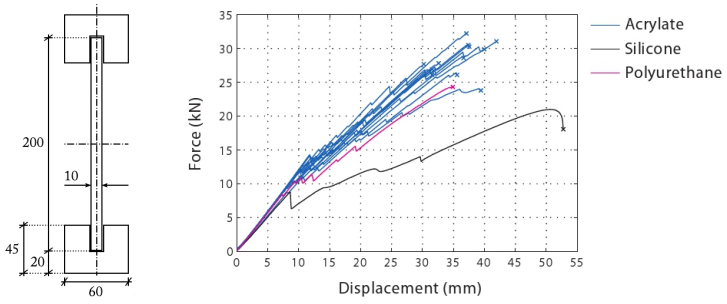

Figure 2.4: Cross-section of hybrid timber-glass beam specimens (left) and force-displacements curves (right) [33]

A different approach was presented by Winter and Hochhauser [40, 41]. In contrast to hybrid beams presented earlier, where the lower timber flange works as reinforcement of the broken glass web, the continuous glass web was split into six glass pieces separated by timber posts. The pieces were adhesively bonded on both sides to the timber framework. Acrylate and epoxy adhesives were used. Thus, it can be said that the beam combines two main load-bearing mechanisms: lattice girder and shear panels. The beam, presented in Figure 2.5, is 837 mm high and 8272 mm long. The cross-section of the beam is composed of timber flanges 100 $\times$ 149 mm and two panes 8 mm thick made of heat-strengthened glass. Three trusses with acrylate adhesive glue lines have been tested in four-point bending tests and showed an average collapse load of 127 kN at a deflection of 77.9 mm [42].

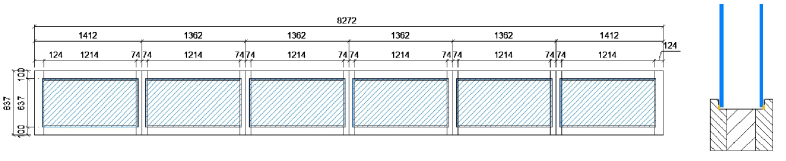

Figure 2.5: Side-view of hybrid timber-glass beam (left) and detail of cross-section (right) [40].

First results on experimental investigation on 4800 long hybrid timber-glass beam were presented by Premov et al. [43]. The specimen with the total height of 240 mm was composed of 8 mm think glass web and timber flanges as two wooden blocks bonded on both sides of the web with silicone adhesive. The specimen presented the ultimate load 225% higher than the load at first cracking. However, the promising findings are based on the only one specimen tested. Moreover, dividing the flanges into two timber blocks may lead to problems as with the beams researched by Hamm [28, 29].

2.2 Example of application

The concept developed by Kreher [30] was tested on a full-scale model and applied in the roof structure of the conference room in The Palafitte Hotel in Switzerland [39, 44], see Fig. 2.6.

The beams support a light roof and are supposed to transfer snow and wind load to steel posts hidden inside external walls. Each 6000 mm long and 580 mm high I-shaped beam composes of a single glass pane and timber flanges bonded on both sides of the glass web. The upper flange consists of two solid timber blocks 100 $\times$ 160 mm whereas the lower flange involves two timber blocks 65 $\times$ 65 mm. For the web a 12 mm thick glass pane made of fully tempered glass was used. Due to the lack of post-breakage strength of toughened glass the upper flanges were designed to resist external loads even in case of total failure of a glass web. This solution ensured the structural safety of the supporting roof structure. The beam was examined in four-point bending test. Due to the use of the fully-tempered glass the specimen presented brittle failure and no post-breakage strength. However, the maximal load obtained during testing was approximately three times bigger than the designed load on the roof structure.

Figure 2.6: The conference hall of Palafitte Hotel: view from inside and outside [44].

2.3 Hybrid glass beams with flanges made of other materials

In the last few decades several projects of combining glass with other materials were started [16, 17]. The section presents selected examples of hybrid beams with flanges made of other materials.

Hybrid steel-glass beams have been researched by Wellershoff [26]. The cross-section of the beam consisted of a glass web adhesively bonded to steel angles screwed to steel rectangular flanges (Fig. 2.7). A prefabricated 3600 mm long I-shaped hybrid beam was build and examined in four-point bending test. At a load of 137.8 kN first crack was observed. At the same time the test was stopped due to a large deflection of the specimen. The load bearing capacity of hybrid beam seems to be impressive if

compared with a pure glass beam. The theoretical load that causes buckling failure of a pure glass beam of the same dimensions as the tested beam was estimated at 29.6 kN.

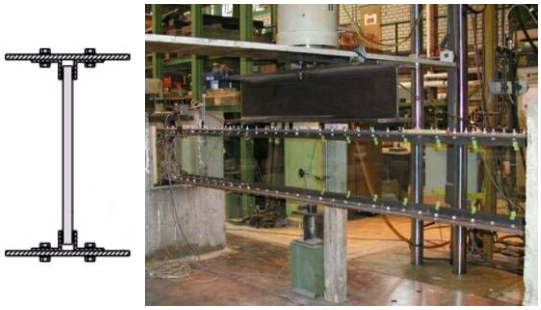

Figure 2.7: Cross-section of the hybrid steel-glass beam and four-point bending test [26].

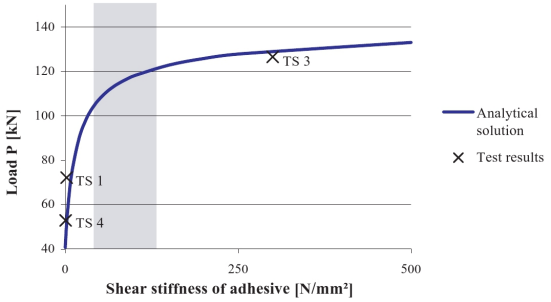

Figure 2.8: Load carrying capacity of hybrid steel-glass beams with joints made of different adhesives: TS4 – silicone, TS1 – polyurethane, TS3 – epoxy resin [24]

Similar studies of hybrid steel-glass beams have been performed by Ungermann [24]. In contrast to Wellershoff's research [26] the steel flanges were bonded directly (with no transitional angles) to the glass web. A 4000 mm long specimens consisted of a web built of two 12 mm toughened glass panes laminated together and steel flanges with a cross-section of 10 $\times$ 80 mm. The flanges were bonded to the web with three different adhesives: polyurethane, epoxy resin and silicone. The beams were examined in four-point bending test. To avoid the failure caused by lateral buckling of the beam a lateral support was built at midspan. To interpret the influence of adding steel flanges on a load bearing capacity of hybrid beams a failure load of a glass fin without flanges was estimated to be 40 kN (based on a glass strength of 120 MPa). The studies proved that stress distribution in hybrid steel-glass beams was highly depended on stiffness of an adhesive connecting the glass web and steel flanges (Fig. 2.8). In case of a silicone adhesive the specimen reached a load of 52.8 kN before the first crack occurred. Due to

low stiffness of silicone the flanges had small contribution in carrying forces and the beam failed due to glass failure. An increase of 32% in relation to the failure load of glass fin without flanges was explained that the glass strength was higher than expected. The beam with polyurethane adhesive (stiffer than silicone) showed the same behaviour at a load of 72.1 kN. An increase of 180% was explained by the glass strength as well. The highest load carrying capacity showed the beam with joints made of epoxy resin – 126.6 kN. The adhesive was so stiff that the steel flanges played a main role in carrying forces and almost reached the yield strength. In the test an 316% increase of failure load was achieved.

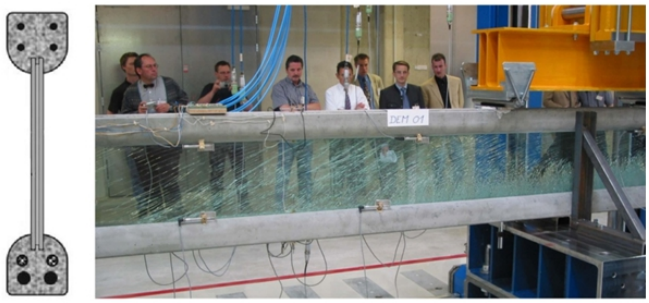

Figure 2.9: The cross-section of the glass-concrete beam (left) and the specimen during test (right) [27].

Research on glass-concrete composite beams has been performed by Freytag [27]. He presented a structural behaviour and detailed theoretical failure mechanism of the hybrid concrete-glass beam, see Figure 2.9. A 7800 mm long beam consisted of a glass web and two flanges made of ultra-high-performance concrete. The web was composed of three 8 mm panes made of fully tempered glass resin laminated together. The direct connection between glass and concrete was made by placing the web into form before pouring liquid concrete. To ensure proper joint the glass was specially pretreated by roughening the surfaces. To validate the concept two experiments were performed. The bottom flange of the first beam was prestressed by bondless tendons placed in the bottom flange of the beam to close the cracks caused by shrinkage of concrete and retrieve the original stiffness. The second specimen was simply reinforced. The experiments showed a strong influence of prestressing on load-bearing capacity of the glass-concrete composite beams. The prestressed beam failed at a load of 257 kN, whereas the second achieved maximum load of 100 kN. The experiments proved the high load-bearing capacity of glass-concrete beams. However, the concept demands complicated manufacturing process and special treatment of glass surface before pouring the liquid concrete into formwork. In the project fully toughened glass has been used. In case of a glass failure there is no post-breakage stiffness of glass web so the shear forces will be transferred only via concrete flanges. Furthermore, the alkaline concrete can corrode the glass.

2.4 Evaluation

The chapter presents the results of research projects on hybrid timber-glass beams accomplished within last twenty years. The studies presented before confirm relatively high post-breakage strength and potential of the concept in applications as load-bearing components of buildings. Despite relatively large number of research projects not all aspects of hybrid timber-glass beams are yet fully investigated.

Firstly, there are no clear conclusions regarding the most suitable adhesive for the bond like connections. For example, Cruz and Pequeno [32] state that silicone adhesive due to its great flexibility is the most advisable while most researchers use stiffer e.g. acrylate adhesives [28, 30, 33]. On the other hand in case of long beams with a stiff adhesive a temperature change may result in potentially high thermal stress. Therefore, there is a need to investigate the effect of temperature changes on the long specimens.

Then, most experiments were performed on short span beams with limited number of specimens. Hence the additional studies on beams with life-size dimensions (4000÷5000 mm) would allow to analyse the scale effect and investigate already tested concepts on the specimens which could be build-in in a real structure.

Finally, most publications do not provide analytical tools or numerical methods (especially including brittle failure of glass) to simulate the behaviour of hybrid timber-glass beams. A simple design analytical tool to estimate the stiffness and load-bearing capacity of hybrid timber-glass beams could be used by engineers who are not always familiar with complex FEM software or used to perform complex calculations. Moreover, the analytical solution, confirmed by test results could be a base for future standardization. An efficient and reliable numerical model could be used for simulating various quasi-static problems related to hybrid timber-glass beams. In addition, it could be used for initial dimensioning of test specimens before designing test a set-up and testing procedures.

3 Experimental investigations on materials

This chapter deals with materials used for manufacturing small- and life-size specimens presented in Chapters 4 and 5. It characterizes mechanically glass, wood and adhesives as well as provides basic mechanical properties used in numerical investigations and analytical considerations (Chapters 6 and 7).

3.1 Background information

The experimental investigations presented in this chapter were conducted in the laboratories of the Faculty of Civil Engineering at the Silesian University of Technology (Gliwice, Poland) and the Department of Building and Energy Technology at the Linnaeus University (Växjö, Sweden). Materials for the research were supported by companies: Pilkington Floatglas AB, Pilkington Poland, Stora Enso Timber AB, Drewno Company, Sika Sverige AB. The contribution regarding technical support and assistance of the following people is acknowledged: Władysław Marchacz, Tomasz Hahn, Karol Konopka (Silesian University of Technology), Bertil Enquist, Michael Dorn (Linnaeus University). Special thanks to Glafo – Swedish Glass Research Institute for lending a polariscope SCALP and help during measurement. The contribution if fully acknowledged.

3.2 Glass

The section presents the results from experimental investigation on two types of glass used to build small-size and life-size hybrid timber-glass beams presented in Chapters 4 and 5, respectively. Glass type A is a monolithic glass beam made of ordinary annealed float glass [45]. Glass type B is a monolithic glass beam made of heat-strengthened glass [45]. The main aim of the research is to determine the basic mechanical properties of glass: modulus of elasticity, ultimate strain (for annealed float glass) and residual stress profile in heat-strengthened glass. The calculated values will be then used in numerical analyses and analytical considerations presented in Chapters 6 and 7, respectively.

3.2.1 Material properties

A glass is usually defined as inorganic product of synthesis which has been cooled to a rigid condition without crystallization [45]. Soda-lime silica glass (annealed glass) is commonly used glass type in the building industry. It is a combination of silica sand (69-74% of mass), lime (5-14%), soda (10-16%), magnesia (0-6%) and alumina (0-3%) [46].

The float process is currently the main production method of float glass. The method is used by 90% of factories all over the world [45]. Continuous float process composes of several stages. During the first phase the raw materials are melted in a furnace at 1550°C. Then, the molten glass is poured onto a bath of molten tin at 1000°C, which ensures forming continuous pane with perfectly smooth surfaces. At the end of the tin bath the glass is cooled down to 600°C and proceeds to an oven called annealing lehr. During that phase the glass is cooled down slowly to 100°C to prevent residual stresses in the material. Finally, after inspection for visual defects, the glass is cut to the final size. The maximum standard size of glass is 6×3.21 m. However, it is possible to produce greater lengths. The standard thicknesses range from 2 to 25 mm.

Table 3.1: Physical properties of soda-lime silicate glass [46].

Property	Value
Density	2500 kg/m^3
Young's modulus	70 GPa
Poisson's ratio	0.23
Tensile strength	45 MPa
Thermal expansion coefficient (at 20°C)	9·10^6
Thermal conductivity	1 W·m^{-1}·K^{-1}

Typical material properties of soda-lime silicate glass are presented in Table 3.1. Glass with a density comparable to reinforced concrete presents modulus of elasticity almost equal to that of aluminium. Glass shows isotropic and almost perfectly elastic behaviour. Due to its brittle manner glass does not yield plastically and therefore is very susceptible to stress concentrations [45].

The strength of glass is not a constant value, but it depends on various parameters such as surface and edge quality, the size of an element, duration of load, residual stress and environmental conditions. Glass is several times weaker in tension than in compression. A theoretical strength of a typical silica glass based on forces of the interatomic bonds is 32 GPa. However, the practical tensile bending strength of annealed soda-lime glass is much lower. According to EN 572-1:2004 the characteristic tensile bending strength is 45 MPa [46]. This significant difference between the theoretical and the practical strength was explained by Griffith in 1920 [47]. Similar to other brittle materials glass presents randomly distributed microscopic flaws at its surface, so-called "Griffith flaws". The flaws act as stress concentrators from which fracture formates. They exist already in glass after production process. Further flaws may occur during processing and service

life from e.g. debris, scratching, impact, etc. The larger flow depths the lower the strength. A compromise is heat-strengthened glass which presents higher bending strength (70 MPa) compared to annealed float glass and fracture pattern is similar to fully-tempered glass [45].

The practical strength of glass can be improved in tempering process which is about introduction of a surface compressive residual stress by heat treatment of glass [45]. Since the surface tensile stress due to actions is smaller than the residual compressive stress in tempered glass, no crack will develop. The fracture pattern of glass is highly dependent on residual stress. Annealed float glass breaks into large fragments whereas fully tempered glass presents high fragmentation and breaks into small pieces which does not affect post-breakage strength.

3.2.2 Laboratory tests

Glass type A is a monolithic glass beam made of ordinary annealed float glass. Figure 3.1 presents the cross-section of the specimen and test set-up for glass type A.

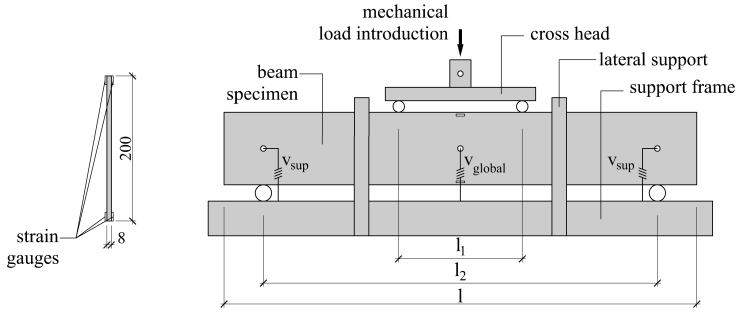

Figure 3.1: Cross-section of specimen and scheme of test set-up used for four-point bending test on glass type A.

The specimens had a rectangular shape with the cross-sectional dimensions of 8×200 mm ($b \times h$) and the length of 1800 mm (l). The theoretical distance between the supports was 1500 mm (l_2). The forces were introduced symmetrically at 1/3 of the span (l_1) through a transitional cross head beam. Two lateral supports were provided approximately 100 mm from the load introduction points to prevent the beam from failing in lateral buckling.

The tests were performed with a number of six specimens (GS.01-GS.06) in a hydraulic testing machine. The specimens were loaded at constant displacement rate of 0.5 mm/min. To read the response of the beams to loading a number of detectors were applied to the specimens. To measure deformations three inductive displacement sensors were installed at the mid-span and at supports. Also a set of strain gauges was attached to the specimens to measure the strains on the top and bottom side of the specimens. To

avoid stress concentration in glass caused by direct contact with steel rolls (at supports and load introduction points) rubber pads were used.

Glass type B is a monolithic glass beam made of heat-strengthened glass. Before testing of life-size hybrid timber-glass beams with the web made of heat-strengthened glass residual stress profile through the thickness of a glass panel was measured using a portable scattered light polariscope SCALP [48], see Figure 3.2. The SCALP device generates a laser beam which passes through the glass panel under the angle of 45°. The stress distribution over the glass thickness modifies the polarisation of the laser beam. Subsequently, a very sensitive camera records the changes in the polarisation along the laser beam and software evaluates the stress profile through the glass panel. In heat-strengthened glass a typical stress profile through the thickness of glass panel shows compressive stress at surface and tensile stress in the core of a glass pane [45].

Figure 3.2: Measurement of residual stress in glass using polariscope SCALP.

3.2.3 Results and discussion

Figure 3.3 presents force versus mid-span displacement plots for testes glass specimens type A. All glass specimens presented similar behaviour under loading. The relationship between the load and vertical mid-span displacement was perfectly linear until failure. The results shows a very good repeatability. In all cases the ultimate failure was brittle and caused by tensile failure of glass.

Modulus of elasticity was calculated with respect to [49]. The standard formula for a simple supported beam with two symmetrically applied forces was transformed to the form:

$$E = \frac{23\,\Delta F\,l_2^3}{54\,b\,h^3\,\Delta u} \tag{3.1}$$

where ΔF [kN] is the increment of the straight line of the load-global deformation curve measured at the neutral axis level at mid-span (see v_{global} in Figure 3.1), Δu [mm] is the increment of the deformation, b and h [mm] are the cross-sectional dimensions, l_2 [mm] is the distance between the supports.

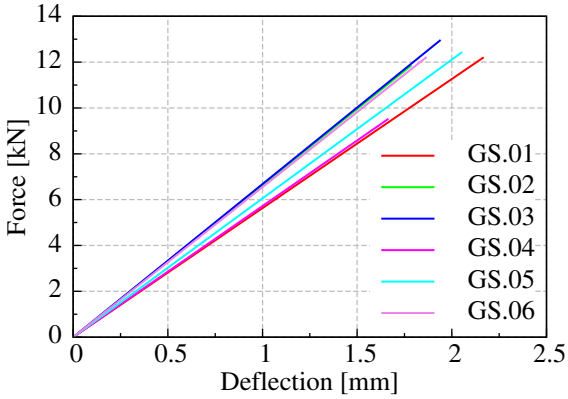

Figure 3.3: Force vs. mid-span displacement curves for glass specimens type A.

The average values of the maximal load, modulus of elasticity, maximal tensile strain and corresponding stress obtained from the test are presented in Table 3.2. The table provides also standard deviation for the obtained values. The average value of the modulus of elasticity of tested specimens was 69.77 $\cdot 10^3$ MPa. The value corresponds to the value of $70 \cdot 10^3$ MPa for basic soda lime silicate glass, reported in [50]. Since the strain gauges were attached to the specimens the tensile strain level at failure in glass could have been obtained and the corresponding stress could have been calculated. For the tested specimens the average value of the maximal tensile strain and corresponding stress were $0.651 \cdot 10^{-6}$ and 45.61 MPa, respectively. The value of maximal tensile stress corresponds to the average failure stress of glass 45 MPa (tested in standing position) reported in [51].

Table 3.2: Four-point bending test results, glass specimens type A.

Specimen	Maximal load [kN]	Modulus of elasticity [MPa$\cdot 10^3$]	Maximal strain [-]	Maximal stress [MPa]
GS.01	12.21	63.25	$0.674 \cdot 10^{-6}$	42.64
GS.02	11.86	74.55	$0.652 \cdot 10^{-6}$	48.61
GS.03	12.96	75.02	$0.723 \cdot 10^{-6}$	54.21
GS.04	9.53	64.29	$0.489 \cdot 10^{-6}$	31.43
GS.05	12.44	67.98	$0.674 \cdot 10^{-6}$	45.83
GS.06	12.22	73.51	$0.693 \cdot 10^{-6}$	50.95
Mean values	11.87	69.77	$0.651 \cdot 10^{-6}$	45.61
Standard dev.	1.19	4.97	$0.080 \cdot 10^{-6}$	7.58

Figure 3.4 presents the glass specimen type A in four-point bending test and typical failure of specimen. The picture shows also a crack formation in the mid-span of the specimen and typical shear crack starting from the support.

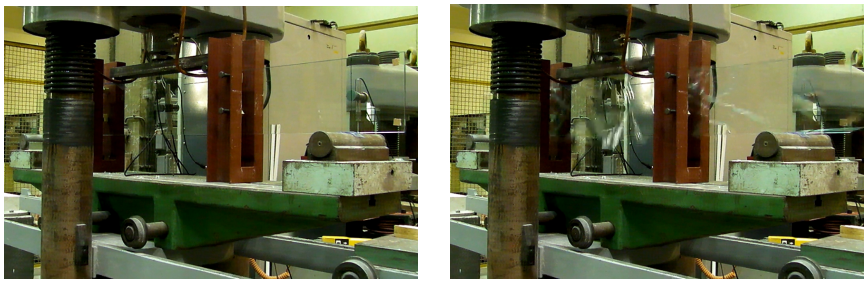

Figure 3.4: Glass specimen GS.01 in four-point bending (left) and typical failure of specimen (right).

Table 3.3 shows the result of the measurement of the residual stress profile through the thickness of 6 glass webs made of heat-strengthened glass (glass type B). The measurements with a use of the polariscope SCALP, were performed in the central part of the glass web. For the tested specimens the average value of middle (tensile) and surface (compressive) residual stress was 53 and 25 MPa, respectively. The value of the compressive residual surface stress of 53 MPa corresponds to the typical value of residual compressive surface stress in heat-strengthened glass of 50 MPa [45]

Table 3.3: Values of residual stress through the thickness of 6 glass panes made of heat-strengthened glass.

Specimen	Residual stress [MPa]	
	Middle (tensile)	Surface (compressive)
E-HS-01	53	24
E-HS-02	51	25
A-HS-01	51	28
A-HS-02	54	22
S-HS-01	55	23
S-HS-02	55	28
Mean values	53	25
Standard deviation	1	2

3.3 Timber

The section presents the results from experimental investigation on two types of timber used to build small-size and life-size hybrid timber-glass beams presented in Chapters 4 and 5, respectively. The main aim of the research is to determine the basic mechanical properties of timber used to build hybrid timber-glass beams (modulus of elasticity and ultimate strain).

3.3.1 Material properties

Timber is natural growing material with highly anisotropic behaviour. Due to the orientation of the wood grains (fibres) and the manner a tree increases in diameter as it grows mechanical properties vary along three perpendicular axes: longitudinal, radial and tangential. The main longitudinal axis is parallel to the fibre direction, the radial axis is perpendicular to the fibre direction and normal to the growth rings, and the tangential axis is perpendicular to the fibre direction and tangent to the growth rings. Although wood properties vary in each of three axis directions, differences between radial and tangential axes is relatively small if compared to the differences between the either of the two: tangential or radial axes and the longitudinal axis.

Timber shows generally low deformation capacity and usually presents brittle type behaviour. The response is strictly dependent on the direction and type of loading. When subjected to compression timber behaves in a rather ductile manner for loading in both directions (parallel and perpendicular to the grain direction). However, when loaded in shear, tension or bending the response is brittle. Typically, modulus of elasticity of wood is $7 \div 20$ GPa along grain and $0.23 \div 1.33$ GPa perpendicular to grain direction. In the grain direction strength is typically equal to $8 \div 42$ MPa in tension and $16 \div 34$ MPa in compression. Across fibres the strength varies from $0.4 \div 0.6$ to $2 \div 8$ MPa in tension and compression, respectively.

Although timber presents heterogenic behaviour due to the presence of weak sections e.g. knots and resin pockets, it is usually considered as homogenous orthotropic material. For structural purposes wood is graded by reducing effects of defects, e.g. removing growth defects or knots in production process of timber or distributing the defects in the final product (laminations). The purpose of grading is to remove week parts such as knots so that only clear, defect-free wood remains. Then, to obtain longer elements the wood is finger-jointed. The wood products used in the research were not graded for structural purposes but for window manufacturing purposes.

Two graded pine wood products were used in the research. Timber specimen type A is a trio beam made from three finger-jointed flat-sided planks bonded together with the grain parallel [52] commonly used for windows framing, see Figure 3.5. Timber specimen B is a finger-jointed solid softwood beam [52], see Figure 3.5. Both beams are knot-less, dimensionally and environmentally stable.

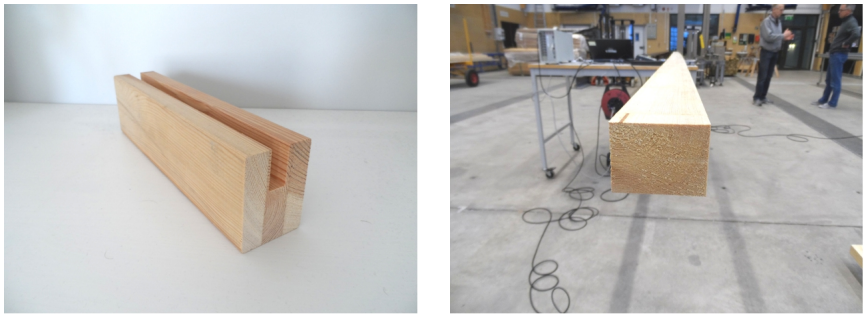

Figure 3.5: Trio beam type A (left) and type B (right).

3.3.2 Laboratory tests

Two types of experiments were performed on timber type A. In the first test three studs were tested in bending to determine modulus of elasticity (in bending) and ultimate strain. Then, three 100 mm long slices, were cut from the same sort of studs and tested in compression to determine the modulus of elasticity (along the fibres) and Poisson's ratio.

Two types of experiments were performed on wood type B. In the first type 30 studs were tested to determine dynamic modulus of elasticity. In the second type test six studs were tested in bending to determine modulus of elasticity (in bending) and ultimate strain.

Timber type A - Bending test

The four-point bending test of specimens was developed with respect to [49]. Figure 3.6 presents the cross-section of specimen and test set-up. Structural size beams have a rectangular shape with the cross-sectional dimensions of 55×75 mm ($b \times h$) and 1800 mm length (l). The theoretical distance between the supports was 1500 mm (l_2). The forces were introduced symmetrically at 1/3 of the span (l_1) through a transitional cross head beam.

The tests were performed with a number of three specimens (TS1-TS3) in a hydraulic testing machine. The beams were loaded at constant displacement rate of 0.5 mm/min. To read the response of the beam to loading a number of detectors were applied to the specimens. To measure deformations three inductive displacement sensors were installed at the mid-span and at supports. Also a set of strain gauges was attached to the specimens to measure the strains on top and bottom side of the specimens.

The formula for modulus of elasticity E (in bending) was derived as explained in Section 3.2:

$$E = \frac{23\,\Delta F\,l_2^3}{108\,b\,h^3\,\Delta u}, \tag{3.2}$$

where ΔF [kN] is the increment of the straight line of the load-global deformation curve

measured at the neutral axis level, at mid-span (see v_{global} in Figure 3.6), Δu [mm] is the increment of the deformation, b and h [mm] are the cross-sectional dimensions, l_2 [mm] is the distance between supports.

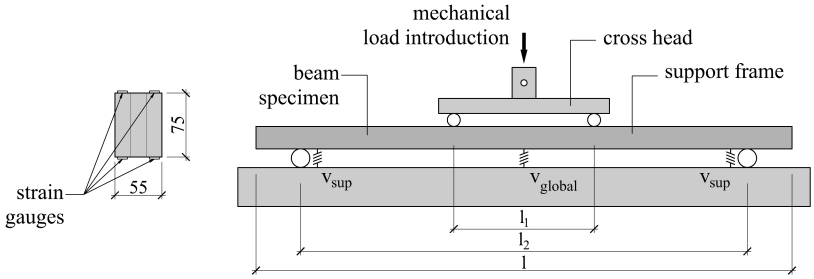

Figure 3.6: Cross-section and scheme of test set-up used for four-point bending test on timber type A.

Timber typa A - Compression test

The compression test of wood was conducted according to [49]. Figure 3.7 presents the specimen and test set-up. The specimens have a rectangular shape with the cross-sectional dimensions of 55×75 mm^2 ($b \times h$) and 100 mm length.

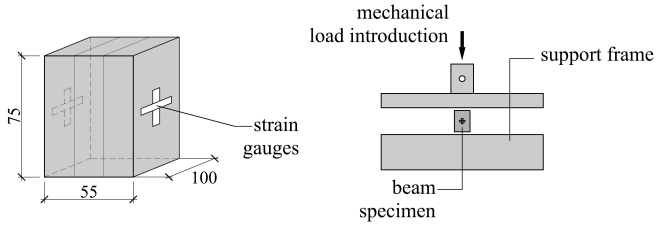

Figure 3.7: Specimen and scheme of test set-up used for compression test on timber type A.

The tests were performed with a number of three specimens (C1-C3) in a hydraulic testing machine. The beams were loaded at constant displacement rate of 0.5 mm/min. To read the response of the beam to loading strain gauges was attached to the specimens to measure the strains on sides of the specimens along and perpendicular to the fibres.

Modulus of elasticity E (in compression) was determined with relation:

$$E = \frac{\Delta\sigma}{\Delta\varepsilon_{axial}}, \tag{3.3}$$

where $\Delta\sigma$ [MPa] is the is the increment of the straight line of the stress-axial strain curve, $\Delta\varepsilon$ is the increment of the axial strain.

To evaluate Poisson's ratio ν the readings from the strain gauges were used. The values of strains: parallel and across the specimen in the middle part of the specimens, see Figure 3.7, were averaged and values of Poisson's ratio were calculated by dividing axial strain by lateral strain, according to:

$$\nu = \frac{\varepsilon_{axial}}{\varepsilon_{lateral}}, \tag{3.4}$$

where $\varepsilon_{\text{axial}}$ is the parallel strain, $\varepsilon_{\text{lateral}}$ is the strain across the specimen.

Timber type B - Dynamic test

Dynamic modulus of elasticity is increasingly being used for the evaluation of wood quality, it allows for quick and appropriate grading solution [53]. The method is based on measurement of the natural frequency of a wood element. During resonance test, the specimen was tapped once on one end with a hammer to determine the response (Fig. 3.8). The response was detected using a sensitive microphone and the resonance frequency was detected with a spectrum analyser (Fig. 3.8). The primary peak with the highest magnitude (the fundamental peak) corresponded to the resonance induced by vibrations in the longitudinal direction.

Dynamic modulus of elasticity was determined with relation:

$$E_{dyn} = \rho\,(2\,L\,f)^2, \tag{3.5}$$

where ρ is the mass density of the specimen [kg/m^3], L is the specimen length [m], f is the fundamental frequency corresponding to the primary peak [Hz].

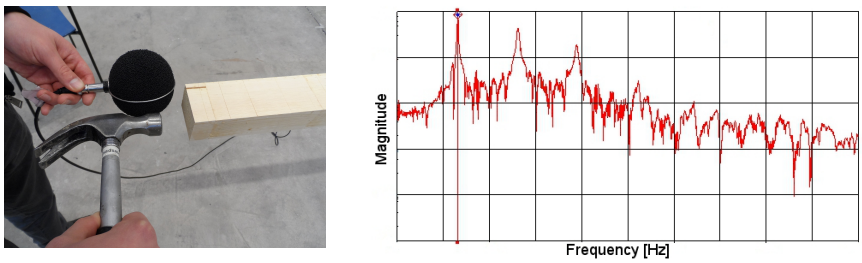

Figure 3.8: Resonance test (left) and resonance frequency detected with spectrum analyser.

Timber type B - Bending test

The four-point bending test of wood was conducted according to [49]. Figure 3.9 presents the cross-section of specimen and test set-up. Beam had a rectangular shape with the cross-sectional dimensions of 45×60 mm ($b \times h$) and 800 mm length (l). Since the specimens were cut off from the beams which were going to be used to build a hybrid beam, the specimens had a groove measuring 12×20 mm. The theoretical distance between the supports was 710 mm (l_2). The forces were introduced symmetrically at 1/3 of the span (l_1) through a transitional cross head beam.

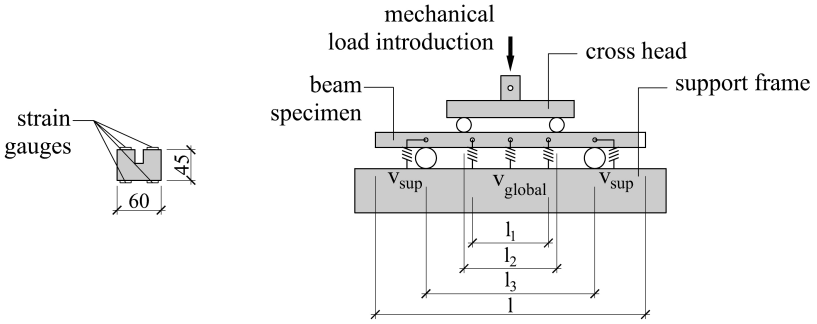

Figure 3.9: Cross-section and scheme of test set-up used for four-point bending test on timber type B.

The tests were performed with a number of six specimens (TSB.1-TSB.6) in a hydraulic testing machine. The beams were loaded at constant displacement rate of 0.5 mm/min. To read the response of the beam to loading a number of detectors were applied to the specimens. To measure deformations five inductive displacement sensors were installed at the mid-span, at supports and between the two loads, over a length of 225 mm to measure curvature of the specimen. Also a set of strain gauges was attached to the specimens to measure the strains on top and bottom side of the specimens.

Local and global modulus of elasticity were determined with relations [49]:

$$E_{local} = \frac{a\, l_1^2\, \Delta F}{16\, I\, \Delta u}, \tag{3.6}$$

$$E_{global} = \frac{l_1^3\, \Delta F}{48\, I\, \Delta u}, \tag{3.7}$$

where a is the distance between the loading position and the nearest support [m], ΔF [kN] is the increment of the straight line of the load-global deformation curve measured at the neutral axis level, at mid-span (see v_{global} in Figure 3.9), Δu [mm] is the increment of the deformation, b and h [mm] are the cross-sectional dimensions, l_1 [mm] is the distance between supports, I is the moment of inertia [m^4].

3.3.3 Results and discussion

Timber type A - Bending test

The obtained results are presented in Figure 3.10 and Table 3.4. All specimens presented similar behaviour under loading. The relationship between the load and vertical mid-span displacement was almost perfectly linear until failure. In all cases the ultimate failure was brittle and caused by failure of finger-joints. The failure occurred at the same force and displacement of approximately 10 kN and 28 mm, respectively.

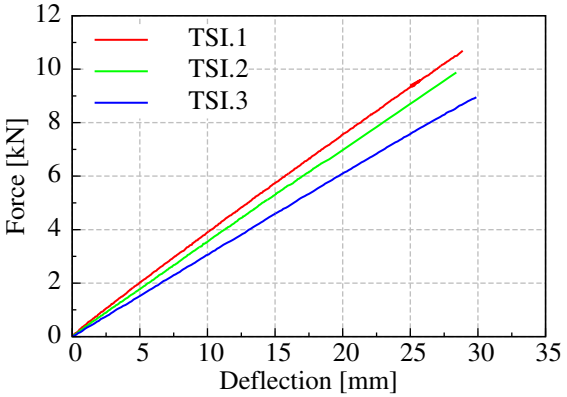

Figure 3.10: Force versus mid-span displacement curves for tested specimens.

The average values of the modulus of elasticity (in bending) E , maximal tensile strain $\varepsilon_{t,u}$ and corresponding stress $\sigma_{t,u}$ are presented in Table 3.4. The table provides also standard deviation for the obtained values. The average value of modulus of elasticity E of tested specimens was 10.54 $\cdot 10^3$ MPa.

Table 3.4: Bending test results, timber type A.

Specimen	E [MPa$\cdot 10^3$]	$\varepsilon_{t,u}$ [-]	$\sigma_{t,u}$ [MPa]
TSI.1	11.47	$3.19 \cdot 10^{-6}$	36.54
TSI.2	10.87	$3.20 \cdot 10^{-6}$	34.56
TSI.3	9.27	$4.28 \cdot 10^{-6}$	35.66
Mean values	10.54	$3.56 \cdot 10^{-6}$	35.58
Standard deviation	0.93	$0.51 \cdot 10^{-6}$	0.81

Since the strain gauges were attached to the specimens the tensile strain level at failure in wood could have been obtained. From the strain the corresponding stress could have been calculated. For tested specimens the average value of the maximal tensile strain $\varepsilon_{t,u}$ and corresponding stress $\sigma_{t,u}$ was equal to $3.56 \cdot 10^{-6}$ and 35.58 MPa, respectively.

Timber type A - Compression test

The obtained results are presented in Figure 3.11 and Table 3.5. All specimens presented similar behaviour under loading. In the first stage the relationship between the load and vertical mid-span displacement was almost perfectly linear. In the next stage the curves started to bend until failure.

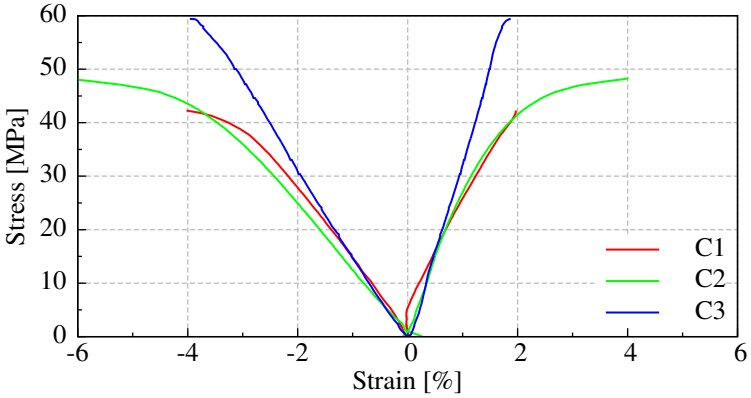

Figure 3.11: Force versus strains curves for tested specimens.

Table 3.5: Compression test results, timber type A.

Specimen	E [MPa·10^3]	ν [-]
C1	13.89	0.411
C2	10.49	0.370
C3	9.32	0.534
Mean values	11.23	0.438
Standard deviation	1.94	0.070

The average values of the modulus of elasticity (in compression) E and Poisson's ratio ν are presented in Table 3.5. The table provides also standard deviation for the obtained values. The average value of the modulus of elasticity E of tested specimens was $11.23 \cdot 10^3$ MPa. In comparison to the value of E (in bending), E (in compression) is approximately 6.5% higher. It can be explained by the fact that E (in bending) is affected by the effect of shear deformation. According to [54] the modulus of elasticity from

bending is approximately 10% higher than modulus of elasticity from the compression test. However, both values correspond to the value of $11 \cdot 10^3$ MPa for pine wood, reported in [55].

Dynamic test

The obtained results are presented in Table 3.6. The average value of the fundamental peak for all tested specimens was 524.3 Hz, which, according to formula 3.5, corresponds to the average value of E= $12.41 \cdot 10^3$ MPa.

Table 3.6: Dynamic test results, timber type B.

	Fundamental peak f [Hz]	E [MPa·10^3]
Mean values	524.3	12.41
Standard deviation	19.7	1.31

Bending test

The obtained results are presented in Figure 3.12 and Table 3.7. All specimens presented similar behaviour under loading. The relationship between the load and vertical mid-span displacement was almost perfectly linear until failure. In all cases the ultimate failure was brittle and caused by failure of finger-joints. The failure occurred at the same force and displacement of approximately 8.6 kN and 12.5 mm, respectively.

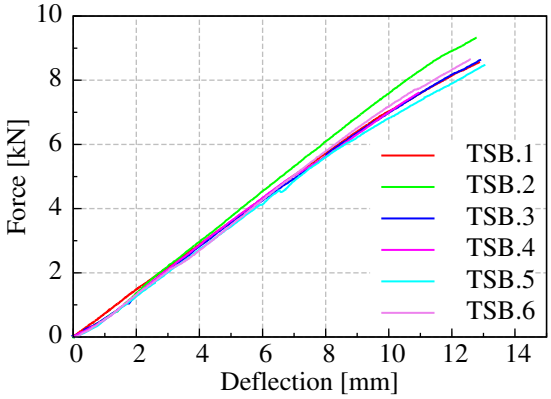

Figure 3.12: Force versus mid-span displacement curves for timber specimens (type B).

The average values of the modulus of elasticity E_{global} and E_{local} (in bending), maximal tensile strain $\varepsilon_{t,u}$ and corresponding stress $\sigma_{t,u}$ are presented in Table 3.7. The table provides also standard deviation for the obtained values. The average value of the global and local modulus of elasticity for tested specimens were $12.78 \cdot 10^3$ and 14.87

$\cdot 10^3$ MPa, respectively. Since the strain gauges were attached to the specimens the tensile strain level at failure in wood could have been obtained. From the strain the corresponding stress could have been calculated. For the tested specimens the average value of the maximal tensile strain $\varepsilon_{t,u}$ and corresponding stress $\sigma_{t,u}$ were $3.49 \cdot 10^{-6}$ and 44.59 MPa, respectively.

Table 3.7: Bending test results, timber type B.

Specimen	E_{global} [MPa·10^3]	E_{local} [MPa·10^3]	$\varepsilon_{t,u}$
TSB.1	12.26	16.22	$3.367 \cdot 10^{-6}$
TSB.2	14.08	14.80	$3.641 \cdot 10^{-6}$
TSB.3	12.51	14.55	$3.124 \cdot 10^{-6}$
TSB.4	12.85	12.13	$3.501 \cdot 10^{-6}$
TSB.5	11.97	14.51	$3.647 \cdot 10^{-6}$
TSB.6	12.99	17.01	$3.647 \cdot 10^{-6}$
Mean value	12.78	14.87	$3.490 \cdot 10^{-6}$
Standard deviation	0.68	1.54	$0.190 \cdot 10^{-6}$

3.4 Adhesives

The section presents results from experimental investigation on adhesives used to build small-size and life-size hybrid timber-glass beams presented in Chapters 4 and 5, respectively. The main aim of the research is to determine basic mechanical properties of adhesives: modulus of elasticity and Poisson's ratio to use the calculated values in numerical and analytical analyses.

3.4.1 Material properties

Structural adhesives are based on resins composition that polymerises to form a load-bearing joint characterized by high-modulus and high-strength features [56]. It is difficult to provide the characteristics of an adhesive based on only its composition, therefore the adhesives used in the research are briefly described.

All adhesives used in the research are dedicated for structural purposes. The main aim during selecting the adhesives was to ensure good adhesion to wood and glass and to cover the full range of stiffness from low (1-3 MPa) to high stiffness (>1000 MPa).

The selected adhesives were:
- the high-strength, two-component epoxy adhesive DP490 [57],
- the fast-curing, flexible two-component acrylate adhesive SikaFast 5215 [58],
- the high-strength, two-component structural silicone adhesive Sikasil SG-500 [59].

3M DP490 is a thixotropic, two-component epoxy adhesive designed for use where toughness and high strength are required [57]. The adhesive shows very good heat and environmental resistance and good adhesion to plastics, metals, glass and composite materials. The epoxy adhesive offers low shrinkage.

SikaFast 5215 is a fast-curing, flexible two-component acrylate adhesive with five minutes open time [58]. It is designed for structural bonding with very good adhesion parameters to a wide range of metals, plastics and glass. It cures by polymerisation. The acrylate adhesive offers also water resistance and durability.

Sikasil SG-500 is a high-strength, two-component structural silicone adhesive, designed for structural glazing and other high-demanding industrial applications [59]. It is UV- and weathering resistant and cures by polycondensation. The silicone adhesive offers also good flexibility and good resistance to high and low temperature.

Table 3.8 presents basic characteristics of the selected adhesives.

Table 3.8: Adhesive technical characteristics [57–59].

Adhesive	3M DP490	SikaFast 5215	Sikasil SG-500
Chemical base	two-component epoxy resin	two-component acrylic based adhesive	two-component silicone adhesive
Producer	3M	Sika	Sika
Curing conditions	ambient temperature	ambient temperature	ambient temperature
Cure mechanism	polymerisation	polymerisation	polycondensation
Open time (at 23degC)	240 min.	9 min.	90 min.

3.4.2 Laboratory tests

The dog-bone shaped specimens were prepared according to ISO 527-2:2012 [60] with respect to ISO 527-1:2012 [61]. The specimen for all adhesives was type 1A (Fig. 3.13). The dog-bone shape of the specimen ensures an uniform stress and strain distribution over the length of interests. The specimens had a prismatic form. To ensure more efficient grip of the ends the total length of the specimen was increased compared to the normalized value. The thickness for all specimens was approximately 4 mm.

All adhesives were supplied in pre-package containers equipped with static mixers which ensure the proper mixing of the components. The specimens were molded in multi-part casting molds, five specimens were produced in each batch. The adhesive was poured into five molds using a pneumatic gun. The molds were filled with sufficient overflow material by one continuous motion. Subsequently, excessive overfill of the wet

adhesive was removed with a spatula guaranteeing the flat upper surface and a thickness of approx. 4 mm. The specimens were stored under ambient laboratory conditions for 24 hours before unmolding and labeling.

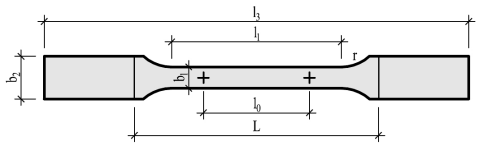

l_0= 50 mm
l_3= 200 mm
L= 115 mm
b_1= 20 mm
b_2= 10 mm
r= 25 mm

Figure 3.13: Standard ISO 527-2 tensile test specimen (type 1A) used in the tests [60].

For all specimens width, thickness and narrowing were measured with a micrometer. The area of the specimens was calculated with respect to the rectangular shape reduced by narrowing due to curing, which was measured additionally. Table 3.9 shows the average values for each adhesive.

Table 3.9: Mean values of dimensions of produced specimens.

Adhesive	Width [mm]	Thickness [mm]	Narrowing [mm]	Area [mm^2]
3M DP490	10.05	4.04	0.15	39.82
Standard dev.	0.02	0.04	0.04	0.52
SikaFast 5215	10.01	3.83	0.00	38.36
Standard dev.	0.03	0.06	-	0.51
Sikasil SG-500	9.98	3.93	0.00	39.26
Standard dev.	0.03	0.04	-	0.45

Cyclic test

The specimens were tested after 7 days of storing under ambient laboratory conditions. The specimens were mounted and loaded in uniaxial testing machine MTS 810 (Fig. 3.14) running in displacement control. Three displacement rates were applied: 1, 5, 50 mm/min (cross-head deformation). The single-axis extensometer was used to measure the strain in the specimens in the longitudinal direction. The base length of the extensometer was 50 mm with a maximum elongation of 4.5 mm. The load was measured with a 1 kN MTS load cell. All data values were sampled and collected by the MTS's computer and then transferred to a PC.

To monitor the strain distribution on the surface of the specimens in order to determine the Poisson's ratio, the optical, non-contact 3D deformation measurement system Aramis was used [62]. The method provides complete, 3D, real-time surface displacement and strain results for multiple measuring positions from the test object surface. ARAMIS recognizes the surface structure of the measuring object at digital camera images and

allocated coordinates to the image pixels. The first picture of the specimen represents the undeformed state of the specimen. During the deformation of the specimen, further images are recorded. Subsequently, ARAMIS compares the images and calculates the displacement and deformation of the object. Then, based on the deformation field the software derives the strain field. ARAMIS replaces the traditional measuring devices (strain gauges, LVDTs extensometers, etc.) especially for experiments where a large number of measuring points is required. It can be also helpful during verification of FEM analyses.

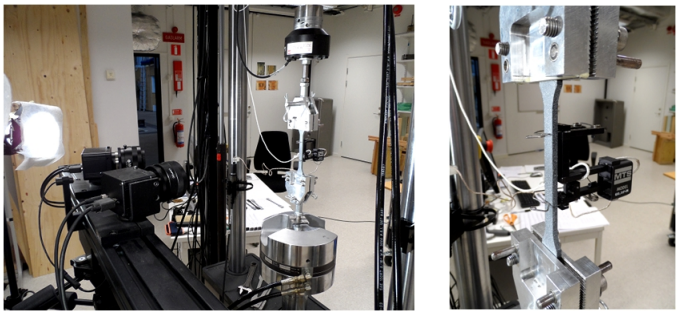

Figure 3.14: Test set-up.

To evaluate the stress-strain relationship based on tension test standard formulas were used to obtain nominal (engineering) stress and strain:

$$\sigma_{axial} = \frac{P}{A_0} \tag{3.8}$$

$$\varepsilon_{axial} = \frac{\Delta l}{l_0}, \tag{3.9}$$

where P and Δl are the applied load and the axial elongation during the test, A_0 the nominal cross-section area, l_0 the extensometer gauge length.

Since Aramis system was planned to be used in the tests, one side of all specimens was painted so that a random pattern was produced. Black and white spray matt paint was used. First a white base layer and next the black paint was applied. To obtain good quality of results special care must have been taken to obtain high-contrast stochastic pattern.

Table 3.10 shows test routines for determination of basic mechanical properties at different load rates to investigate time-depended behaviour of selected adhesives. To determine Young's modulus and Poisson's ratio the specimens were loaded in displacement control to a certain level, then unloaded and reloaded above the previous value.

Table 3.10: Details of test procedures.

Adhesive	Load rate [mm/min]	Load/unload level
3M DP490	1, 5, 50	980 N / 300 N
SikaFast 5215	1, 5, 50	8 mm / 10N
Sikasil SG-500	1, 5, 50	10 mm / 1 N

Monotonic test
Testing was performed in accordance to PN ISO 527-1:2012 [61] with respect to PN ISO 527-2:2012 [60]. For the research available 7-months old specimens, stored under ambient laboratory conditions, were used. After 7 months of storing some ageing process might have occurred therefore the main aim of the test was only to load the specimens up to the maximum piston elongation, which was 160 mm and try to bring the specimens to failure. The main aim of the monotonic test is to get a picture of the behaviour of the adhesives when specifying material models. The specimens were mounted into an uniaxial testing machine, MTS 810, with steel grips. The initial length between grips was 115 mm. The tests were conducted under ambient laboratory conditions of $23\pm1^{\circ}$ and $50\pm5\%$ relative humidity. The loading was run with displacement control with the loading rate of 5 mm/min governed by the piston movement. Therefore, the resulting plots are built as force-elongation curves (based on the piston movement).

Relaxation test
The main aim of the relaxation test is to determine an infinite modulus of elasticity when all relaxation process is finished. The test was performed on epoxy and acrylate adhesives since the adhesives present viscoelastic behaviour, what reveals in the dependence of the behaviour of loading rate.

The tests were conducted under ambient laboratory conditions, at $23\pm1^{\circ}$ and $50\pm5\%$ relative humidity. To investigate relaxation behaviour and identify the instantaneous E_{inst} and infinite Young's modulus E_{∞} the specimens were loaded to a certain loads at a load rate of 100 mm/min. Deformation was then held constant for at least 1000 s. The changes of load were monitored. Since the deformation is constant after loading the specimens to a certain load level the instantaneous modulus of elasticity E_{inst} decreases with decreasing load (stress) due to relaxation. The modulus of elasticity stabilizes at a certain level which is defined as the infinite modulus of elasticity E_{∞}. Table 3.11 shows test routines for the relaxation test for the adhesives.

Table 3.11: Details of relaxation test on selected adhesives.

Adhesive	Load levels [N]
Epoxy	250, 500, 750
Acrylate	30, 60, 90

3.4.3 Results and discussion

Cyclic test

Figures 3.15÷3.16 present tensile stress-strain curves for all specimens tested under cyclic loading at different load rates. Values of stress and strain are based on undeformed geometry (see formulas 3.8 and 3.9). Since the main aim of the tests was to determine modulus of elasticity the specimens were not loaded up to failure.

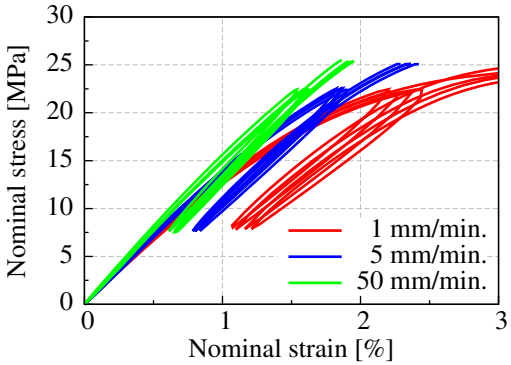

Figure 3.15: Stress-strain curves for 3M DP490 at different load rates.

The epoxy specimens (Fig. 3.15) presented homogeneous stress-strain curves. Very good repeatability of results was observed. After unloading the curves did not return the same path. However, at a higher loading rate this phenomenon was less pronounced. It can be explained by the adhesive viscoelasticity; at higher load rates the material has simply no time to relax.

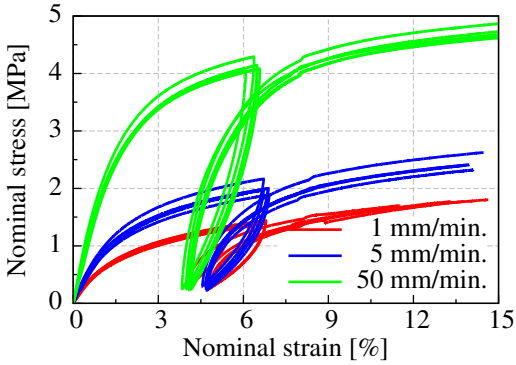

Figure 3.16: Stress-strain curves for SikaFast 5215 at different load rates.

Compared to the epoxy, the acrylate specimens (Fig. 3.16) presented similar behaviour, however, the repeatability of results is not equally good. There may be several reasons

but the most probable is related to manufacturing process and very short open time of the acrylate adhesive which is only 5 minutes. After filling the molds, which takes usually couple of minutes, the overflow material was removed by a spatula. During the process some hardening might have started influencing the results. After unloading the curves did not return along the same path, which is even more pronounced then the behaviour showed by the epoxy specimens.

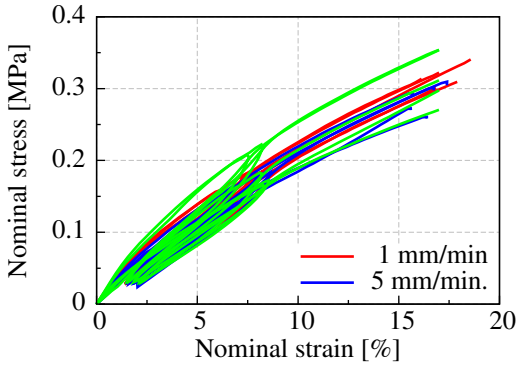

Figure 3.17: Stress-strain curves for SikaSil SG-500 at different load rates.

The lowest influence of loading rate on strain-stress curves and relatively low stress in specimens were observed for the silicone adhesive (Fig. 3.17). Due to 1 kN load cell used in experiments considerable dispersion of results was obtained.

Viscoelastic properties of epoxy and acrylate adhesives are clearly pronounced. However, the phenomenon was not observed in case of silicone specimens.

Based on stress-strain relationship curves (Fig. 3.15 ÷ 3.17) the values of the modulus of elasticity for all tested specimens were evaluated. MOE was calculated based on the slope of a secant line between 0.05% and 0.1% strain on a stress-strain plot. Due to the limitations of measuring devices smaller values of strain were not possible to be recorded.

The following formula was used to calculate MOE:

$$MOE = \frac{\Delta\sigma_{axial}}{\Delta\varepsilon_{axial}} \tag{3.10}$$

where $\Delta\sigma_{axial}$ and $\Delta\varepsilon_{axial}$ are the increments of the axial stress and strain, respectively. Table 3.12 summarizes the results for MOE for the adhesives.

Table 3.12: Values of MOE [MPa] of tested specimens at different load rates.

Adhesive	Load rate [mm/min]		
	1	5	50
3M DP490	1595	1664	1750
Standard dev.	45	135	50
SikaFast 5215	78.12	140.97	284.12
Standard dev.	3.67	4.59	25.10
Sikasil SG-500	3.17	2.86	2.34
Standard dev.	1.59	0.76	0.64

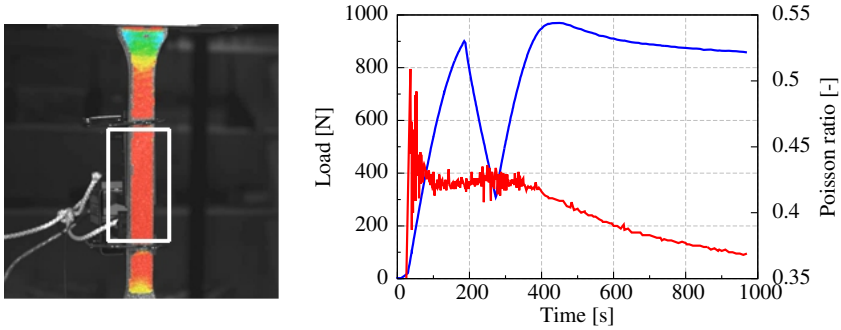

Figure 3.18: Strain map (left) and load (Poisson's ratio)-time plot obtained from Aramis system.

To evaluate Poisson's ratio ν the strains results from the non-contact optical 3D deformation measurement system were used. The values of strains (parallel and across the specimen) in the central part between clamps of the extensometer (white box in Fig. 3.18) were averaged and values of Poisson's ratio were calculated by dividing axial strain by lateral strain, according to:

$$\nu = -\frac{\epsilon_{axial}}{\epsilon_{lateral}} \tag{3.11}$$

Figure 3.18 presents comparison between load-time and calculated Poisson's ratio-time curves for a selected specimen. The values of Poisson's ratio at the beginning of loading are unstable due to the initial movement of a specimen (in the initial phase the specimen is slightly bent). Then the values stabilise and decrease when the material is in the plastic domain. Table 3.13 summarizes the values of the Poisson's ratio for all adhesives.

Table 3.13: Mean values of Poisson's ratio of tested specimens at different load rates.

Adhesive	Load rate [mm/min]		
	1	5	50
3M DP490	0.422	0.414	0.401
Standard dev.	0.003	0.017	0.011
SikaFast 5215	0.459	0.458	0.451
Standard dev.	0.008	0.006	0.004
Sikasil SG-500	0.462	0.462	0.470
Standard dev.	0.001	0.010	0.006

Monotonic test

Figures 3.19÷3.21 present tensile stress-strain curves for all specimens tested under monotonic loading at load rates of 5 mm/min. The epoxy adhesive presented elastic, almost linear behaviour until failure. The failure occurred at the nominal value of load of 1416 N and ultimate elongation of 0.032 mm/mm. The acrylate adhesive demonstrated clear bi-linear behaviour, however, the ultimate load was not reached. Alike the acrylate adhesive the silicone sealant presented elastic almost linear behaviour and the ultimate load was not reached.

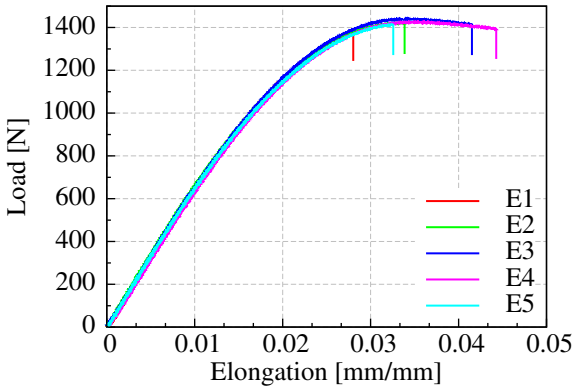

Figure 3.19: Load-specimen's elongation (based on the piston movement) for 3M DP490 (epoxy) at 5mm/min.

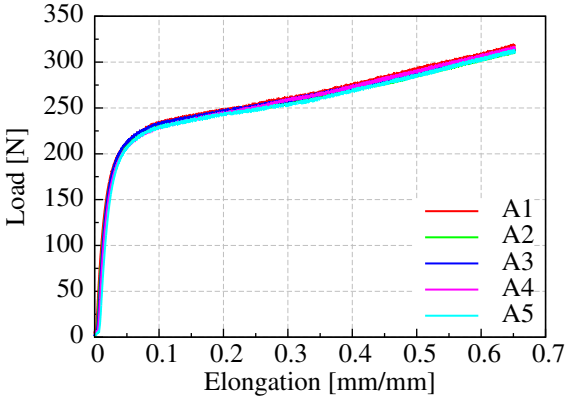

Figure 3.20: Load-specimen's elongation (based on the piston movement) for SikaFat 5215 (acrylate) at 5mm/min.

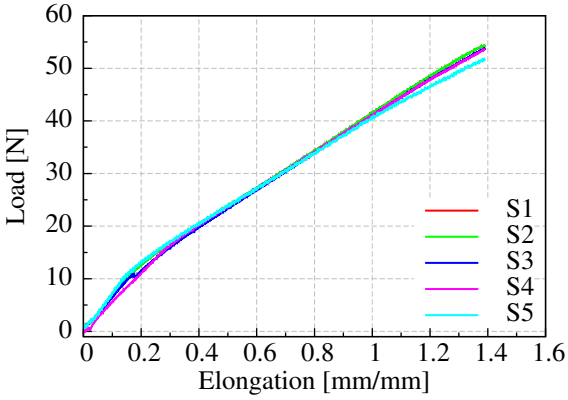

Figure 3.21: Load-specimen's elongation (based on the piston movement) for SikaSil SG500 (silicone) at 5mm/min.

Table 3.14 summarizes tensile test results for the epoxy adhesive since the adhesive was the only one which failed during testing. The table includes the tensile ultimate load $F_{t,u}$ and tensile ultimate strain $\varepsilon_{t,u}$. The failure of the epoxy adhesive occurred far beyond the range of the extensometer hence the values ($F_{t,u}$ and $\varepsilon_{t,u}$) were calculated based on the piston movement.

Table 3.14: Results of monothonic test on selected adhesives.

Specimen	$F_{t,u}$ [N]	$\varepsilon_{t,u}$ [−]
3M DP490	1416.1	0.032
Standard dev.	18.8	0.003

Relaxation test

Figures 3.22 and 3.23 present the results of the relaxation test for the acrylate end epoxy adhesives. Both adhesives show highly viscoelastic behaviour, after 1000 s a significant decrease of the modulus of elasticity was observed. However, the phenomenon was more pronounced for the acrylate adhesive.

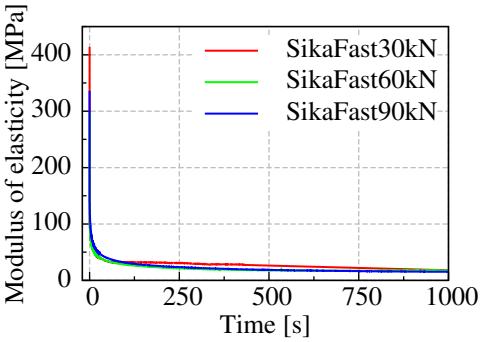

Figure 3.22: Results of relaxation test for acrylate adhesive.

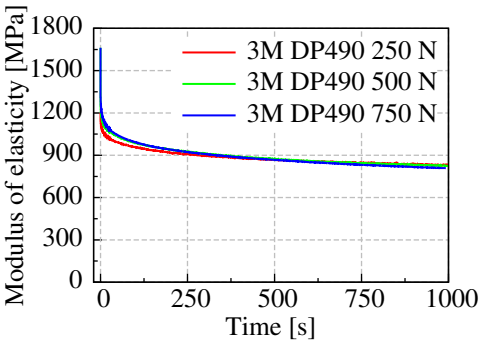

Figure 3.23: Results of relaxation test for epoxy adhesive.

For the acrylate and epoxy adhesive the ratio between the infinite modulus of elasticity E_∞ and the instantaneous modulus of elasticity E_{inst} was equal to 0.05 and 0.49, respectively. For the acrylate and epoxy adhesive the ratio between the infinite modulus of elasticity E_∞ and the the modulus of elasticity determined in the cyclic test was equal to 0.53 and 0.22, respectively. Comparing the results of the relaxation test to the results of the cyclic test it can be concluded that the load rate of 1 mm/min is still too high to determine the modulus of elasticity which is at least close to the infinite modulus of elasticity E_∞. Further relaxation tests on adhesives are necessary.

Table 3.15: Results of relaxation test on selected adhesives.

Specimen	E_{inst} [MPa]	E_∞ [MPa]	E_∞/E_{inst} [MPa]	$E_\infty/E_{1mm/min}$ [MPa]
3M DP490	1698	840	0.49	0.53
Standard dev.	57	34		
SikaFast 5215	349	17.02	0.05	0.22
Standard dev.	50	0.97		

4 Experimental investigations on small-size specimens

This chapter deals with testing of small-size beam specimens. It provides information regarding test specimens, test set-up and test procedures. It presents results, discussion and conclusions.

4.1 Background information

The experimental investigations presented in this chapter were conducted in the laboratory of the Faculty of Civil Engineering at the Silesian University of Technology (Gliwice, Poland). Materials for the research were supplied by Sika Poland and Zakład Szklarski S.C. Leś. The contribution regarding technical support and assistance of the following people is acknowledged: Władysław Marchacz, Tomasz Hahn, Karol Konopka (Silesian University of Technology), Michał Pieroń, Rafał Siwek (Sika Poland). The contribution is gratefully acknowledged.

4.2 Introduction

To investigate the influence of stiffness of bond connection on behaviour under loading, stiffness and load-bearing capacity of small-size hybrid timber glass beams a series of beam specimens were investigated. Three hybrid beams with a web made of ordinary annealed float glass and timber flanges, bonded with three types of adhesives of different stiffness were tested in four-point bending.

4.3 Test specimens and test set-up

Figure 4.1 presents a cross-section of the beam specimens. The cross-section consists of a glass web and timber flanges combined together with a bond line adhesive connection. All specimens were 300 mm high and 1800 mm long. The glass for all webs was made of annealed float glass according to European standard PN-EN-572 [50]. All webs had

dimensions of 200 × 1800 mm with a thickness of 8 mm. To minimize the influence of edge quality on the glass strength, widely described in [63], after the traditional cutting to desired dimensions all edges were polished. For the wooden flanges finger jointed pine studs were used. All flanges were 1800 mm long with a rectangular cross-section of 55 × 75 mm. Since the glass web was planned to be bonded to the flanges, 30 mm deep machined grooves were milled in the studs. Three different groove widths were used: 12, 13 and 15 mm. The width of the grooves depended on the adhesives used. After consultation with technical advisors, which were representatives of manufacturers, optimum values of the thickness of bond line connection were chosen. The values ranged from 2.0 to 3.5 mm (on both sides of the web). For the adhesive bonding three different types of adhesives of different stiffness were used: Sikasil SG-500 (silicone), SikaFast 5215 (acrylate) and Icosit KC 640/7 (polyurethane). Icosit KC 640/7 is a pourable, two-component flexible polymer grout based on polyurethane resin [64]. The resin is designed as flexible, vibration absorbing grout usually used for load-bearing undersealing layers of rails and turnouts but increasingly for mounting free standing glass balustrades.

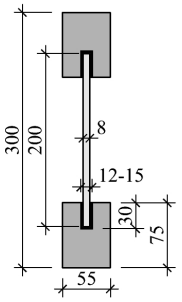

Number of specimens	9
Glass web	200 × 1800 mm
Timber flanges	55 × 75 mm
Groove width	(12-15) × 30 mm
Beam height	300 mm
Beam length	1800 mm

Figure 4.1: Cross-sections of the beam specimens; nominal dimensions.

All specimens were manufactured manually in a custom-made steel frame. After filling the groove with adhesive the glass pane was placed in the groove. The overflow of adhesive was removed with a spatula. To ensure the same bond line thickness on both sides of the web wooden sticks were used. When the adhesives cured, the sticks were removed and remaining holes were filled with adhesive. Next, the half-beam was reversed and the same procedure was conducted. In total, nine hybrid beam specimens were produced. Table 4.1 presents the notation system of the produced specimens and thickness of the bond line connection.

Table 4.1: Notation system for the beams and thickness of bond connections.

Beam type	Adhesive	Groove width [mm]	Bond line thickness [mm]
BA1, BA2	Acrylate	12.0	2.0
BA3		13.0	2.5
BS1	Silicone	13.0	2.5
BS2, BS3		15.0	3.5
BI1, BI2	Polyurethane	13.0	2.5
BI3		15.0	3.5

The test set-up was a four-point bending test presented in Figure 4.2. Theoretical distance between the supports was 1500 mm. Forces were introduced symmetrically at 1/3 of the span (500 mm) through a cross head steel beam. Due to high slenderness of the specimen two additional lateral supports were provided at the ends to protect the beam against sloping out of the plane.

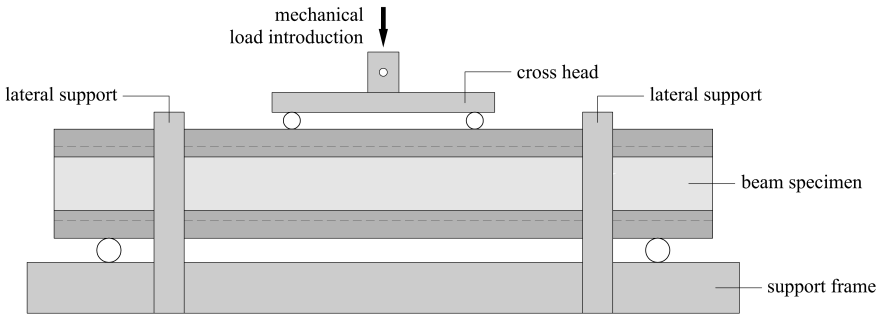

Figure 4.2: Scheme of test set-up used for four-point bending test on small-size beam specimens.

The tests were performed in a hydraulic testing machine. The beams were loaded at constant vertical displacement rate of 2 mm/min until failure. To read the response of the beam to loading a number of detectors were applied to the specimens. To measure deformations six inductive displacement sensors were installed at the mid-span, load introduction points, supports and at half-height of the glass web. To measure the strain distribution in components a set of strain gauges was attached to the substrates.

4.4 Results and discussion

Figure 4.3 illustrates force versus mid-span displacement curves for all tested beams. The beams bonded with acrylate, silicone and polyurethane adhesives presented different initial stiffness, load-bearing capacity and deformations at failure [65, 66]. For most beams, the load at which initial crack formed was much lower than the failure load.

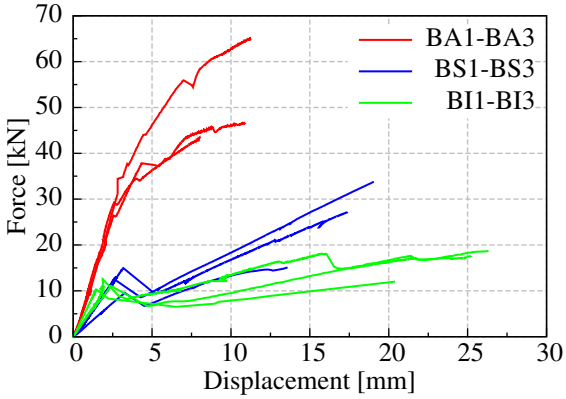

Figure 4.3: Force versus mid-span displacement curves for tested beams.

The beams bonded with acrylate adhesive (BA1÷3) demonstrated almost perfectly linear elastic response until initial glass failure. It was followed by a sudden drop of bending stiffness and an increase of vertical displacement. Multiple cracks occurred in the glass, usually located under the load introduction points. Outside the maximum bending moment zone (outside the load introduction points) typical diagonal shear cracks occurred. Ultimate failure of the beams was usually caused by failure of the flange working in tension, see Figure 4.4.

The beams bonded with silicone adhesive (BS1÷3) demonstrated almost perfectly linear elastic response until initial glass failure. Compared to beams with acrylate adhesive, the initial stiffness and the load at initial glass failure was much lower and the drop of bending stiffness and increase of vertical displacement was more pronounced. No diagonal shear cracks occurred. The beams with silicone adhesives presented also much lower load-bearing capacity and larger ultimate deformation. The initial crack usually occurred in the mid-span of the beam and was much bigger as compared to the beams with acrylate adhesive, see Figure 4.5. Ultimate failure of the beams BS1-BS3 was usually caused by explosion of the compressive zone of the glass web and failure of the flange working in tension.

The beams bonded with polyurethane adhesive (BI1÷3) demonstrated almost perfectly linear elastic response until initial glass failure. Alike the beams with silicone adhesive, the beams presented much lower initial stiffness as compared to the beam with acrylate

adhesive. Only one crack occurred during testing. The crack was formed along all hight of the glass web. After this phase increase of vertical deformation with slight increase of force was observed. Ultimate failure of the beams BI1-BI3 was caused by the failure of both flanges.

Figure 4.4 present selected frames from a video of the four-point bending test of the beam BA2. It presents initial failure (first crack) of the glass web under the load introduction point, second crack formed symmetrically to the first one, successive failure of the glass web and ultimate failure of the beam (failure of the flange working in tension).

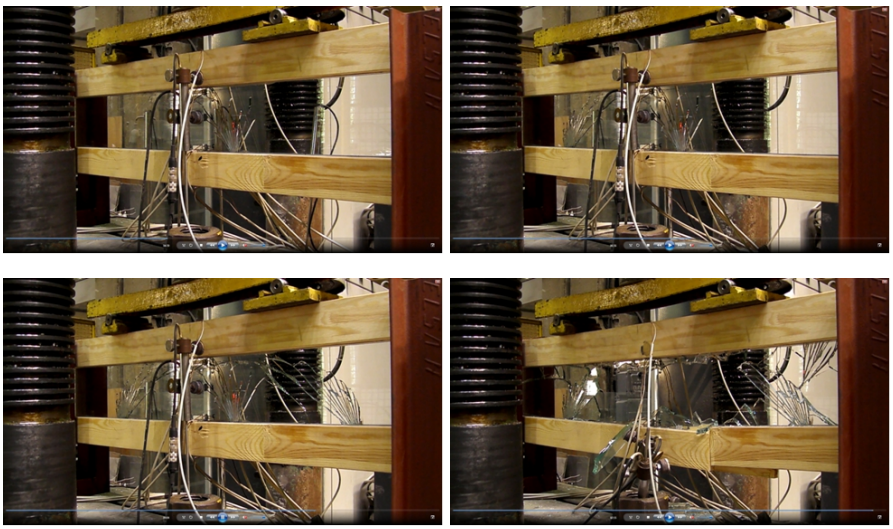

Figure 4.4: Selected frames from four-point bending test of specimen BA2.

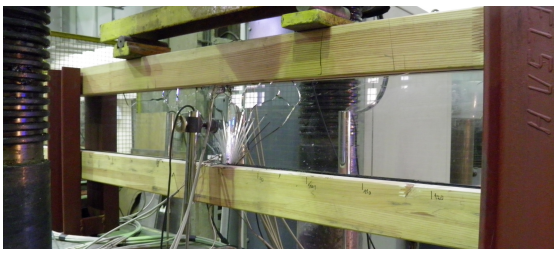

Figure 4.5: Failure of glass web of specimen BS1 in four-point bending test.

Figures 4.6÷4.8 present load-deformation diagrams and sequential set of sketches showing the crack pattern development during testing for selected specimens. A black cross-mark indicates the places where the flange failed.

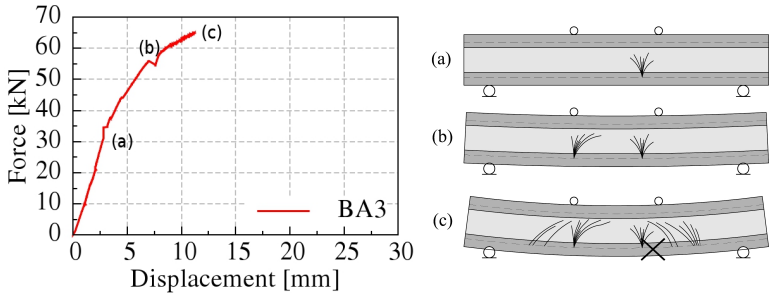

Figure 4.6: Bending test results for selected small-scale beam specimens with acrylate adhesive.

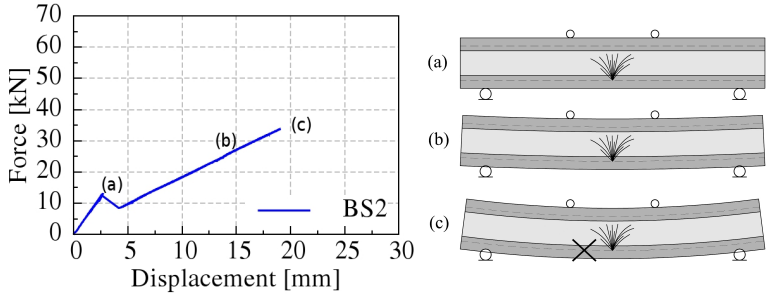

Figure 4.7: Bending test results for selected small-scale beam specimens with silicone adhesive.

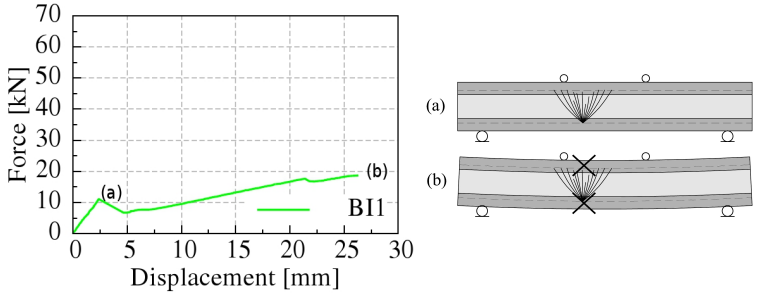

Figure 4.8: Bending test results for selected small-scale beam specimens with adhesive based on polyurethane.

Table 4.2: Test results, beams made of annealed float glass.

Beam type	Load at first crack [kN]	Maximal load [kN]	Increase of load [%]
BA1	26.4	66.2	150
BA2	29.3	43.6	50
BA3	26.4	46.7	75
Mean values	27.4	52.2	91.7
Standard deviation	1.37	10.0	42.5
BS1	12.7	25.1	100
BS2	12.6	34.1	170
BS3	9.6	15.1	60
Mean values	11.6	24.8	110
Standard deviation	1.4	7.8	45.5
BI1	11.1	18.7	65
BI2	12.5	18.1	45
BI3	10.3	12.0	20
Mean values	11.3	16.3	43.3
Standard deviation	0.9	3.0	18.4

Table 4.3: Values of failure stress in glass for all tested beams.

Specimen	Failure stress [MPa]
BA1	49.38
BA2	44.99
BA3	54.09
BS1	44.64
BS2	51.20
BS3	45.81
BI1	46.20
BI2	45.81
BI3	58.67
Mean value	48.92
Standard deviation	4.61

Table 4.2 presents the loads at initial cracking, ultimate load and increase of value of the load for all tested beams. The increase of the load is referred to the load when first crack in glass web occurs. The highest load-bearing capacity, with respect to the initial crack, was achieved by the beams BA1-3 bonded with acrylate adhesive. The average value of the load at first crack was 27.4 kN and the maximal load 52.2 kN. This corresponds to the post-breakage strength of 192%. The beams BS1-3 and BI1-2 bonded with silicone and polyurethane adhesives showed almost 50% lower load-bearing capacity,

the average value of the load at first crack was 11.6 kN and 11.3 kN respectively. In contrast to the beams BS1-3, which showed almost the same value of the increase of load after first cracking of glass as the beams BA1-3, the maximal load for the beams BI1-3 increased by only 43%.

Since strain gauges were mounted to the glass web, the strain level at failure of the glass could have been obtained. From these strains the maximum strains over the cross section could have been extrapolated and the corresponding stresses in the glass could have been calculated. Table 4.3 presents mean values of failure stress in glass for all tested beams. For all beams the average failure stress was approximately 49 MPa calculated using modulus of elasticity of glass 70 GPa (determined in the four-point bending test, see Chapter 3). The value corresponds to the average failure stress of annealed float glass 45 MPa (tested in a standing position) reported in [51].

Table 4.4 presents the initial bending stiffness obtained during loading calculated from global deflection. The beams bonded with acrylate adhesive presented the highest bending stiffness. The beams bonded with silicone and polymer grout based on polyurethane resin showed approximately 60% lower stiffness. The values of stiffness for the beams BI1-3 are unreliable since great scatter of results was observed. The polymer grout based on polyurethane resin, in contrast to the other two adhesives, was prepared and mixed manually, which probably resulted in a variety of mechanical properties. Therefore, the beams were excluded from further analyses.

Table 4.4: Values of initial bending stiffness for all tested beams.

Specimen	Initial bending stiffness [MNm^2]
BA1	0.692
BA2	0.623
BA3	0.632
Mean values	0.649
Standard deviation	0.030
BS1	0.292
BS2	0.289
BS3	0.178
Mean values	0.253
Standard deviation	0.053
BI1	0.270
BI2	0.430
BI3	0.314
Mean values	0.338
Standard deviation	0.067

4.5 Evaluation

The section presents the results of experimental investigation on small-size hybrid I-shaped beams made of ordinary annealed glass and timber flanges, bonded with three types of adhesives of different stiffness. Based on a qualitative research with a limited number of specimens main conclusions are drawn.

Experimental studies on hybrid timber-glass beams show that the beams are able to withstand much higher load than the load that causes initial failure of a glass web. The post-breakage strength relates to an increased value of a load at a total collapse of a beam in relation to the load at which first crack in the web occurs. The combination of a single pane web, made of ordinary annealed float glass, and timber flanges provides ductility and a warning signal relatively long before the total collapse. It gives time to temporarily support the element before the replacement and ensures the safety of users.

The results obtained from experiments of hybrid timber-glass beams compared with testing of timber flanges and pure glass beams, presented in Chapter 3, prove the synergistic feature of the hybrid beams. The maximal load obtained by beams bonded with acrylate adhesive is much higher than a sum of maximum loads taken by two timber flanges and a glass beam. In case of hybrid timber-glass beams the timber provides the ductility and the glass resistance and stiffness. Regarding hybrid beams bonded with silicone sealant and polymer based on polyurethane resin the synergistic feature was not observed. However, these beams allowed for much greater deformations before the total collapse.

Regarding the initial stiffness, post-breakage residual strength and maximal load hybrid beams bonded with stiff adhesive presented much better behaviour than corresponding beams bonded with softer adhesives. Beams BA1÷3, bonded with acrylate adhesive, were much stiffer in the elastic phase and reached almost double load before total failure (high post-breakage, relatively low ductility ratio). However, beams BS1÷3, bonded with silicone sealant, although characterised with lower stiffness and post-breakage strength, allowed for much greater deformations (high ductility ratio, relatively low post-breakage strength). The average value of post-breakage strength for the beams with acrylate, silicone and polyurethane adhesive was 192, 210 and 143%, respectively.

The results for the beams bonded with polymer grout based on polyurethane resin (BI1÷3) are unreliable since great spread of behaviour was observed. Additionally, applied Icosit KC 640/7 resin, in contrast to the other two adhesives, was prepared and mixed manually, which probably resulted in a variability of mechanical properties. Therefore, the resin was excluded from further analysis and it is not recommended for hybrid timber-glass beam purposes.

5 Experimental investigations on life-size specimens

This chapter deals with testing of life-size beam specimens. It provides information regarding test specimens, test set-up and test procedures. It presents results, discussion and conclusions.

5.1 Background information

The experimental research on life-size specimens was made within the WoodWisdom-Net research project "LBTGC - Load bearing timber-glass composites". The experimental investigations presented in this chapter were conducted in the laboratory of the Department of Building and Energy Technology at the Linnaeus University (Växjö, Sweden). Materials for the research were supplied Pilkington Floatglas AB, Stora Enso Timber AB and Sika Sverige AB. The contribution regarding technical support and assistance of Bertil Enquist and Michael Dorn (Linnaeus University) is acknowledged.

5.2 Introduction

To investigate the influence of stiffness of bond connection and type of glass on the behaviour under loading, stiffness and load-bearing capacity of life-size hybrid timber glass beams a series of beam specimens were investigated.

Twelve hybrid beams with web made of ordinary annealed float and heat-strengthened glass and timber flanges, bonded with three types of adhesives of different stiffness were tested in four-point bending. The results of experimental investigations on small-scale hybrid beams showed that the beams with stiff adhesive presented the best performance. Therefore, regarding life-size specimens with web made of annealed float glass a stiff adhesive was selected. The reason of use of the heat-strengthened glass was its higher bending strength caused by residual stress introduced in tempering process. However, this type of glass presents intermediate fracture pattern between annealed float glass, which breaks into big shards, and fully-tempered glass, which disintegrates in small

pieces after failure. For the beams with web made of heat-strengthened glass three different adhesives were applied.

5.3 Test specimens and test set-up

Figure 5.1 presents a cross-section of the beam specimens. The cross-section consists of a glass web and timber flanges combined together with a bond line adhesive connection.

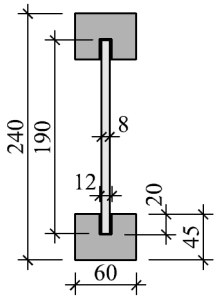

Number of specimens	12
Glass web	190 × 4800 mm
Timber flanges	45 × 60 mm
Groove width	12 × 20 mm
Beam height	240 mm
Beam length	4800 mm

Figure 5.1: Cross-sections of the beam specimens; nominal dimensions.

All beams were 240 mm high and 4800 mm long. For the webs two types of glass were used: annealed float and heat heat-strengthened glass. In comparison to annealed float glass, which breaks into large pieces, the fracture pattern of heat-strengthened glass is more like for tempered glass. All webs had dimensions of 190 × 4800 mm with a thickness of 8 mm. To minimize the influence of edge quality on the glass strength, widely described in [63], after the traditional cutting to desired dimensions all edges were polished. The polishing of the edges of glass webs had to be done before the tempering process since any treatment of heat-strengthened glass leads to brittle and rapid failure [45]. For the wooden flanges finger-jointed pine studs measuring 45 × 60 mm were used. The dynamic elastic modulus along the fibres of timber flanges was 12.4 GPa, which was determined based on the lowest natural frequency in axial excitation of the timber flanges reported in Section 3.3. In order to fit the glass web, a groove measuring 12 × 20 mm was milled in the flanges. Thus, the bond line thickness for all beams was 2 mm (on both sides of the glass web). For the adhesive bonding three different types of adhesives of different stiffness were used: 3M DP490 (epoxy) [57], SikaFast 5221 (acrylate) [58] and Sikasil SG-500 (silicone) [59].

All specimens were manufactured manually in a custom-made stabilising steel frame consisting of a stiff I-shaped steel section and seven lateral supports mounted at every 800 mm along the steel base. Each support was adjustable by a screw point support with a rubber disc at its end to protect the glass surface when mounting. First, the glass web was mounted in the lateral supports 50 mm above the steel base and cleaned

with alcohol. A masking tape was used to protect the glass surface from the adhesive which flows out of the groove when lowering the web. All adhesives were supplied in pre-package containers and were applied using static mixers compatible with the nozzles of the containers in order to ensure the proper dosage and mixing of the components. Before applying the adhesive, the flange, alike the web, was protected with a masking tape. The adhesive was poured into the groove using a pneumatic gun and the wet adhesive was spread with a spatula. Subsequently, the flange was placed below the web, which was then lowered and placed into the groove and stabilised. At this stage accuracy was crucial and thus, before fixing the web in the lateral supports, the height of the half-beam was measured with high precision. To ensure a uniform adhesive bond line thickness, rubber strips were used.

Subsequently, the excess amount of the wet adhesive was removed with a spatula, alike the masking tape. After mounting the web in the supports it was impossible to remove the rubber strips without tearing them off so they were shortened and left in the groove. The stabilised specimens were left until the adhesive cured. In contrast to the acrylate adhesive, which curing time was approximately 10 minutes, the specimens with silicone and epoxy adhesives were left for 12 hours before the other flange was bonded to the glass web.

Table 5.1: Notation system, number and components of manufactured specimens.

Glass type	Adhesive	Number of specimen
Annealed float glass (AF)	3M DP490 (E)	6
Heat-strengthened glass (HS)	Sikasil SG-500 (S)	2
	SikaFast 5221 (A)	2
	3M DP490 (E)	2

In total, twelve hybrid timber-glass beams with three adhesives of different stiffness and two types of glass were manufactured. Table 5.1 presents the notation system, number and components of manufactured specimens. The notation system for specimens is constructed as follows: adhesive type-glass type-specimen number.

To monitor strain in the components strain gauges were used. Two beams with annealed glass and all beams with heat-strengthened glass were equipped with the strain gauges. These were mounted at mid-span, on the tensile and compression side of the glass web and two gauges on the flange working in tension (on upper and lower side).

Before testing of the beams with heat-strengthened glass, the residual-stress profile through the thickness of the glass panels was measured using a portable scattered light polariscope SCALP [48]. The test revealed average value of residual surface compressive stress 53 MPa and middle tensile stress 25 MPa, see Section 3.4.

The test set-up was a four-point bending test (Fig. 5.2). The nominal distance between the supports was 4320 mm while the total beam length was 4800 mm. The forces were

introduced symmetrically at 1/3 of the span (1440 mm) through hydraulic jacks fixed to vertical steel frames. The tests were run in displacement control at load rate of 12 mm/min. Two lateral supports were provided approximately 300 mm from the load introduction points to prevent the beam from failing in lateral buckling. Apart from measuring the loads and the mid span displacement v_{global}, the curvature over a length of 1200 mm between the two loads was also measured, see v_{local} (Fig. 5.2).

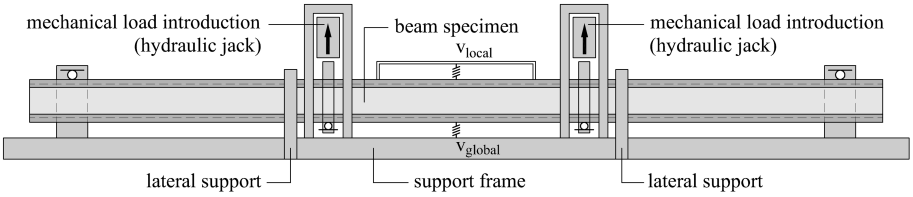

Figure 5.2: Scheme of test set-up used for four-point bending test on small-size beam specimens.

5.4 Results and discussion

Figure 5.3 illustrates force versus mid-span displacement curves of all beams. The specimens with the web made of annealed float glass and epoxy adhesive presented a multi-stage mechanism of failure during loading [67–69]. In the first stage the relationship between the load and vertical mid-span displacement is almost perfectly linear until initial cracking. This is followed by a sudden drop of bending stiffness and an increase of vertical displacement, see Figure 5.3.

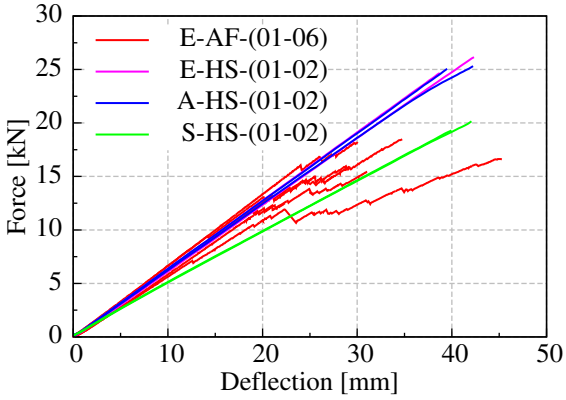

Figure 5.3: Load-displacements for testes beams.

After the initial failure of the annealed float glass the bottom flange acted as a crack bridge which together with a non-cracked compression zone of the web and top flange allowed the beam to still carry the load. In the next stage the existing crack grow and subsequent cracks formed in another part of the web. Multiple cracks occurred in the glass, usually located between the load introduction points. Despite the failure of the glass web the beam could still carry load until the final collapse, which was usually caused by failure of the flange working in tension. Figure 5.4 presents the mechanism of failure of hybrid timber-glass beam with a web made of annealed float glass.

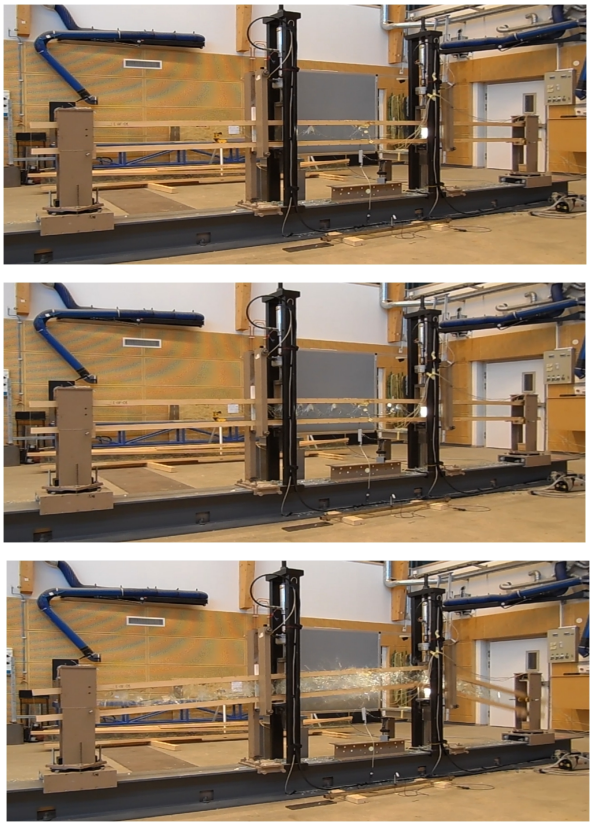

Figure 5.4: Four-point bending test of life-size hybrid beams with web made of annealed float glass.

The beams with webs made of heat-strengthened glass presented higher load at initial cracking than the beams with webs made of annealed float glass. However, the failure was brittle with no warning, see Figure 5.5. Thus no post-breakage strength was presented. It is unclear whether the failure was caused by explosion of the glass with high residual stress or tensile failure of the timber flanges.

Figure 5.5: Four-point bending test of life-size hybrid beam with web made of heat-strengthened glass.

Table 5.2 presents the values of loads at first cracking and ultimate load for the tested beams. For the beams with annealed float glass these loads were 11.6 kN and 16.4 kN, respectively. This corresponds approximately to a 50% increase of the load after the first crack, and the beams can be said to fail in a rather ductile manner.

The specimens with webs made of heat-strengthened glass withstood approximately 100% higher load than the beams with annealed float glass but showed no post-breakage strength. Although the stiffness of the specimens bonded with the soft silicone adhesive was lower than that of beams made with a stiff adhesive, the failure occurred at the same displacement of approximately 40 mm.

Table 5.3 presents the comparison of the stiffness obtained during loading: calculated from global and local deflection. The stiffness calculated from local deflection was approximately 6% higher in comparison to the stiffness calculated from global deflection. The difference can be explained by the fact that global stiffness was measured from global deformation which is a combination of bending and shear deflection [70]. In this case bending deflection represents the main part, the shear deflection gives a contribution to the total deflection. Unlike global deformation, local deformation represents only a pure bending deflection. The stiffness of beams with silicone adhesive was approximately 25% lower as compared to the beams bonded with stiffer adhesives.

Table 5.2: Test results, beams made of annealed float glass.

Beam type	Load at first crack [kN]	Maximal load [kN]	Increase of load [%]
E-AF-01	9.4	19.5	107.5
E-AF-02	7.1	16.6	133.8
E-AF-03	12.0	15.5	29.2
E-AF-04	13.2	15.8	19.7
E-AF-05	11.9	12.5	5.0
E-AF-06	16.0	18.2	13.8
Mean values	11.6	16.4	50.0
Standard deviation	2.81	2.2	-
E-HS-01	26.2	26.2	-
E-HS-02	24.7	24.7	-
Mean values	25.5	25.5	-
A-HS-01	25.1	25.1	-
A-HS-02	25.2	25.2	-
Mean values	25.2	25.2	-
S-HS-01	20.2	20.2	-
S-HS-02	19.3	19.3	-
Mean values	19.8	19.8	-

Since strain gauges were mounted to the glass web, the strain level at failure of the glass could have been obtained. From these strains the maximum strains over the cross section could have been extrapolated and the corresponding stresses in the glass could have been calculated. For the beams E-AF-(01-02), equipped with strain gauges, the average failure stress was approximately 44.5 MPa, see Table 5.4. The value corresponds to the average failure stress of glass 45 MPa (tested in a standing position) reported in [51]. However, these specimens turned out surprisingly the weakest among the beams with annealed glass. For the beams with web made of heat-strengthened glass the average failure stress was 127 MPa, see Table 5.4. If the average tensile stress of annealed float glass is approximately 45 MPa [51], the level of residual stress in the tested beams can be estimated to be 127-45=82 MPa. The SCALP measurements revealed the value of surface residual compressive stress of 53 MPa, see Section 3. The difference can be explained by the observation that in heat-strengthened glass the residual edge stress tends to be up to 50% higher than the residual stress away from the edges [45]. Since the residual surface stress was measured far from the edges of the glass, the residual edge stress can be calculated as $1.5 \times 53.2 = 79.8$ MPa, which explains the estimated value of 82 MPa.

Table 5.3: Initial bending stiffness (MNm^2) of beams

Specimen	Calculated from v_{global}	Calculated from v_{local}	
	EI_{global}	EI_{local}	Δ_{local} [%]
E-AF-01	0.939	0.973	3.62
E-AF-02	0.834	0.825	-1.08
E-AF-03	0.864	0.915	5.90
E-AF-04	0.904	0.965	6.75
E-AF-05	0.890	0.969	8.88
E-AF-06	0.958	1.042	8.77
Mean value	0.898	0.948	3.01
Standard deviation	0.042	0.066	-
E-HS-01	0.885	0.947	7.01
E-HS-02	0.899	0.949	4.29
Mean value	0.898	0.948	5.57
A-HS-01	0.916	0.976	6.55
A-HS-01	0.899	0.954	6.12
Mean value	0.907	0.965	6.39
S-HS-01	0.722	0.752	4.16
S-HS-01	0.718	0.792	10.31
Mean value	0.720	0.772	7.22

Table 5.4: Values of failure stress in glass for all tested beams.

Specimen	Failure stress [MPa]
E-AF-01	49.38
E-AF-02	44.99
Mean value	44.48
E-HS-01	141.78
E-HS-02	112.90
A-HS-01	126.85
A-HS-02	136.86
S-HS-01	125.30
S-HS-02	118.04
Mean value	126.96

5.5 Evaluation

The section presents the results of experimental investigation on life-size hybrid I-shaped beams made of ordinary annealed float and heat-strenghtened glass and timber flanges, bonded with three types of adhesives of different stiffness. Based on a qualitative research with a limited number of specimens main conclusions are drawn.

Experimental studies on hybrid timber-glass beams with web made of annealed float glass show that the beams are able to withstand much higher load than the load that causes initial failure of the glass web. The average value of an increase of load for all beams with annealed glass was 50% higher as compared to the load at initial crack. Alike the small-size beams presented in Chapter 4 the combination of a single pane web, made of ordinary annealed float glass, and timber flanges provides ductility and a warning signal relatively long before the total collapse. It gives time to temporarily support the element before the replacement and ensures the safety of users.

Beams with a web made of heat-strengthened glass, despite much higher load-bearing capacity, presented brittle failure with no warning signal. Due to the residual stress in the heat-strengthened glass the hybrid beams did not exhibit any post-breakage strength. The fracture pattern after glass failure was so advanced that the stiffness of the web was not large enough to hold the shards in place. Probably high-speed camera would have revealed the mechanism of cracks formation and the cause of the explosive final failure.

Despite significant difference in modulus of elasticity of epoxy (1595 MPa) and acrylate (78 MPa) adhesives no difference in initial bending stiffness of hybrid beams were observed. The beams bonded with silicone adhesives with modulus of elasticity of 3 MPa presents the initial bending stiffness approximately 25% lower when compared with others.

Readings from extensometers attached to the annealed glass revealed the average tensile strength of glass 44.5 MPa which corresponds to the values reported in literature [51]. Good agreement was found when comparing the average tensile strength of heat-strengthened glass with measured values of residual stress with SCALP device.

To translate the results of the life-size specimens with the web made of annealed float glass to a real situation an additional analysis was performed. It was assumed that a hybrid timber-glass beam with the cross-section dimensions and length as in the experiments is a structural component of a roof structure as presented in Figure 1.1. The beams support insulated glass panels with the total thickness of glass of 24 mm. A 1.5 m spacing of the beams was assumed. Comparing the bending moments from the four-point bending test (based on the load at first cracking, see Table 5.2) and a simple supported beam with uniformly distributed loading (including the dead load from glass panels, self-weight of the beams and a snow load for I snow zone in Poland) a global safety factor of 2.0 was obtained. Obviously, it is possible to control the load-bearing capacity of hybrid timber-glass beams by modifying the geometry of the glass web and timber flanges.

6 Numerical modelling of the structural response

This chapter focuses on numerical modelling of the structural response of hybrid timber-glass beams. It presents an introduction on numerical methods used in analysis. The experimental results, reported in Chapters 4 and 5, are used as a reference to validate the models. The findings from the numerical investigations are presented.

Introduction

This chapter deals with numerical modelling of the structural response of hybrid timber-glass beams. The numerical models make use of the commercial Finite Element Analysis software ABAQUS and the *brittle cracking* feature dedicated for modelling brittle failure of materials [35].

To validate the numerical models they were applied to describe the structural response of small- and life-size hybrid timber-glass beams investigated experimentally in Chapters 4 and 5. Moreover, the models were checked for sensitivity to variable parameters: element type, element size and value of fracture energy of glass. In addition, a simple thermal stress analysis is performed.

6.1 Background information

Numerical calculations were performed in ACK CYFRONET in Cracow funded by a grant MNiSW/SGI3700/PSlaska/030/2011. All numerical calculations were performed using the ABAQUS/CAE 6.12 [35]. The software is an advanced non-linear Finite Element Analysis software dedicated for various types of analyses in structural, mechanical, biomedical and related engineering applications. It provides finite element solution techniques to simulate a wide range of dynamic and quasi-static problems.

6.2 Numerical methods applied in the research

6.2.1 Review of numerical methods

Regarding modelling brittle behaviour of glass different simulation strategies have been used. Nielsen at al. [71, 72] presented a simplified method for modelling cracking of glass. In the method glass was modelled as a linear-elastic material in plane stress state. The crack initiation criterion was governed by maximum principal stress. After the stress reaches critical value, the stiffness material point is reduced so it is not able to carry any stresses. Comparing numerical results with experiments a fairly good agreement was observed. However, the approach assumed that stiffness of the cracked material is reduced in all directions which is not true. Even though the cracked material cannot carry any tensile stress, some shear can be still transferred through the crack.

Louter at al. [73] proposed two smeared crack models, in which to avoid convergence problems due to negative tangent stiffness of the softening law two strategies were adopted. Within the first strategy the incremental-iterative analysis was replaced by a series of scaled linear analyses. In the further, the stress-strain softening law of glass was replaced by a "saw-tooth" reduction curves. In therms of load-displacements curves numerical results presented very good predictions in comparison to experimental results. However, in therms of amount and shape of cracks the results of computational models differs from the experimental results.

Correia at al. [74] presented multi-fixed smeared crack model, which included a linear tensile-softening law. In the model new crack was initiated when two conditions were satisfied: principal stress exceeds the tensile strength of glass and the angle between the direction of existing cracks and direction of maximum principal stress in glass exceeds the prodefined treshold value of 30°. Good agreement between numerical simulations and experimental results was observed.

Bedon and Louter [75] used brittle cracking model available in ABAQUS/Explicit to simulate behaviour of laminated reinforced glass beams. Interesting results were found regarding load-displacement plots and crack patterns. However, in the model plane stress state was applied.

Despite promising results of the numerical analyses presented before, in most cases the approaches make use of plane stress methods and require implementations of own computational code. The main aim of the thesis to model structural response of hybrid timber-glass beams using an available software ABAQUS. The models will make use of a three-dimensional model.

6.2.2 Brittle cracking model (ABAQUS/Explicit)

The finite element method is a popular computational tool used in engineering research. Regarding field of solid mechanics and non-linear quasi-static problems, finite element equation solution methods can basically be classified as either implicit or explicit. Both methods are solved incrementally.

In the standard implicit finite element method a solution for each increment involves iterations until a convergence criterion is satisfied. However, the method can meet numerical difficulties when solving non-linear quasi-static problems involving large element deformation, brittle failure of material, highly non-linear plasticity or contact between surfaces [35].

In contrast to implicit finite element method, the explicit approach provides an alternative, efficient and more robust solution. In the method, the finite element equations are formulated as dynamic and thus can be solved directly, without iterations. The solution is determined at a constant size of the time increment:

$$\Delta_t = \left(\frac{L^e}{c^d} \right), \tag{6.1}$$

where L^e is the characteristic element length and c^d is the dilatational wave speed:

$$c^d = \sqrt{\frac{\lambda + 2\mu}{\rho}}, \tag{6.2}$$

where λ and μ are the Lame constants and ρ is the material density. Thus the total calculation time of explicit solution depends on the element size and material density.

For the numerical analysis of hybrid timber-glass beams, presented further, the ABAQUS/-Explicit solver was used since it provides a *brittle cracking model* which is the most suitable for modelling of tensile cracking in brittle materials [35].

Brittle cracking model provides capability for modelling behaviour of brittle materials (e.g. ceramics, brittle rocks, concrete, glass, etc.) in which the behaviour is dominated by tensile cracking [35]. It assumes that the compressive behaviour is always linear elastic and the model must be used with linear elastic material only.

ABAQUS/Explicit uses a smeared crack model to represent the discontinuous brittle behaviour in material. Constitutive calculations are performed independently at each material point of the finite element model. The existence of discontinuities (cracks) comes into these computations in such a way that the cracks affect the strain and material stiffness associated with the material point.

A simple criterion is used to detect the crack initiation. A crack starts forming when the maximum principal tensile stress exceeds the tensile strength of brittle material. Subsequent cracks may form in another material point independently. Once a crack occurs at a point it remains throughout the rest of calculations. Nevertheless, it may close and reopen along the directions of the crack surface normals. When the stress at a material point becomes compressive the crack can close completely.

Within *brittle cracking model* crack criterion makes use of Hillerborg's fracture energy proposal [76]. Hillerborg defined the energy which is required to open a unit area of crack in Mode I $G_{\mathrm{f}}^{\mathrm{I}}$ as a material parameter. Mode I applies to a situation when tensile stress is normal to the plane of the crack (Fig. 6.2). In this approach brittle behaviour is

defined as stress-displacement response (Fig. 6.1). A specimen made of brittle material is subjected to tensile force, sufficiently short so the elastic strain is small enough that the specimen will crack primarily by the opening at the crack, independently on the specimen's length.

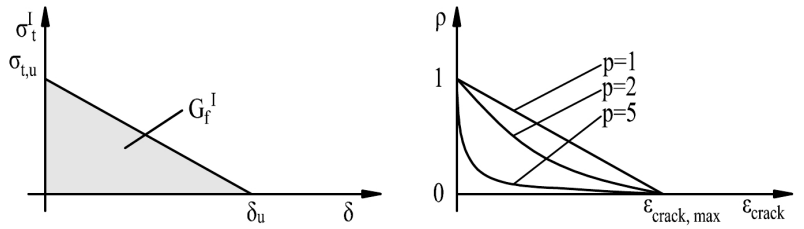

Figure 6.1: Crack criterion in Mode I and postfailure stress-fracture energy curve.

In ABAQUS/Explicit the Mode I fracture energy G_f^I can be specified directly as a material property. The model assumes a linear loss of strength after cracking (Fig. 6.1). The failure stress σ_t^I decreases until complete loss of strength takes place (at the crack normal displacement δ_u). Since the fracture energy is the area under the curve, the crack normal displacement is, therefore:

$$\delta_u = 2\,\frac{G_f^I}{\sigma_{t,u}}. \tag{6.3}$$

The definition of the characteristic length associated with a material point is required to implement the stress-displacement concept in a finite element model. The characteristic length is based on the element geometry, usually it is a length of a line across the element.

Within *brittle cracking model* crack initiation is based on Mode I fracture only, when post-cracking behaviour includes Mode I and Mode II (Fig. 6.2).

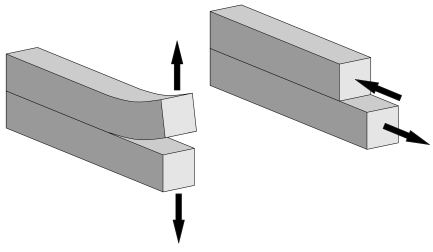

Figure 6.2: Fracture Mode I (left) and Mode II (right).

The mode II shear behaviour is based on observation that the shear behaviour depends on the magnitude of crack opening, namely, the shear modulus decreases with crack

opening. The ABAQUS/Explicit provides the shear retention model, in which post-cracked shear stiffness is formulated as a function of opening strain throughout the crack. In the model the relationship is formulated by expressing the post-cracking shear modulus G_{crack}, as a fraction of the uncracked shear modulus:

$$G_{crack} = \rho(\varepsilon_{crack})\, G \tag{6.4}$$

where G is the shear modulus of uncracked material, $\rho(\varepsilon_{\text{crack}})$ is the shear retention factor which depends on the crack opening strain $\varepsilon_{\text{crack}}$. The shear retention factor should meet $0.0 \leq \rho \leq 1.0$, in which 0 represents no shear retention, whereas 1.0 represents full shear retention. The shear retention factor can be defined in the power law form:

$$\rho(\varepsilon_{crack}) = \left(1 - \frac{\varepsilon_{crack}}{\varepsilon_{crack,max}}\right)^{p} \tag{6.5}$$

where p and $\varepsilon_{\text{crack,max}}$ are material parameters (the dependence is shown in Figure 6.1. It satisfies the requirements that $p \to 1$ as $\varepsilon_{\text{crack,max}} \to 0$, which correspond to the state before crack initiation, and $p \to 0$ as $\varepsilon_{\text{crack}} \to \varepsilon_{\text{crack,max}}$ which corresponds to the state when the crack cannot transfer any shear stress (no shear interlock). To get more stable explicit finite element simulation Ivanov and Sadowski [77] recommend $\varepsilon_{\text{crack,max}} \geq \varepsilon_{\text{crack}}(\delta_u)$.

Computations where elements can no longer carry stress may lead to excessive distortion of the elements and subsequent premature termination of the simulation [35]. Therefore, a *brittle failure* criterion is provided within *brittle cracking model*. When local direct cracking displacement components at a material point reach defined value, the element is removed from the mesh. The *brittle failure* criterion must be used with care. The main consequence is that the elements are removed from the mesh until the end of calculations.

To perform a quasi-static analysis and avoid the influence of inertial forces on mechanical response using the ABAQUS/Explicit, which is a dynamic analysis solver, special care must be taken when setting the analysis step time period. Incorrect step time period of explicit analysis can result in unrealistic dynamic effects [78]. Kutt et al. [79] recommend that the ratio of step time period and natural period of the structure should be greater than five.

In addition, Chung at al. [80] suggest that dynamic effects in the model can be neglected and the quasi-static response can be ensured by keeping the ratio of kinetic energy to the internal strain energy at <5% during entire time period. In such a way the external work done by the load is balanced mostly by the internal energy of the whole structure, which in fact happens in static analysis. In this approach, based on the conservation of energy principle, the kinetic energy is an indicator for the quasi-static response. Limitation of the kinetic energy is usually archived by adjusting the step time period and controlling the plots of the kinetic and internal energy before any results are accepted. Usually, the optimum step time period is obtained after several trials.

6.3 Numerical models

The section describes numerical models and materials properties applied. Two models were investigated: small- and life-size beam elements, see Figures 6.3 and 6.4.

The consistency of the numerical models was investigated for selected small-size beam by varying the element type, element size and fracture energy of glass. Based on findings from parametric studies the optimum model parameters were set and final numerical models were investigated. In addition, thermal analyses for final model of the life-size beam with different adhesives were performed.

6.3.1 Set-up 3D models

Due to symmetries of the specimens, only quarter beams were taken into account with appropriate boundary conditions simulating a four-point bending test, see Figures 6.3 and 6.4.

Load introduction points and supports were modelled using 50 mm long rigid surfaces ensuring distribution of forces to larger number of elements. In experimental investigations the loads was distributed to the timber flange by steel plates measuring 50×50 mm with a thickness of 8 mm.

All components were modelled using 3D solid elements. For the flanges and bond connections 8-node linear brick elements (C3DR8) with reduced integration and large-strain formulation were used. For the web two types of elements were used: 8-node linear brick elements (C3DR8) with reduced integration and large-strain formulation and 6-node linear triangular prism elements (C3D6). In all models 5 mm and 2 mm element size was applied for the flanges and adhesive connection, respectively. All calculations were run in displacement control including non-linear effects of large deformations. The displacement was increased linearly using a smooth amplitude function.

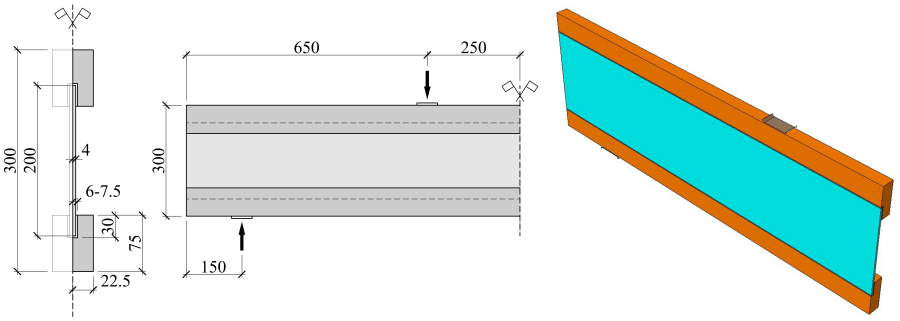

Figure 6.3: Cross-section, loading and boundary conditions for 3D model of small-size beam.

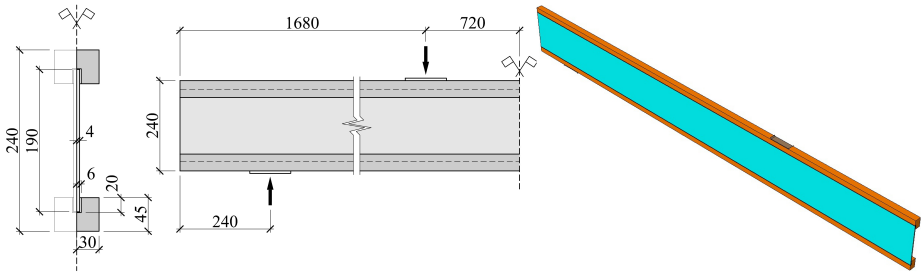

Figure 6.4: Cross-section, loading and boundary conditions for 3D model of life-size beam.

6.3.2 Material models

The glass material, in both models (small-size and life-size beams), was modelled with isotropic, linear elastic material properties. The values of modulus of elasticity E and maximal tensile stress f_t were determined based on experimental results presented in Section 3.2. The value of Poisson's ratio ν and density ρ were take from literature [50].

To model the mechanism of glass failure a smeared crack model along with *brittle cracking* and *brittle failure* damage evolution sub-options available in ABAQUS/Explicit software were used, see Section 6.2. In this approach a crack initiation is governed by the maximal tensile stress f_t and crack propagation is based on the fracture energy of glass G_f. The value of G_f was preliminary set equal to 3.0 J/m^2 according to [45]. Based on f_t and G_f the crack normal displacement δ_u was calculated according to formula 6.3. Post-cracking behaviour (decrease of shear modulus with crack opening) was modelled using the shear retention model. The values of $\varepsilon_{crack,max}$ were calculated taking into account the size of finite elements. In the analyses it was assumed after Ivanov and Sadowski [77] $\varepsilon_{\text{crack,max}} = 2 \times \varepsilon_{\text{crack}}(\delta_u)$. Mechanical characterization of glass material model is summarized in Table 6.1.

Table 6.1: Mechanical characteristics of glass material model.

E [MPa·10^3]	ν	f_t [MPa]	G_f [J/m^3]	δ_u [m]
70	0.23	45	3	1.333·10^{-7}

The timber material was modelled with orthotropic, linear elastic material properties. Since the flanges of small-size and life-size beams were made of different timber types two material models were used. For the timber type A the values of modulus of elasticity E_{1-3} and Poisson's ratio ν were determined based experimental results presented in Section 3.3. For the timber type B the values of modulus of elasticity E_{1-3} and ultimate

tensile stress f_t were determined based on experimental results presented in Section 3.3. Other parameters were calculated proportionally based on the literature [54, 55]. Mechanical characterization of wood material models (type A and B) are summarized in Tables 6.2 and 6.3.

Table 6.2: Mechanical characteristics of wood type A material model.

E_1	E_2 [MPa·10^3]	E_3	ν_{12}	ν_{13}	ν_{23}	G_{12}	G_{13} [MPa·10^3]	G_{23}
10.54	0.75	0.75	0.44	0.40	0.52	0.93	0.93	0.12

Table 6.3: Mechanical characteristics of wood type B material model.

E_1	E_2 [MPa·10^3]	E_3	ν_{12}	ν_{13}	ν_{23}	G_{12}	G_{13} [MPa·10^3]	G_{23}
12.41	0.88	0.88	0.44	0.40	0.52	1.09	1.09	0.14

Three types of adhesives were considered: epoxy, acrylate and silicone. Depending on the behaviour of tested specimen in tension, see Section 3.4, different material models were applied. The epoxy adhesive (3M DP490) was modelled as isotropic with linear elastic behaviour. The epoxy linear model is characterized by the tensile elastic modulus $E_{t,e}$, the tensile ultimate stress $f_{t,e}$ the tensile ultimate strain $\varepsilon_{t,u}$ and Poisson's ratio ν. The tensile elastic modulus $E_{t,e}$ was based on cyclic test on the epoxy adhesive while the tensile ultimate strain $\varepsilon_{t,u}$ was based on monotonic test, see Chapter 3. The acrylate adhesive (SikaFast 5215) was modelled as isotropic, bilinear elastic plastic behaviour. The acrylate bilinear model is characterized by the tensile elastic modulus $E_{t,e}$, the tensile plastic modulus $E_{t,p}$, the tensile elastic stress $f_{t,e}$ and Poisson's ratio ν. Since the acrylate specimens exhibited large deformation during testing without failing the ultimate tensile strain was not considered. The bilinear material model was created based on the cyclic and monotonic tests. The elastic domain was based on the cyclic test while the plastic domain was based on monotonic test, see Chapter 3. Since in ABAQUS software plastic behaviour is formulated in terms of Cauchy stress and its strain, the nominal stress and strain were transformed into the true stress and strain. Assuming that specimen volume does not change, the true stress and strain were calculated respectively with the following formulas:

$$\sigma_{t,t} = \sigma_t(1 + \varepsilon_t) \tag{6.6}$$

$$\varepsilon_{t,t} = ln(1 + \varepsilon_t) \tag{6.7}$$

where $\sigma_{t,t}$ is the true stress, σ_t is the nominal stress, ε_t is the nominal strain.

The silicone adhesive (Sikasil SG-500) was modelled as isotropic with linear elastic behaviour. The silicone linear model is characterized by the tensile elastic modulus $E_{t,e}$

and Poisson's ratio ν. The values were based on cyclic test on the silicone adhesive, see Chapter 3.

Figure 6.5 summarizes the tensile mechanical properties for the adhesive models. Table 6.4 presents the tensile model stress-strain curves for the three adhesives.

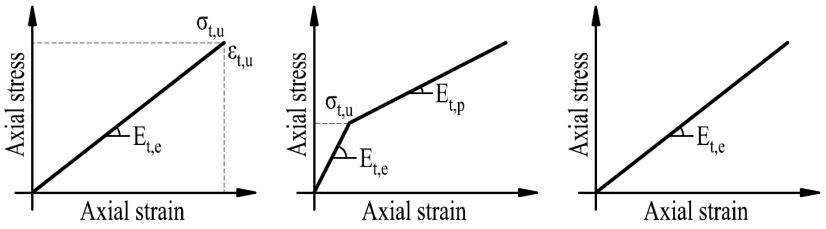

Figure 6.5: Tensile model axial stress-strain for adhesives: epoxy (left), acrylate (middle) and silicone (right).

Table 6.4: Mechanical characteristics of adhesive material models.

Adhesive	$E_{t,e}$ [MPa]	$f_{t,e}$ [MPa]	$E_{t,p}$ [MPa]	$\epsilon_{t,u}$	$f_{t,u}$ [MPa]	ν
Epoxy	1595	-	-	0.032	36.5	0.422
Acrylate	78.12	8.42	4.84	-	-	0.459
Silicone	3.17	-	-	-	-	0.462

6.3.3 Parametric studies and final models

To find the optimum model parameters some factors were varied to investigate their effect on the numerical results. Due to computational cost of simulations it was performed for the small-size beam model bonded with acrylate adhesive with groove dimensions of 13×30 mm. Variations of model parameters, presented in Table 6.5, are briefly described below.

Firstly, the geometry of the elements was varied. Since the smeared model is susceptible to elements shape, the geometry of the elements was varied between rectangular and prism with triangular base elements, see Figure 6.6. Secondly, the size of rectangular and prism elements was altered among 8, 4 and 2 mm, see Figure 6.6. The value of 8 mm corresponds to the thickness of glass used in the research. Finally, the fracture energy of glass was varied between 3 and 8 J/m^2, the values were reported in [45] and [81], respectively. Also an intermediate value of 5.5 J/m^2 was considered.

For all models the values of direct cracking failure strain $\epsilon_{\text{crack,max}}$ was calculated.

Table 6.5: Mechanical and geometrical properties of parametric models.

	Model	Mesh geometry	Mesh size [mm]	Fracture energy G_f [J/m^2]	$\epsilon_{crack,max}$
Variation of mesh type and mesh size	P-01	rectangular	8	3	$8.33 \cdot 10^{-5}$
	P-02		4		$6.67 \cdot 10^{-5}$
	P-03		2		$1.33 \cdot 10^{-5}$
	P-04	prism	8		$8.33 \cdot 10^{-5}$
	P-05		4		$6.67 \cdot 10^{-5}$
	P-06		2		$1.33 \cdot 10^{-5}$
Variation of fracture energy	P-07	prism	4	5.5	$6.67 \cdot 10^{-5}$
	P-08		4	8	

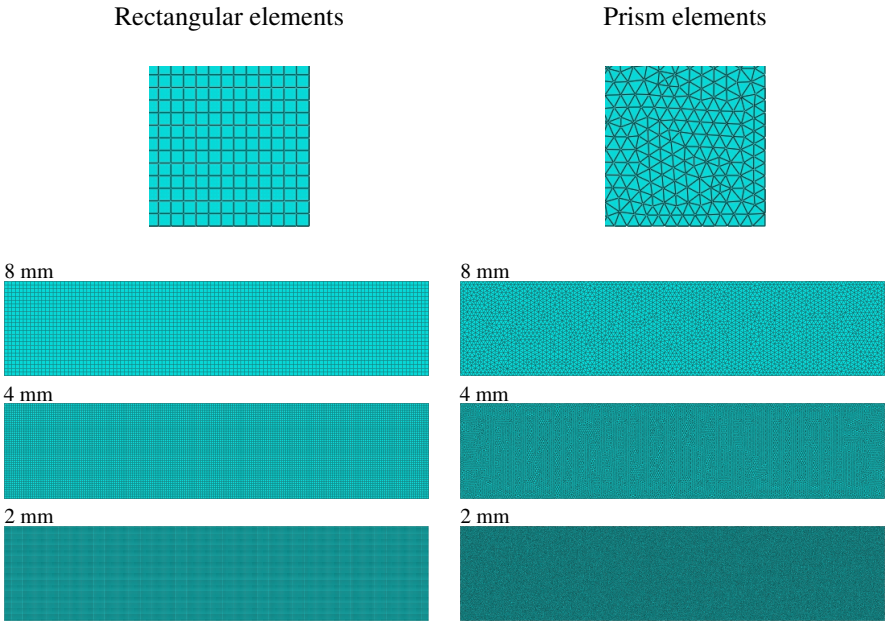

Figure 6.6: Parametric numerical studies - mesh patterns of glass web.

Based on the findings from parametric studies analyses of the final numerical models of small- and life-size beams were performed. The optimum model parameters were: prismatic element type, element size 4 mm and fracture energy of glass 3 J/m^2. Numerical investigation on small-size beams includes four models with variable parameters:

groove dimensions and adhesives, see Table 6.6. Numerical investigations on life-size beams include four models with variable parameters: adhesive and glass type, see Table 6.7.

Table 6.6: Variables of final numerical models of small-size beams.

Model	Groove dimensions [mm]	Adhesives
F-SSB-01	12×30	Acrylate
F-SSB-02	13×30	
F-SSB-03		Silicone
F-SSB-04	15×30	

Table 6.7: Variables of final numerical models of life-size beams.

Model	Adhesive	Glass type
F-LSB-01	Epoxy	Annealed float glass
F-LSB-02	Acrylate	Heat-strenghtened glass
F-LSB-03	Silicone	

Experimental investigation on small- and life-size specimens showed that stiff adhesive is suggested to reach high load-bearing capacity. Since the hybrid beams are composed of constituents made of different materials with different thermal expansion coefficients a rigid connection between the web and flanges may lead to high thermal stress due to temperature changes. Thus a thermal stress analysis was performed. Table 6.8 shows the values used in the numerical analyses. A simple supported beam with temperature change of $\pm 25°C$ was considered.

Table 6.8: Values of thermal expansion coefficients for materials [45, 55, 82].

Material	Thermal expansion coefficient [10^{-6}/°C]
Glass	9
Timber	3.5
Epoxy adhesive	25
Acrylate adhesive	20
Silicone adhesive	100

6.4 Results and discussion

As discussed in Section 6.2 to ensure the quasi-static response the ratio of kinetic energy to the internal strain energy must be kept at <5% during entire analysis. Before any numerical results were accepted, every time the ratio was evaluated.

As an example, Figure 6.7 presents plots of kinetic and internal energy as well as the ratio for numerical model P-01. Only within the first second the ratio reaches value of approximately 35% which is related to initial increase of loading and small value of internal energy. Subsequently, the curve stabilises at approximately 0.05 and follow the level until the first cracking in glass occurs (at 6 s). A sudden increase of deformation, related to drop of bending stiffness, generates high kinetic energy which affects slightly the energies. Then, the ratio returns to a very low level and continues until the ultimate failure of model. In this stage the internal energy suddenly reaches an extremely low (negative) value and the kinetic energy a high (positive) value. For clarity, last increment is not shown in the plot.

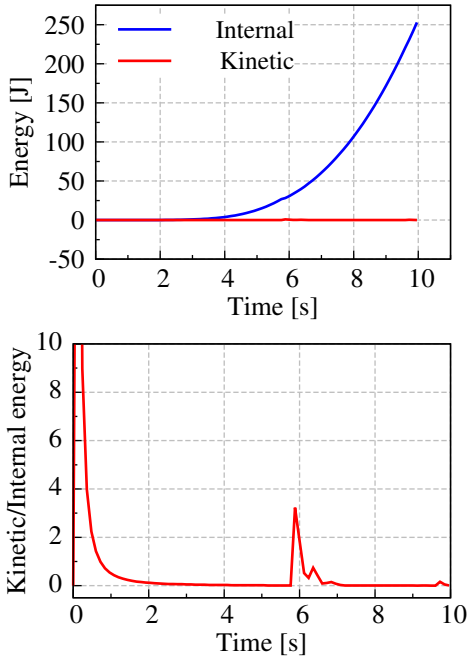

Figure 6.7: Energy levels for numerical analysis of model P-01.

As ABAQUS/Explicit solver is a dynamic analysis tool, despite ensuring a quasi-static response by applying an adequate step time period and keeping low ratio of kinetic-to-internal energy, dynamic effects such as oscillation cannot be avoided. Thus, the results obtained from numerical analysis were smoothed using a smoothing function available in ABAQUS to eliminate the oscillation effect, see Figure 6.8.

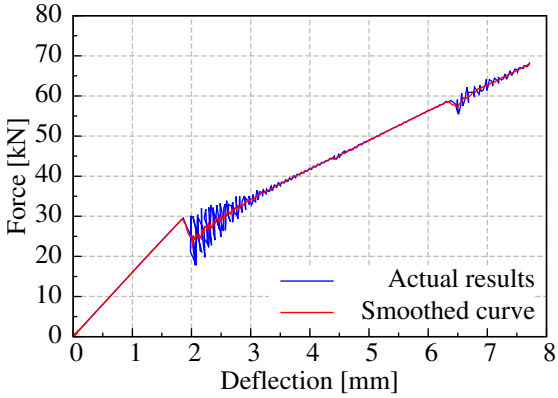

Figure 6.8: Numerical results. Force versus mid-span displacement plot for numerical model P-01: actual results and smoothed curve.

Regarding variation of element geometry and element size, models P-02÷06 (rectangular and prism elements and 8÷2 mm element size) compared to the reference model P-01 (rectangular elements and 8 mm element size) were investigated.

In terms of the load-displacement curves, the results present very small differences, see Figure 6.9. For all models in the first stage the relationship between the load and vertical mid-span displacement is almost perfectly linear until initial cracking. This is followed by a sudden drop of bending stiffness and an increase of vertical displacement. Initial cracking of glass web, for all models, occurs at the same load of 29 kN and displacement of 1.8 mm. Subsequently, the existing crack propagates and at the load of approximately 65 kN next crack forms. The ultimate failure of all models occurs at the load of 120-142 kN and displacement of 16-20 mm. The ultimate failure is caused by explosion of the glass web, see Figure 6.10.

Despite close results regarding load-displacement curves, mesh refinement does significantly alter the cracking pattern. Figures 6.11÷6.13 show crack pattern for numerical models P-01÷ P-06 with variable type and size of finite elements. Two element types (brick and prism element) and three element sizes (8, 4 and 2 mm) were considered in the analyses. Mesh refinement, regarding reduction of the size of elements, significantly alters the numerical results. Models with a coarse mesh (8 mm) show a relatively limited number of cracks when compared to the models with finer mesh (4 and 2 mm mesh size). It can be explained by the fact that the higher number of elements the more cracking

originates in the model. In terms of the element type, models with brick elements show a relatively limited number of cracks, while models with prism elements demonstrate more extensive cracking. Moreover, the models with prism elements show presence of diagonal cracks. The model P-06 with 2 mm prism elements the most correctly simulates the structural behaviour of beams investigated experimentally.

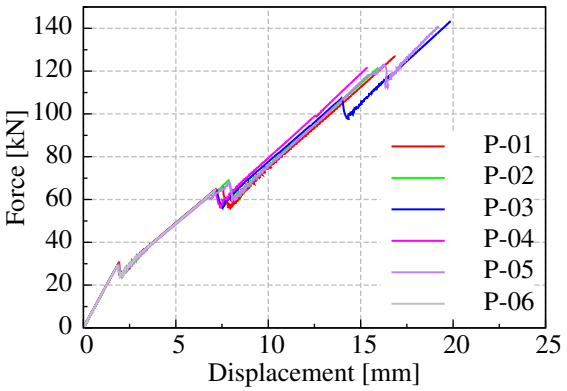

Figure 6.9: Load-displacement curves for numerical models F-01÷06.

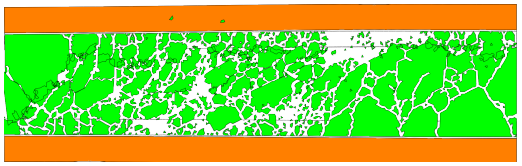

Figure 6.10: Ultimate failure of model P-04.

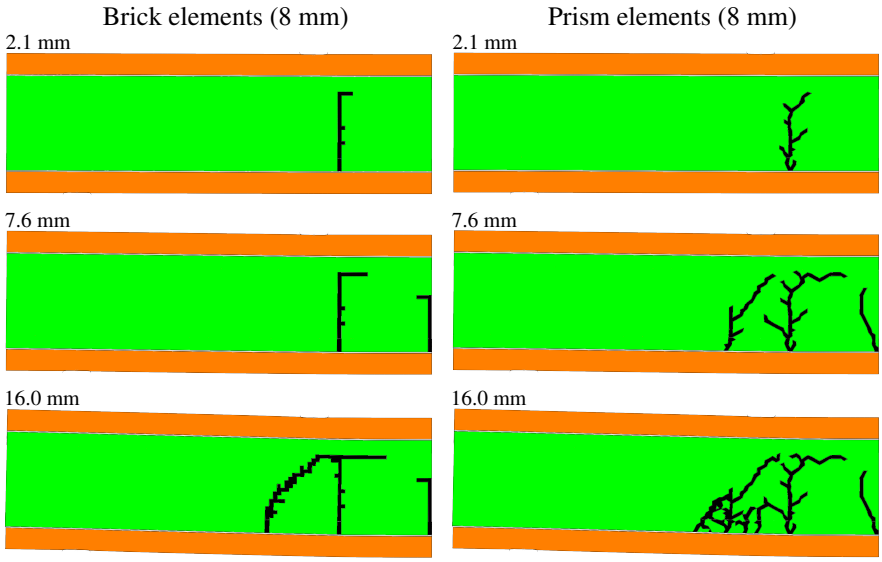

Figure 6.11: Crack pattern for numerical models P-01 and P-04.

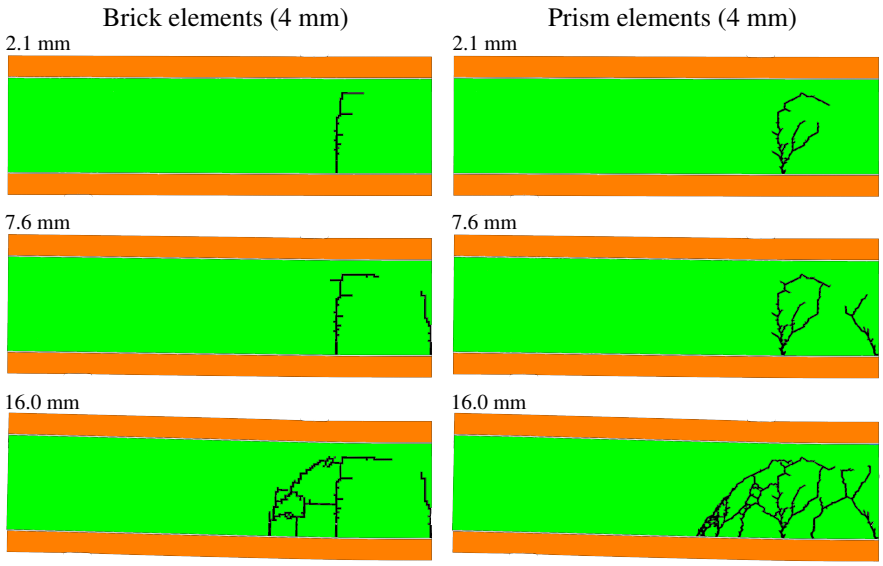

Figure 6.12: Crack pattern for numerical models P-02 and P-05.

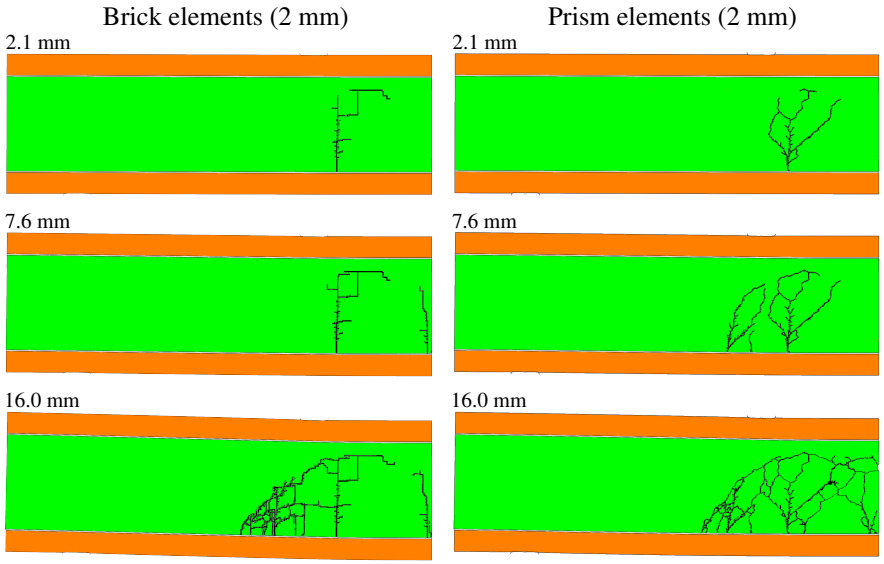

Figure 6.13: Crack pattern for numerical models P-03 and P-06.

A comparison obtained from models P-05, P-07 and P-08 is presented in Figures 6.14 and 6.15. Varying the value of fracture energy of glass not alter numerical results, no significant effects were found in the global resistance and structural performance. However, major discrepancies were found in the cracking patterns. In terms of load-displacement behaviour the results of these models are similar until second crack in glass occurs, see Figure 6.14. From this point the models present small differences in the occurrence of subsequent cracks. However, the global performance is similar and ultimate failure occurs at the same displacement. In terms of cracking patterns, the increase of fracture energy, in general, results is a decrease of a number of cracks in glass, see Figure 6.15. The cracking pattern of model F-03 the most correctly simulates the structural behaviour of beams investigated experimentally.

From the parametric analyses it is concluded that variation of model parameters assumed not alters significantly the results. In terms of load-displacement plots the type and size of elements the results present minor differences regarding the load and displacement at ultimate failure. In terms of cracking pattern models with larger number of elements (fine mesh with prism elements) results in larger number of cracks which correspond to the results observed in experimental investigations. Alike the effect of type and size of elements the variation of fracture energy does not change the load-displacement plots. However, the increase of fracture energy results in decrease of a number of cracks.

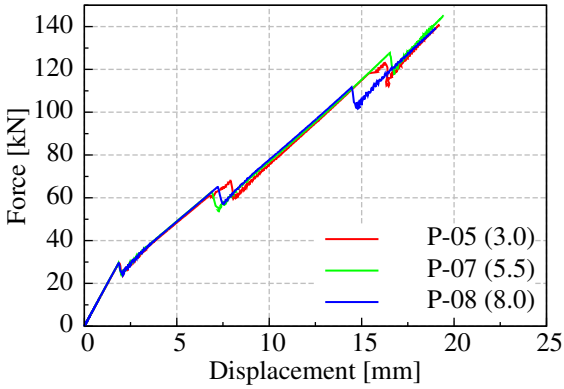

Figure 6.14: Load-displacement curves for numerical models P-05, P-07 and P-08. Values in brackets indicate fracture energy applied in analyses.

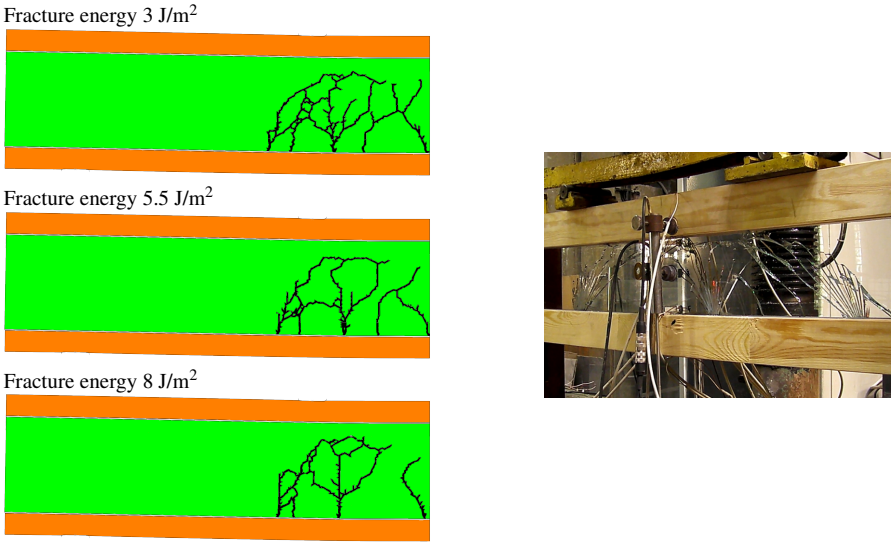

Figure 6.15: Crack patterns for models P-05, P-07 and P-08 with different fracture energy at displacement of 12.4 mm (left) and crack formation in the test (Specimen BA1).

Taking into account the results of parametric studies the prism elements with element size of 4 mm and the lowest value of fracture energy (3 J/m^2) are recommended to be used in final models of small- and life-size beams.

6.4.1 Numerical predictions compared with test results (small-size beams)

In the subsection a comparison of the numerical predictions and test results of small-size hybrid timber-glass beams is presented. Figure 6.16 and Table 6.9 present the results of the numerical investigations compared to the experimental testing of small-size beams bonded with acrylate adhesive.

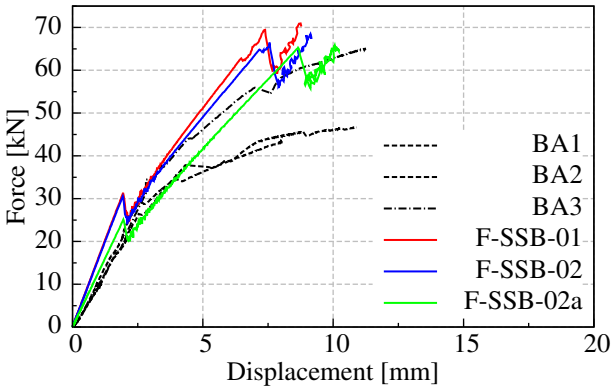

Figure 6.16: Load-displacement curves obtained from experimental and numerical analyses for small-size beams with acrylate adhesive.

Table 6.9: Experimental and numerical results of small-size beams with acrylate adhesive.

Model	Experimental investigations		Numerical investigations	
	F_{crack} [kN]	EI [MNm^2]	F_{crack} [kN]	EI [MNm^2]
F-SBB-01	27.9	0.658	31.38 (+12.5%)	0.966 (+46.8%)
F-SBB-02	26.4	0.632	30.56 (+15.8%)	0.941 (+48.9%)
F-SBB-02a	26.4	0.632	25.26 (-4.3%)	0.779 (+23.3%)

In Figure 6.16 it can be seen that the numerical results are in fairly good agreement with the experimental results. Despite different geometry of the groove, no difference in the initial stiffness and load at first glass cracking between models F-SSB-01 and F-SSB-02 can be observed. The curves start diverging from the load of approximately 60 kN, when shear cracks form. At this stage due to large strain in the adhesive different behaviour is observed. The stiffness of the bond line connection, due to wider groove and larger volume of adhesive, allows for greater deformations in model F-SSB-02 as compared to model F-SSB-01.

For both models (F-SSB-01 and F-SSB-02) the initial stiffness obtained from the numerical analyses overestimate the results from experiments, see Table 6.9. It can be explained by the fact that the actual stiffness of the acrylate adhesive is lower than obtained from testing the adhesive in tension, see Section 3.4, even for the the lowest load rate. For numerical models F-SSB-01 and F-SSB-02 the load when first cracking in glass occurs and initial stiffness is approximately 14 % and 48 % higher, respectively, as compared to the experiments. Therefore, additional model F-SSB-02a with reduced modulus elasticity of acrylate adhesive was computed and corresponding initial bending stiffness was calculated. The reduced value of the modulus of elasticity (E=17 MPa) corresponds to the results of relaxation tests on acrylate adhesive, see Section 3.4. The results of the model F-SSB-02a are in much better agreement (regarding the initial bending stiffness and the load at first cracking) with the experimental results. In this case, compared to experimental results the load which causes first cracking in glass is approximately 4% lower and the initial bending stiffness is 23% higher.

The numerical models simulate correctly the ultimate failure of the beams. During testing it was observed that the final failure was caused by the failure of the flange working in tension. Thus the numerical calculations were stopped at the stage when when tensile stress in the timber flanges exceeds the ultimate tensile stress obtained from experimental investigation on wood specimens (type A) in four-point bending, see Section 3.3.

In terms of crack pattern numerical models simulate correctly the tested beams, see Figure 6.17. No differences regarding crack patterns between models F-SSB-01, F-SSB-02 and F-SSB-02a were observed.

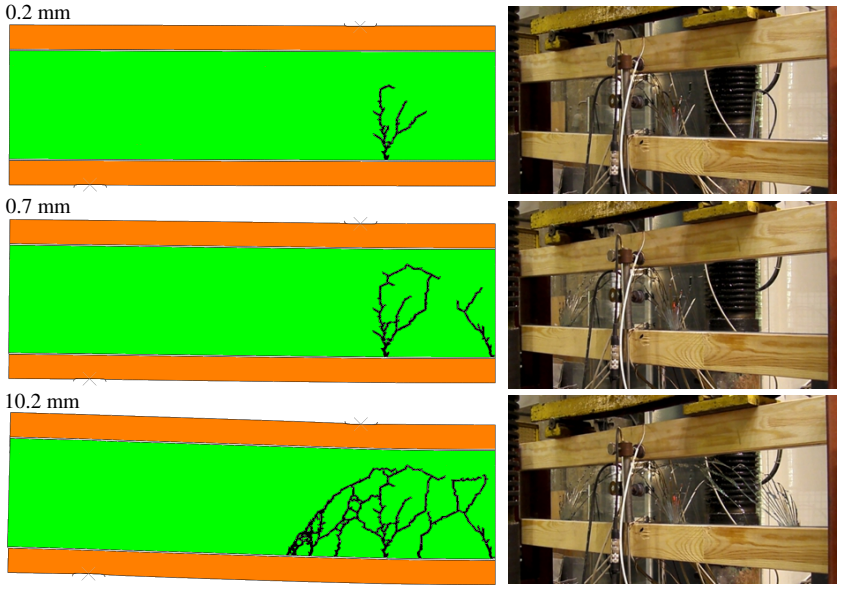

Figure 6.17: Crack patterns at different displacements obtained from numerical and experimental analyses.

Figure 6.18 and Table 6.10 present the results of numerical investigations and experimental testing of small-size hybrid timber-glass beams with silicone adhesive.

From Figure 6.18 it can be seen that the numerical results are in very good agreement with the experimental results. Despite different geometry of the groove, no difference in the initial stiffness and load at glass cracking between models F-SSB-03 and F-SSB-04 can be observed. The curves start diverging from the point when first crack occurs. At this stage due to large strain in the adhesive different behaviour is observed. The stiffness of the bond line connection, due to wider groove, allows for greater deformations in model F-SSB-04 as compared to model F-SSB-03.

In terms of the load at first cracking in glass the numerical models underestimates the experiments by approximately 10%, see Table 6.10. However, regarding the initial stiffness, the numerical models overestimates the results from the experiments by approximately 7%.

The numerical models simulate correctly the ultimate failure of the beams. During testing it was observed that the final failure was caused by the failure of the flange working in tension. Thus the numerical calculations were stopped at the stage when when tensile stress in the timber flanges exceeds the ultimate tensile stress obtained from experimental investigation on wood specimens (type A) in four-point bending, see Section 3.3.

In terms of cracking pattern the numerical models are in good agreement with the

experimental results. From both methods only one crack localized in the center of the specimen was observed, see Figure 6.19.

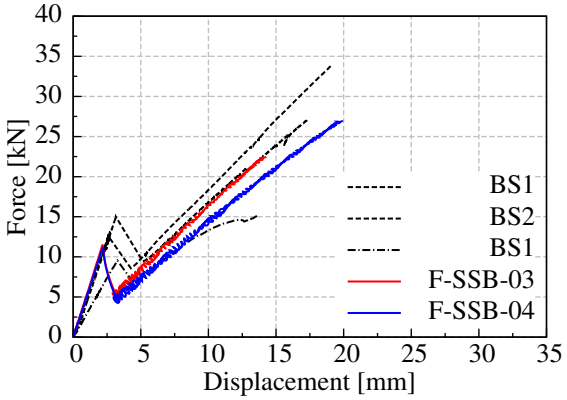

Figure 6.18: Load-displacement curves obtained from experimental and numerical analyses for small-size beams with silicone adhesive.

Table 6.10: Experimental and numerical results of small-size beams with silicone adhesive.

Model	Experimental investigations		Numerical investigations	
	F_{crack} [kN]	EI [MNm^2]	F_{crack} [kN]	EI [MNm^2]
F-SBB-03	12.7	0.292	11.5 (-9.5%)	0.315 (+7.9%)
F-SBB-04	12.6	0.289	11.1(-11.9%)	0.307 (+6.2%)

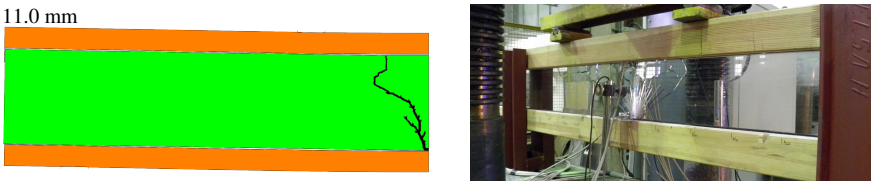

Figure 6.19: Crack patterns at different displacements obtained from numerical and experimental analyses.

6.4.2 Numerical predictions compared with test results (life-size beams)

As discussed in Chapter 5 only beams with web made of annealed float glass presented any post-breakage strength during experiments while the beams with web made of heat-strengthened glass failed right after first cracking in glass. Thus only for beams with ordinary glass a numerical model with brittle cracking model was calculated. For beams with tempered glass in order to determine an initial bending stiffness a linear elastic model (without brittle failure of glass) was applied.

Figure 6.20 presents the load-displacement curves obtained from numerical investigations and experimental testing of life-size hybrid timber-glass beams with epoxy adhesive.

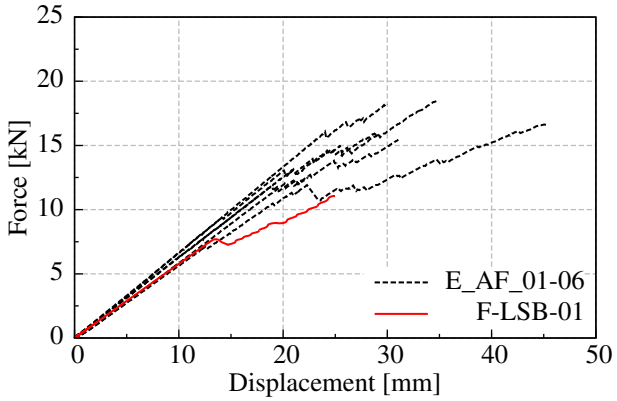

Figure 6.20: Load-displacement curves obtained from experimental and numerical analyses for life-size beams with epoxy adhesive.

From Figure 6.20 it can be seen that the numerical results are in very good agreement with the experimental results. However, the numerical models underestimate the ultimate failure. During testing it was observed that the final failure was caused by the failure of the flange working in tension. Thus the numerical calculations were stopped at the stage when when tensile stress in the timber flanges exceeds the ultimate tensile stress obtained from experimental investigation on wood specimens (type B) in bending, see Section 3.3.

Table 6.11 presents the results from numerical investigations and experimental testing of life-size hybrid timber-glass beams. In the table only results form beams with strain gauges attached were included. In terms of the load at first cracking in glass the results from numerical investigation vary from -8 to +10%. Regarding the initial bending stiffness the variation of results is $\pm 4\%$.

In terms of cracking pattern the numerical models are in good agreement with the

experimental results. From both methods several cracks were observed, see Figures 6.21 and 6.22. However, in the numerical analyses cracks forming outside the load introduction points were observed, what did not occur during experiments.

Table 6.11: Experimental and numerical results of life-size beams with epoxy, acrylate and silicone adhesives.

Model	Experimental investigations		Numerical investigations	
	F_{crack} [kN]	EI [MNm^2]	F_{crack} [kN]	EI [MNm^2]
E-AF-01÷02	8.25	0.887	9.11 (+10.4%)	0.920 (+3.72%)
E-HS-01÷02	25.5	0.898	25.48 (-0.08%)	0.920 (+2.45%)
A-HS-01÷02	25.2	0.907	24.60 (-3.53%)	0.904 (+0.67%)
S-HS-01÷02	19.8	0.720	18.27 (-7.73%)	0.692 (-3.89%)

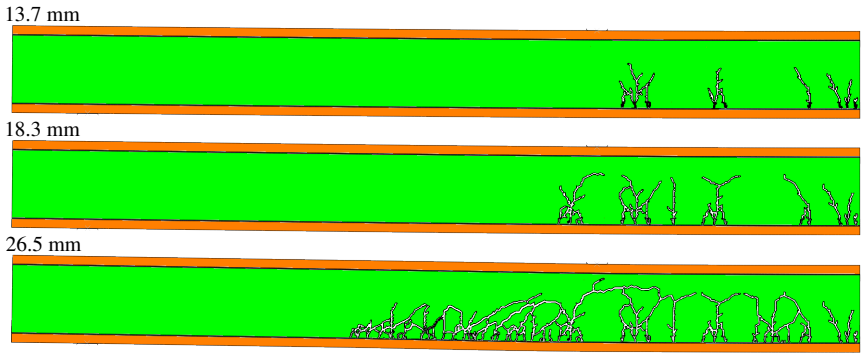

Figure 6.21: Crack patterns obtained from numerical analyses.

Figure 6.22: Crack patterns obtained from experimental analyses.

Thermal stress analysis

Figures 6.23 and 6.24 present stress profiles in the mid-span of the hybrid timber-glass beam with life-size dimensions due to the variation of the temperature by ±25°C. The loading results in relatively low stresses in the components. No significant differences were observed for the beams with epoxy, acrylate and silicone adhesives. Maximum thermal stress in glass is approximately 4 MPa (at ΔT= -25°C), which is 9% of the tensile strength of glass (45 MPa according to [50]). Relatively low stress was obtained for the adhesive and timber. Numerical analyses show that even the beams with stiff bond line connection no failure of glass web, timber flanges and adhesive could be predicted.

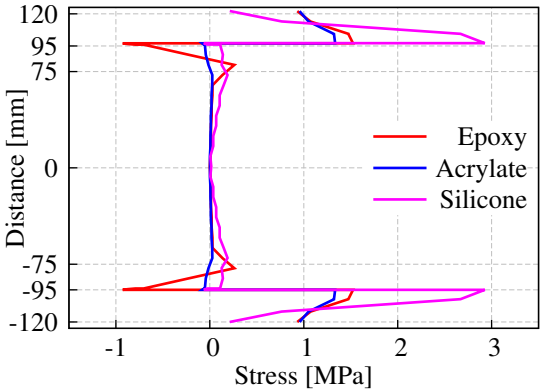

Figure 6.23: Thermal stress profile caused by increasing the temperature of +25°C.

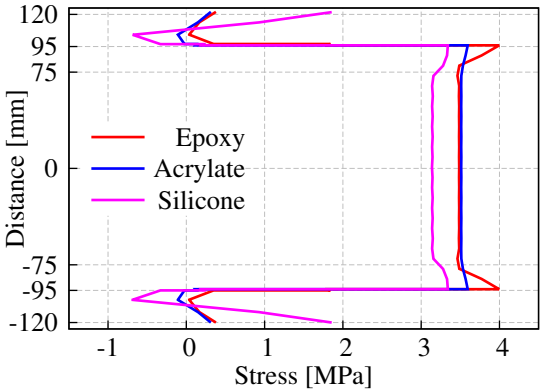

Figure 6.24: Thermal stress profile caused by increasing the temperature of -25°C.

6.5 Evaluation

In this section the results of numerical modelling of the structural response of small- and life-size hybrid I-shaped beams were presented. Parametric studies were performed to find the optimum model parameters for final beam models. Then, the model results were compared with the experimental results. In addition, a simple thermal stress analysis was performed to check how much temperature change results in thermal stress. Based on a qualitative research with a limited number of models main conclusions are drawn.

From the parametric investigations it is concluded that Explicit solver and *Brittle cracking* feature, available in Abaqus software, offer a suitable technique for simulating cracking of the glass. Regarding the effect of the element geometry and element size on the numerical results it is concluded that the parameters do not affect the response of the model in terms of load-displacement plots. The same observation was made for models with varying fracture energy of glass. However, mesh refinement does significantly alter the cracking pattern. The models with larger number of elements result in a larger number of cracks. In terms of the element type, models with brick elements show a relatively limited number of orthogonal cracks while models with prism shape elements demonstrate more extensive cracking and diagonal cracks. It was also observed that the increase of fracture energy results in a decrease of number of cracks. If taking into account the calculation time, load-displacement plots and cracking pattern 4 mm prism elements with the the value of fracture energy of $3 J/m^2$ is the optimum combination of parameters. The combination was used in the final models to be compared with the experimental results.

From the final models of small-size hybrid beams it is concluded that the numerical results of models with the modulus of elasticity of the acrylate adhesive determined in the cyclic test overestimate the experimental results. To obtain better agreement the results of the relaxation test must be used. The numerical models simulate correctly the load at first cracking in glass and overestimate slightly the initial bending stiffness. In terms of number of cracks and cracking pattern the numerical simulations are in good agreement with experiments.

From the final models of life-size hybrid beams with annealed float glass it is concluded that the numerical results (including the load at first cracking and initial bending stiffness) are in very good agreement with the experimental results. From the final models of life-size hybrid beams with heat-strengthened glass only the value of initial bending stiffness could be obtained.

From thermal stress analyses at the temperature change of $\pm 25°C$ it is concluded that the load does not lead to failure of glass. The stress corresponds to the level of approximately 9% of the tensile strength of glass.

7 Analytical considerations

This chapter focuses on a simple analytical tool to investigate the structural response of hybrid timber-glass beams. The test results presented in Chapters 4 and 5 are used as a reference to validate the model. The findings from the analytical investigations are presented.

7.1 Introduction

When considering a hybrid beam, in which materials with different stiffness are combined, a key element is the shear stiffness of the connecting media. It has a significant influence on the overall stiffness, strain distribution through the cross-section and also on the load-bearing capacity of the beam component.

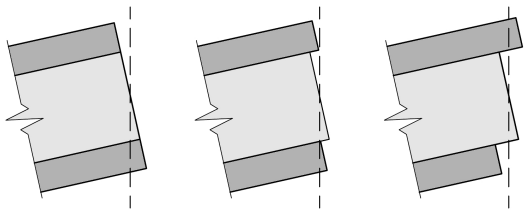

Figure 7.1: Behaviour of a hybrid beam depending of the flexibility of joints: full composite action (left), partial composite action (center), non-composite action (right).

Figure 7.1 presents the behaviour of a hybrid beam depending of the flexibility of joints. Two bounds can be distinguished:

- a lower bound - the stiffness of the connecting media is negligible and the components act separately (non-composite action),
- an upper bound - the stiffness of the connecting media is infinite (rigid connection) and the components act together (fully composite action).

Regarding the hybrid timber-glass beams with adhesive bond connections under loading there is always a slip between the components and thus a partial composite action has to be considered. The following section presents a simplified method to determine the effective bending stiffness and the load at first cracking in glass of a hybrid I-shaped beam with elastic connections between components.

7.2 Analytical solution

An I-shaped hybrid timber-glass beam presented in Figure 7.2 composed of two flanges and a web, combined with adhesive bond connections, is considered. Although the notation system relates to asymmetric cross-section, in the following calculations a symmetrical cross-section is assumed.

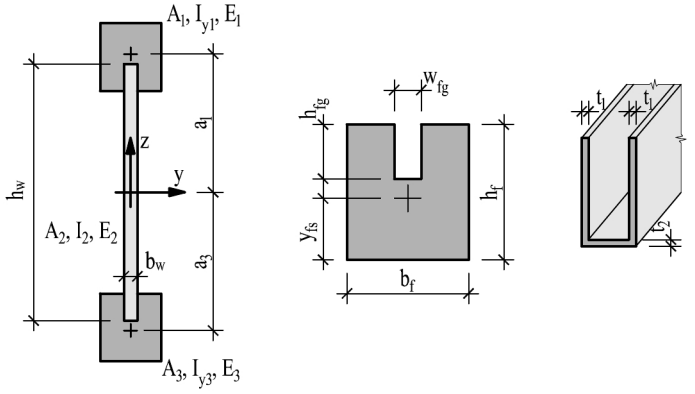

Figure 7.2: Notation system for the cross-section (left), timber flange (center) and bond connection (right).

In case of a very stiff connection between the web and flanges there is no slip between components under loading. Therefore the beam presents fully composite action and to determine the moment of inertia of the cross-section the parallel axis theorem can be used:

$$I_y = 2\,I_{y1} + I_{y2} + 2\,A_1\,{a_1}^2 \tag{7.1}$$

Another case relates to a situation when there is no connection between the web and flanges or the stiffness of the connection is negligible. The connection cannot take any shear stress and the components act separately. The moment of inertia in case of non-composite action comes down to a sum of the properties of the components:

$$I_y = 2\,I_{y1} + I_{y2} \tag{7.2}$$

The structural behaviour of hybrid timber-glass beams combined with adhesive bond

connections cannot be classified to any situations presented before. To determine the effective stiffness of such a component a partial composite action must be considered.

The approach with a gamma-factor used in timber engineering, see PN-EN 1995-1-1 [83] was applied in the work. The gamma-factor reduces the second component of the parallel axis theorem contribution of bending stiffness, depending on the stiffness of the connecting media:

$$I_{y,ef} = 2\,I_{y1} + I_{y2} + \gamma\,2\,A_1\,{a_1}^2 \quad \text{where} \quad 0 \leq \gamma \leq 1 \tag{7.3}$$

The connection efficiency factor γ was introduced by Möhler in 1956 [84]. A derivation of the gamma-factor can be found in [85]. It is expressed as:

$$\gamma = \frac{1}{1+k} \quad \text{where} \quad k = \frac{\pi^2\,E\,A_1}{L^2\,K_k} \tag{7.4}$$

The γ factor depends on the properties of the flanges E and A_1, length of the beam L and stiffness of the connections K_k. According to [83] the gamma-method applies to composite beams with mechanical connections. Based on dimensions of the bond line connection presented in Figure 7.2 a formula to determine K_k is proposed:

$$K_K = \frac{2\,G\,h_{fg}}{t_1} + \frac{G\,w_{fg}}{t_2} \tag{7.5}$$

where G is the shear modulus of adhesive, h_{fg}, w_{fg}, t_1, t_2 are the dimensions presented in Figure 7.2.

The general formula to determine the effective bending stiffness for the cross-section built with several components with different values of modulus of elasticity can be expressed:

$$I_{y,eff} = \sum_{1}^{3} n_i\,I_{yi} + \gamma_i\,n_i\,A_i\,a_i^2 \tag{7.6}$$

where:
$n_i = E_i/E_v$
E_i modulus of elasticity of i-component,
E_v comparative modulus of elasticity,
I_i moment of inertia of i-component,
γ_i connection efficiency factor,
A_i area of cross-section of i-component,
a_i distance between the center of gravity of i-component and center of gravity of the entire cross-section.

For the symmetrical cross-section presented in Figure 7.2, with $n_1 = n_3$, $\gamma_1 = \gamma_3$, $A_1 = A_3$ and $a_1 = a_3$, the formula (7.6) is expressed:

$$I_{y,ef} = 2\,n_1\,I_{y1} + n_2\,I_{y2} + 2\,\gamma_1\,n_1\,A_1\,{a_1}^2 \tag{7.7}$$

where:

$$I_{y1} = \left[\frac{b_f\,{h_f}^3}{12} + \left(\frac{h_f}{2} - y_{fs}\right)^2 b_f\,h_f\right] - \left[\frac{w_{fg}\,{h_{fg}}^3}{12} + \left(h_f - y_{fs} - \frac{h_{fg}}{2}\right)^2 w_{fg}\,h_{fg}\right] \tag{7.8}$$

$$y_{fs} = \frac{h_f}{2} + \frac{{h_g}^2\,w_{fg} - h_f\,h_{fg}\,w_{fg}}{2\,b_f\,h_f - 2\,h_{fg}\,w_{fg}} \tag{7.9}$$

$$I_{y2} = \frac{b_w\,{h_w}^3}{12} \tag{7.10}$$

$$a_1 = h_w + 2(t_2 + (h_f - h_{fg} - y_{fs})) \tag{7.11}$$

The following formulas are used to determine stress in the components:

- flange (centroid):

$$\sigma_{f,c} = \pm\frac{M}{I_{eff}}\gamma\,a_1\,n_1 \tag{7.12}$$

- flange (outer edge):

$$\sigma_f = \pm\frac{M}{I_{eff}}(\gamma\,a_1 + y_{fs})n_1 \tag{7.13}$$

- web (edge):

$$\sigma_w = \pm\frac{M}{I_{eff}}\frac{h_w}{2} \tag{7.14}$$

where M is the bending moment, I_{eff} is the effective bending stiffness, γ is the connection efficiency factor, a_1 is the distance between the center of gravity of flange and center of gravity of the entire cross-section, y_{fs} is the distance between the center of gravity of flange and its outer edge, h_w is the height of the web.

7.3 Comparison of analytical, experimental and numerical results

The section presents the results of analytical studies compared to the experimental and numerical results. Tables 7.1 and 7.2 present a comparison of results from analytical considerations and experimental and numerical investigations of life-size hybrid timber-glass beams. The analytical solution is in very good agreement with the experimental and numerical results. In terms of initial bending stiffness mean deviations of results were about 0.5 to 8.7%, see Table 7.1.

Table 7.1: A comparison of initial bending stiffness [MNm^2] obtained from experimental investigations, numerical simulations and analytical solution for life-size hybrid timber-glass beams.

Specimen	Experimental investigation	Numerical investigation	Analytical solution	Δ_{exp} [%]	Δ_{num} [%]
E-AF-01÷06	0.898	0.920	0.925	+3.01	+0.54
E-HS-01÷02	0.898	0.920			
A-HS-01÷02	0.907	0.904	0.923	+1.76	+2.10
S-HS-01÷02	0.720	0.692	0.752	-3.89	+4.44

Table 7.2: A comparison of load at first cracking in glass [kN] obtained from experimental investigations, numerical simulations and analytical solution for life-size hybrid timber-glass beams.

Specimen	Experimental investigation	Numerical investigation	Analytical solution	Δ_{exp} [%]	Δ_{num} [%]
E-AF-01÷06	11.6	9.11	8.7	-25.0	-4.5
E-AF-01÷02	8.25	9.11	8.7	+5.3	+5.3
E-HS-01÷02	25.5	25.5	24.5	-3.8	-3.9
A-HS-01÷02	25.2	25.2	24.4	-3.0	-3.2
S-HS-01÷02	19.8	18.3	19.7	-0.5	+7.7

Alike the initial bending stiffness, the load at first cracking calculated analytically shows very good agreement with experiments and numerical calculations, see Table 7.2. The value of ultimate tensile stress in glass of 45 MPa was taken into account in analytical calculations. Regarding the results for the beams with epoxy adhesive and annealed float glass (E-AF), if taking the mean value from all specimens (E-AF-01÷06) the analytical solution underestimate the experiments by 25%. However, only two specimens were equipped with strain gauges (E-AF-02÷02) and the ultimate stress in

glass could have been calculated. For remaining specimens (E-AF-03÷06) the value of ultimate tensile stress in glass was probably higher. If comparing the analytical solution with the experimental results for specimens E-AF-01÷02 the analytical solution is in much better agreement, it overestimates the load only by 5%. The analytical solution for beams with heat-strengthened glass presents very good agreement with experiments and numerical analyses (mean deviations are about -3.9 to +7.7%. Figures 7.3÷ 7.6 present a comparison between the stress profiles derived using the gamma-method and the stresses calculated from the strain gauge readings. A very good agreement was obtained.

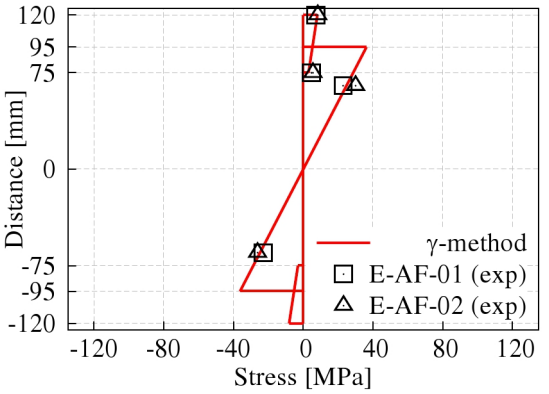

Figure 7.3: Stress profile derived using gamma-method compared to reading from strain gauges at a load of approximately 80% of ultimate load for specimens E-AF.

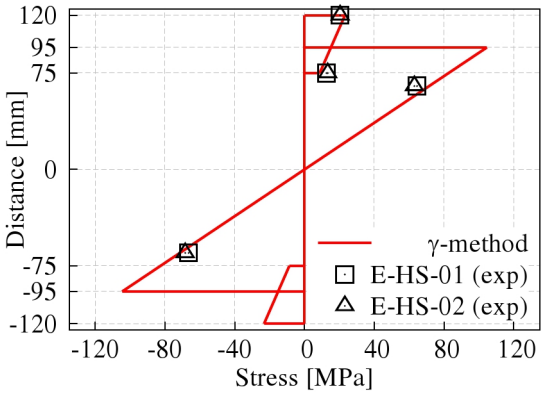

Figure 7.4: Stress profile derived using gamma-method compared to reading from strain gauges at a load of approximately 80% of ultimate load for specimens E-HS.

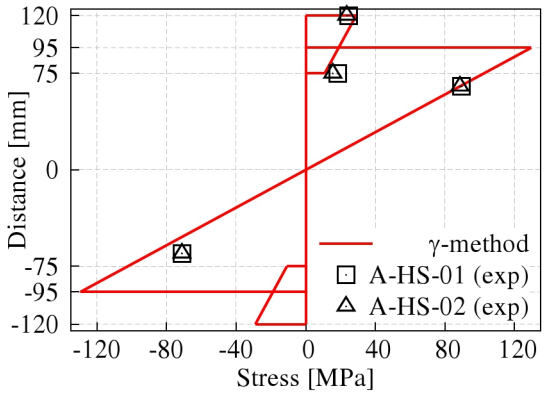

Figure 7.5: Stress profile derived using gamma-method compared to reading from strain gauges at a load of approximately 80% of ultimate load for specimens A-HS.

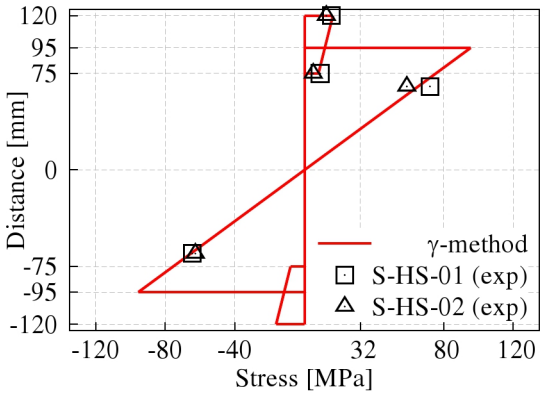

Figure 7.6: Stress profile derived using gamma-method compared to reading from strain gauges at a load of approximately 80% of ultimate load for specimens S-HS.

Figure 7.7 shows the influence of adhesive stiffness on the load level when first cracking in glass occurs for the life-size beam model with epoxy, acrylate and silicone adhesives. In the figure two levels are highlighted: the load for the beam model with fully-composite and non-composite action calculated with the analytical method presented in this chapter. Since the adhesives used in the research cover a wide range of stiffness, from approximately 3 to 1600 MPa, the horizontal axis was shown in a logarithmic scale. The epoxy is approximately twenty times stiffer if compared to the acrylate adhesive. Despite significant difference in stiffness of epoxy and acrylate adhesives almost the same load level at initial cracking in glass was observed. For the

beam model with the silicone adhesive, five hundred times less stiff, the load level was lower only by 22% compared to the load level for the beams with stiff adhesives and the theoretical beam with fully-composite action.

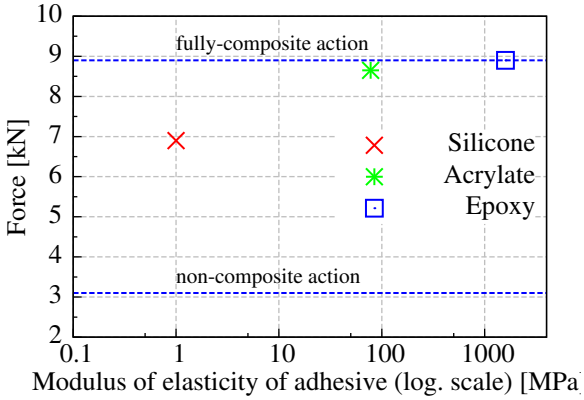

Figure 7.7: Influence of adhesive stiffness on force at first cracking in glass.

7.4 Evaluation

In this section the results of analytical method were presented. Based on a qualitative research main conclusions are drawn.

The analytical solution presented in the chapter confirms that the modified gamma method included in PN-EN 1995-1-1 can be successfully adapted for determination of initial bending stiffness and a load at initial cracking in glass of hybrid timber-glass beams. The results of the analytical method show very good agreement with the experimental testing and numerical simulations. In terms of the initial bending stiffness and the load at first cracking in glass the mean deviation of the results were about $\pm$ 5% and $\pm$ 8%, respectively.

8 Conclusions and future research

This chapter provides the conclusions from the research presented in the preceding chapters. It also presents the directions for future research.

The main purpose of the thesis was to extend the knowledge about structural response of hybrid timber-glass beams. Moreover, it was focused on the try to simulate numerically the behaviour under loading and failure mechanism including formation and propagation of cracks in the glass web. In addition, it aimed at a simple method to estimate the stiffness and load-bearing capacity of hybrid timber-glass beam components.

The following objectives were successfully accomplished:

- Preparation of a literature review. Current state of knowledge within the subject of the thesis was presented and current research was situated within the work done by others;
- Experimental investigations on materials (glass, timber and adhesives) used in the research. In this part mechanical properties of materials were evaluated;
- Experimental testing of 1800 mm long small-scale beam specimens bonded with three different types of adhesives. Within the part the concept was tested, results were evaluated and conclusions were drawn;
- Experimental testing of 4800 mm long life-scale beam specimens bonded with three different types of adhesives. In this part the results were evaluated and conclusions were drawn;
- Numerical modelling of the structural response of hybrid timber-glass beam. Within the part a numerical model which includes brittle failure of glass was presented and results were evaluated;
- Analytical model. In this part the hybrid timber-glass beams were investigated analytically and a analytical tool to determine bending stiffness and load at initial

cracking was proposed. The results were compared with numerical analyses and experiments;

Referring to the hypotheses presented in Chapter 1 it is concluded that:

- Experimental investigations on models of hybrid timber-glass beam specimens confirm that a combination of a glass web and timber flanges bonded with structural adhesives provides a practical, durable and environmentally-friendly basis for a building system;
- Four-point bending tests on hybrid timber-glass beams, both small- and life-scale specimens, confirm that the hybrid timber-glass beam components make possible predictable and safe structures by providing ductility and high post-breakage strength (from 140 to 210% of the load at initial cracking of glass). The conclusion is valid only for beams with the web made of annealed float glass, the beams with the web made of heat-strengthened glass, despite almost double load-bearing capacity, show no post-breakage strength; it was observed that the ultimate failure of the hybrid beams was caused by failure of the flange working in tension. Thus a material with higher strength is recommended for future research;
- The bending stiffness and load-bearing capacity of hybrid beams are highly influenced by the stiffness of the bond line adhesive connection; it was observed that the beams bonded with stiff adhesives present higher bending stiffness and load-bearing capacity; Epoxy adhesive is recommended for the bond line connection;
- Numerical analyses performed confirm the ability to reliable model the behaviour of the hybrid beams under loading; Explicit solver and *Brittle cracking* material model, available in Abaqus software, offer a suitable technique for simulating cracking of the glass; based on parametric studies it is concluded that the element geometry, element size and variation of fracture energy do not affect the response of the models in terms of load-displacement plots; however, the factors affect the cracking pattern of glass; the models with prism elements, size of 2 mm and the value of fracture energy of 3 J//m^2 prisent the cracking pattern the closest to the pattern observed in experiments; the numerical models of small- and life-scale specimens show very good agreement with experiments regarding the value of bending stiffness, a load at initial cracking of glass; the numerical models allow for reliable simulations of formation and propagation of cracks in the glass web;
- Analytical solution proposed in the thesis confirms that the modified gamma method included in PN-EN 1995-1-1 can be successfully adapted for determination of initial bending stiffness and a load at initial cracking of glass; the results of analytical method show good agreement with experiments and numerical simulations; in terms of initial bending stiffness and load at first cracking in glass the mean deviation of results were about about $\pm$ 5% and $\pm$ 8%, respectively;
- From the practical point of view it is possible to apply the hybrid beams investigated in a real structure; however, modifying the geometry of the components

(hight and thickness of a web, the cross-section of flanges) it is possible to control the stiffness and the load-bearing capacity of the elements.

The above conclusions are based on studies including short, repetitive series and can not be considered as universal.

Based on studies and analyses performed a number of topics is recommended to investigate in future research:

- Experimental investigations on adhesives including long-term behaviour, ageing, climate loading;
- Experimental investigations on beam specimens with a web made of laminated glass;
- Use of more homogeneous and stable wood material for flanges (e.g. laminated veneer lumber LVL);
- Experimental investigation on hybrid beams under long-term loading;
- Experimental investigation on hybrid beams under climate loading (e.g. temperature change);
- Improvement of the analytical methods and numerical models including the results of additional studies.

References

[1] Robbins C. *Daylighting: design and analysis*. Van Nostrand Reinhold Company, 1986.

[2] Kaplan R. "The role of nature in the context of the workplace". In: *Landscape and Urban Planning* 26 (1993), pp. 193–201.

[3] Citherlet S., Di Guglielmo F., and Gay J. "Window and advanced glazing systems life cycle assessment". In: *Energy and Buildings* 32 (3) (2000), pp. 225–234.

[4] *Kyoto Protocol*. United Nations Framework Convention on Climate Change, 1997.

[5] Schittich C. et al. *Glass Construction Manual. 2nd revised and expanded edition*. Birkhauser, 2007.

[6] Kozłowski M. "Glass as structural material". In: *XII Scientific Conference for Civil Engineering PhD Students, Conference Proceedings*. 2011.

[7] D. Aslop et al. *Structural use of glass in buildings*. The Institution of Structural Engineers, London, 1999.

[8] Nijsse R. *Glass in structures: elements, concepts, designs*. Birkhauser, 2003.

[9] Wurm J. *Glass Structures: Design and Construction of Self-supporting Skins*. Birkhauser, 2007.

[10] Kozłowski M. "Glass as structural material". MA thesis. Silesian University of Technology, Gliwice, 2009.

[11] Kozłowski M. "Projects that inspire". In: *The World of Glass* 06 (2010).

[12] Kozłowski M. "Glass staircase in Toronto". In: *The World of Glass* 07-08 (2010).

[13] Kozłowski M. "Load-bearing glass walls". In: *The World of Glass* 01 (2011).

[14] Kozłowski M. "Steel-glass composite bridge in Grand Canyon National Park". In: *The World of Glass* 06 (2011).

[15] Hulimka J. and Kozłowski M. "Timber-glass beams. A new solution to design of light roofs". In: *The World of Glass* 01 (2013), pp. 30–32.

[16] Kozłowski M. "Hybrid glass beams. Review of research projects and applications". In: *ACEE Journal* 5 (2012).

[17] Kozłowski M. and Kadela M. “Hybrid glass beams. Review of research projects and applications”. In: *The World of Glass* 3 (2014).

[18] Belis J. et al. “The Effect of Post-Tensioning On the Buckling Behaviour of a Glass T-beam”. In: *ISAAG Conference, Conference Proceedings*. Munich, 2006, pp. 129–136.

[19] Bos F. et al. “Stainless steel reinforced and post-tensioned glass beams”. In: *ICEM12 - 12th International Conference on Experimental Mechanics, Conference Proceesings*. Politecnico di Bari, 2004, pp. 1–9.

[20] Louter C. et al. “Post-Tensioned Glass Beams”. In: *Fracture of Nano and Engineering Materials and Structures*. Ed. by E. Gdoutos. Springer Netherlands, 2006, pp. 597–598.

[21] Louter P.C. “Adhesively bonded reinforced glass beams”. In: *Heron* 52 (2007), pp. 31–57.

[22] Palumbo M. “A New Roof for the XIIIth Century Loggia de Vicari (Arqua Petrarca -PD - Italy) Based on Structural Glass Trusses: a Case Study”. In: *Glass Processing Days, Conference Proceedings*. Tempere, 2005.

[23] Louter C., Bos F., and Veer F.A. “Structural Glass Beams with Embedded Glass Fibre Reinforcement”. In: *Challenging Glass 2, Conference Proceedings*. Delft, 2010.

[24] Ungermann D. and Preckwinkel E. “Structural Behaviour of Hybrid Steel-Glass Beams”. In: *Challenging Glass 2, Conference Proceedings*. Delft, 2010, pp. 485–495.

[25] Weller B., Meier A., and Weimar T. “Glass-Steel Beams as Structural Members of Facades”. In: *Challenging Glass 2, Conference Proceedings*. Delft, 2010, pp. 517–524.

[26] Wellershoff F. and Gerhard S. “Structural Use of Glass in Hybrid Elements: Steel-Glass-Beams, Glass-GFRP-Plates”. In: *Glass Processing Days, Conference Proceedings*. Tempere, 2013, pp. 268–270.

[27] Freytag B. “Glass-Concrete Composite Technology”. In: *Structural Engineering International* 14 (2) (2004), pp. 111–117.

[28] Hamm J. “Tragverhalten von Holz und Holzwerkstoffen im statischen Verbund mit Glas”. PhD thesis. École Polytechnique Fédérale de Lausanne, Switzerland, 2000.

[29] Hamm J. “Development of Timber-Glass Prefabricated Structural Elements”. In: *Innovative Wooden Structures and Bridges IABSE Conference* 1 (Lahti, 2001), pp. 41–46.

[30] Kreher K. “Tragverhalten und Bemessung von Holz-Glas-Verbundträgern unter Berücksichtigung der Eigenspannungen im Glas”. PhD thesis. École Polytechnique Fédérale de Lausanne, Switzerland, 2004.

[31] Kreher K. “Load Introduction with Timber Timber as Reinforcement for Glued Composites (Shear-Walls, I-Beams) Structural Safety and Calculation-Model”. In: 9^{th} *World Conference on Timber Engineering, Conference Proceedings*. Portland, 2006.

[32] Cruz P. and Pequeno J. “Timber-Glass Composite Beams: Mechanical Behaviour and Architectural Solutions”. In: *Challenging Glass Conference*. Vol. 1. Delft, 2008, pp. 439–448.

[33] Blyberg L. and Serrano E. “Timber/Glass Adhesively Bonded I-beams”. In: *Glass Performance Days, Conference Proceedings*. Tampere, 2011, pp. 507–512.

[34] Blyberg L. et al. “Glass, timber and adhesive joints as Innovative load bearing building components”. In: *Construction and Building Materials* 55 (2014), pp. 470–478.

[35] Hibbit D., Karlsson B., and Sorensen P. *ABAQUS/Standard User’s Manual. Ver. 6.10*. Pawtucket, Rhode Island, 2004.

[36] Stiell W. et al. *Geklebte Glaselemente in Holztragwerken. Abschlussbericht*. Inst. fur Fenstertechnik, Rosenheim, 1996.

[37] Schmidt J. et al. *Einsatz von geklebten Glaselementen bei Holztragwerken - ein Beitrag zur Innovation in der Holzbauarchitektur*. Inst. fur Fenstertechnik, Rosenheim, 1996.

[38] Schmidt J. et al. *Einsatz von geklebten Glaselementen bei Holztragwerken - ein Beitrag zur Innovation in der Holz-bauarchitektur (Objektversuche)*. Inst. fur Fenstertechnik, Rosenheim, 1996.

[39] Natterer J. and Kreher K. “New joining techniques for modern architecture”. In: *Rosenheimer Fenstertage* (2002).

[40] Hochhauser W. “Ein Beitrag zur Berechnung und Bemessung von geklebten und geklotzten Holz-Glas-Verbundscheiben”. PhD thesis. Vienna University of Technology, Austria, 2011.

[41] Winter W., Hochhauser W., and Fadai A. “Timber-glass composite trusses and plates”. In: *World Conference of Timber Engineering, Conference Proceedings*. Auckland, 2012, pp. 69–74.

[42] Fadai A. and Winter W. “Application of timber-glass composite (TGC) structures for building construction”. In: *Challenging Glass 4 & COST Action TU0905 Final Conference, Conference Proceedings*. Lausanne, 2014, pp. 235–242.

[43] Premrov M., Zlatinek M., and Strukelj A. “Experimental analysis of load-bearing timber-glass I-beam”. In: *Construction of Unique Buildings and Structures* 4 (19) (2014), pp. 11–20.

[44] Kreher K. and Natterer J. “Timber-Glass-Composite Girders for a Hotel in Switzerland”. In: *Structural Engineering International* 14 (May 2004), pp. 149–151.

[45] Haldimann M., Luible A., and Overend M. *Structural Use of Glass*. IABSE, 2008.

[46] *EN 572-1:2004 Glass in building - Basic soda lime silicate glass products - Part 1: Definitions and general physical and mechanical properties*.

[47] Griffith A. "The Phenomena of Rupture and Flow in Solids". In: *Philosophical Transactions* 221 (1920), pp. 163–198.

[48] Aben H. et al. "On non-destructive residual stress measurement on glass panels". In: *Estonian Journal of Engineering* 16 (2) (2010), pp. 150–156.

[49] *EN 408:1995 Timber structures. Structural timber and glued laminated timber. Determination of some physical and mechanical properties*.

[50] *EN 572-2:2012 Basic soda lime silicate glass products - Part 2: Float glass*.

[51] Veer F., Riemslag T., and Romein T. "The failure strength of glass, a non transparent value". In: *Glass Performance Days, Conference Proceedings*. 2007, pp. 610–614.

[52] Herzog T. et al. *Timber Construction Manual*. Birkhauser, 2004.

[53] Horacek P., Tippner J., and Hassan K. "Nondestructive evaluation of static bending properties of scots pine wood using stress wave technique". In: *Wood Research* 57 (3) (2012), pp. 359–366.

[54] Bergman R. et al. *Wood handbook. Wood as an Engineering Material. General Technical Report FPL-GTR-190*. Tech. rep. Forest Products Laboratory, 2010.

[55] Neuhaus H. *Budownictwo drewniane*. Polskie Wydawnictwo Techniczne, 2006.

[56] Kinloch A. J. *Adhesion and Adhesives: Science and Technology*. Springer, 1987.

[57] 1996 3M. Technical data sheet DP490. Technical report.

[58] Version 08/2002 SIKA SCHWEIZ AG. Technical data sheet SikaFast 5215. Technical report.

[59] Version 03/2010 SIKA SCHWEIZ AG. Technical data sheet Sikasil SG-500. Technical report.

[60] *ISO 527-2:2012 Plastics - Determination of tensile properties - Part 2: Test conditions for moulding and extrusion plastics*.

[61] *ISO 527-1:2012 Plastics - Determination of tensile properties - Part 1: General principles*.

[62] *ARAMIS / User Manual. v. 6.1*. GOM mbH, Germany, 2009.

[63] Veer F. and Zuidema J. "The strength of glass, effect of edge quality". In: *Glass Processing Days, Conference Proceedings*. Tampere, 2003, pp. 106–109.

[64] Version 08/2009 SIKA SCHWEIZ AG. Technical data sheet Icosit KC 340/7. Technical report.

[65] Hulimka J. and Kozłowski M. “Synergy of hybrid timber-glass beams”. In: *Symposium Composites. Polish Society of Theoretical and Applied Mechanics, Conference proceedings*. 2012.

[66] Hulimka J. and Kozłowski M. “Load-bearing capacity of hybrid timber-glass beams”. In: *ACEE Journal* 2 (2014).

[67] Kozłowski M., Serrano E., and Enquist B. “Experimental investigation on timber-glass composite I-beams”. In: *Challenging Glass 4 and COST Action TU 0905 Final Conference, Lausanne, Conference Proceedings*. 2014.

[68] Dorn M., Kozłowski M., and Serrano E. “Development of large-scale load-bearing timber-glass structural elements (in review)”. In: *World Conference in Timber Engineering, Quebec City*. 2014.

[69] Dorn M., Kozłowski M., and Serrano E. “Design approaches for timber-glass beams (in review)”. In: *Engineered transparency. International Conference at glasstec, Dusseldorf*. 2014.

[70] Solli K. “Modulus of elasticity - local or global values”. In: *6th World Conference on Timber Engineering, Conference Proceedings*. Whistler, 2000.

[71] Nielsen J.H. and Olesen J.F. “Mechanically Reinforced Glass Beams”. In: *Recent Developments in Structural Engineering, Mechanics and Computation. Conference Proceedings*. 2007, Cape Town, pp. 655–657.

[72] Olgaard A.B., Nielsen J.H., and Olesen J.F. “Design of Mechanically Reinforced Glass Beams - Modelling and Experiments”. In: *Structural Engineering International* 19(2) (2009), pp. 130–136.

[73] Louter C., Van de Graaf A., and Rots. J. “Modeling the Structural Response of Reinforced Glass Beams using an SLA Scheme”. In: *Challenging Glass 2, Conference on Architectural and Structural Applications of Glass. Conference Proceedings*. 2010.

[74] Correia J.R., Valarinho L., and Branco F.A. “Ductility and post-cracking strength of glass beams stresngthened with GFRP pultruded composites”. In: *Composite Structures* 93(9) (2011), pp. 2299–2309.

[75] Bedon C. and Louter C. “Parametric 2D numerical investigations of the structural response of SG-laminated reinforced glass beams”. In: *Challenging Glass 4 & COST Action TU0905 Final Conference. Conference Proceedings*. 2014.

[76] Hillerborg A., Modeer M., and Petersson P. “Analysis of Crack Formation and Crack Growth in Concrete by Means of Fracture Mechanics and Finite Elements”. In: *Cement and Concrete Research* 6 (1976), pp. 773–782.

[77] Ivanov I.V. and Sadowski T. “Efficient finite element models of laminated glass structures subjected to low-velosity impact”. In: *Challenging Glass 4, Conference Proceedings*. 2014, pp. 499–506.

[78] Harewood F.J. and McHugh P.E. “Comparison of the implicit and explicit finite element methods using crystal plasticity”. In: *Computational Materials Science* 39(2) (2007), pp. 481–494.

[79] Kutt L. et al. “Slow-dynamic finite element simulation of manufacturing processes”. In: *Computers & Structures* 66(1) (1998), pp. 1–17.

[80] Chung W.J., Cho J.W., and Belytschko T. “On the dynamic effects of explicit FEM in sheet metal forming analysis”. In: *Engineering Computations* 15(6) (1998), pp. 750–776.

[81] Bernard F., Krour B., and Fahsi B. “Analysis of the debonding risks and the failure of laminated glass thanks to a coupled analytical-numerical investigation”. In: *COST Action TU0905 Mid-term Conference on Structural Glass. Conference Proceedings*. 2013, pp. 391–403.

[82] Castro san Roman J. “System ductility and redundancy of FRP structures with ductile adhesively-bonded joints”. PhD thesis. EPFL, 2005.

[83] *PN-EN 1995-1-1 2010 Part 1-1: General - Common rules and rules for buildings*.

[84] Möhler K. “Über das Verhalten von Biegeträgern und Druckstäben mit zusammengesetzten Querschnitten und nachgiebigen Verbindungsmitteln”. PhD thesis. Universität Karlsuhe, 1956.

[85] Flinterhoff A. “Tragverhalten von geklebten Stahl-Glas-Verbundkonstruktionen unter Biegebeanspruchung”. MA thesis. Dortmund University, 2002.

List of Figures

List of Tables